NASA Contractor Report 175063

Effect of Liquid Droplets on Turbulence in a Round Gaseous Jet

A.A. Mostafa and S.E. Elghobashi

University of California at Irvine
Irvine, California

February 1986

NASA
National Aeronautics and
Space Administration

SUMMARY

The main objective of this investigation is to develop a two-equation turbulence model for dilute vaporizing sprays or in general for dispersed two-phase flows including the effects of phase changes. The model that accounts for the interaction between the two phases is based on rigorously derived equations for the turbulence kinetic energy (K) and its dissipation rate (ϵ) of the carrier phase using the momentum equation of that phase. Closure is achieved by modeling the turbulent correlations, up to third order, in the equations of the mean motion, concentration of the vapor in the carrier phase, and the kinetic energy of turbulence and its dissipation rate for the carrier phase. The governing equations are presented in both the exact and the modeled forms.

It is assumed that no droplet coalescence or breakup occurs. This implies that the droplets are sufficiently dispersed so that droplet collisions are infrequent. The droplets are considered as a continuous phase interpenetrating and interacting with the gas phase, and are classified into finite-size groups. Further, constant properties for both the carrier fluid and droplets are assumed.

The Eulerian approach adopted here leads to two sets of transport equations, one set for the carrier phase (primary air issuing from the pipe plus the evaporated material) and the other for the droplets. These equations are coupled primarily by three mechanisms, the mass exchange, the displacement of the carrier phase by the volume occupied by droplets, and the momentum interchange between droplets and the carrier phase.

An expression for calculating the turbulent Schmidt number of the droplets (the ratio of droplet diffusivity to fluid point diffusivity) is developed via comparison with the experimental data (Snyder and Lumley, 1971,

and Wells and Stock, 1983).

The governing equations are solved numerically using a finite-difference procedure to test the presented model for the flow of a turbulent axisymmetric gaseous jet laden with either evaporating liquid droplets or solid particles. The predictions include the distribution of the mean velocity, volume fractions of the different phases, concentration of the evaporated material in the carrier phase, turbulence intensity and shear stress of the carrier phase, droplet diameter distribution, and the jet spreading rate. Predictions obtained with the proposed model are compared with the data of Shearer et al. (1979) and with the recent experimental data of Solomon et al. (1984) for Freon-11 vaporizing sprays. Also, the predictions are compared with the data of Modarress et al. (1984) for an air jet laden with solid particles. The predictions are in good agreement with the experimental data.

TABLE OF CONTENTS

a : droplet radius;

a_1, a_2 : major and minor radii of a droplet;

B : transfer number;

C : concentration of the vapor in the carrier phase;

c : concentration fluctuation of the vapor in the carrier phase;

C_D : drag coefficient of a liquid droplet;

C_{Ds} : drag coefficient of a solid particle;

C_{Db} : drag coefficient of a gas bubble;

c_ϕ : coefficient in the momentum equations;

c_μ : coefficient in the turbulence model;

$c_{\varepsilon 1}, c_{\varepsilon 2}, c_{\varepsilon 3}$: coefficients in ε equation;

d : droplet diameter;

D : nozzle diameter;

Et : Eotvos number, $\rho_1 (U-V)^2 d / \gamma$;

$E_p(\omega)$: particles normalized energy spectrum function;

$E(\omega)$: fluids normalized energy spectrum function;

F : momentum exchange coefficient;

f : particle's free fall velocity;

g : gravitational acceleration;

I : evaporation rate;

K : kinetic energy of turbulence;

L : latent heat of vaporization per unit mass;

L_f : fluid Lagrangian length scale;

m : droplet mass;

$\dot{m}$: evaporation rate per droplet volume;

P : mean static pressure;

p	: static pressure fluctuation;
ΔP	: static pressure difference;
r	: distance in radial direction;
R	: ratio between a_1 and a_2;
Re	: Reynolds number;
$R_L(\tau)$	: Lagrangian velocity autocorrelation for the gas;
R_o	: universal gas constant;
$R_p(\tau)$	: Lagrangian velocity autocorrelation for the droplet;
S	: droplet surface area;
Sc	: Schmidt number of the gas;
Sh	: Sherwood number;
t	: time;
T_B	: boiling temperature of the droplet;
T_L	: temperature at the droplet surface;
T_S	: saturation temperature of the droplet;
U	: mean velocity of the carrier phase;
$\vec{U}$	: total mean velocity of the carrier phase;
u	: velocity fluctuation of the carrier phase;
V	: mean velocity of the droplets;
$\vec{V}$	: total mean velocity of the droplets;
v	: velocity fluctuation of the droplets;
We	: Weber number;
W_v	: molecular weight of the evaporating material;
X_o	: ratio of the mass of the particles to that of the gas at the nozzle exit;
X_v	: molecular fraction of the evaporating material;
$\overline{Y^2(t)}$	: mean square displacement of the gas;

$\overline{Y_p^2(t)}$: mean square displacement of the particles;

z : distance in the axial direction;

Greek symbols

μ : dynamic viscosity of the carrier phase;

ν : kinematic viscosity of the carrier phase;

ν_t : momentum eddy diffusivity of the carrier phase;

ν_p : momentum eddy diffusivity of the droplets;

δ : molecular mass diffusivity of the vapor;

ρ : density;

α : coefficient;

τ_p : droplet's relaxation time;

τ_L : lagrangian time scale of the gas;

β, β_h, β_v : coefficients;

η : Kolmogorov length scale;

γ : surface tension of the liquid-air interface;

Φ : mean volume fraction of the droplets;

ϕ : volume fraction fluctuation of the droplets;

ψ : gaseous phase stream function;

ω : circular frequency;

ε : rate of turbulence energy dissipation per unit volume;

ε_f : mass eddy diffusivity of the carrier phase;

ε_h : mass eddy diffusivity of the praticles in the normal direction to the mean relative velocity;

ε_v : mass eddy diffusivity of the paritcles in the prarllel direction to the mean relative velocity;

σ_k : coefficient in K equation;

σ_ε : coefficient in ε equation;

σ_p : droplet's Schmidt number;

σ_v : coefficient in the dispersed phase momentum equation.

Subscripts

o   : conditions at the nozzle exit;

1   : carrier phase;

2   : dispersed phase;

c   : conditions at the jet centerline;

c.s.   : corresponding values for the single phase (air only);

L   : conditions at the droplet surface;

r   : radial direction;

z   : axial direction.

Superscript

k   : droplets in k^{th} size range.

1.0 INTRODUCTION

1.1 The Problem Considered

Dispersed flow is a particular class of two-phase flows, characterized by the dispersion of solid particles, liquid droplets, or gas bubbles in a continuous fluid phase. Different flow regimes may be encountered. Of particular interest here is the case where liquid droplets occupy a small fraction, less than 1%, of the total volume of a gas-droplet mixture. This spray regime (Fig. 1-1), which has been termed "thin spray" (O'Rourke, 1981) or "dilute spray," (Mostafa and Elghobashi, 1984) is important in a variety of applications. Steam generators, nuclear reactors, cooling systems, premixed-prevaporized gas turbine combustors, diesel-engine sprays, spray-cooling and spray-drying systems, and rocket plumes are some examples. Understanding the interaction between the particles and surrounding gas is essential for predicting dispersed two-phase flows.

A quantitative definition of "dilutness" in turbulent two-phase flows is not readily available. For laminar flow the dilutness requires that the center-to-center distance between particles should be larger than $2(a+\delta_b)$ where a is the particle radius and δ_b is the thickness of the boundary layer around that particle. The experimental data of Tsuji et al. (1982) indicates that the fluid dynamic force on a suspended particle can be assumed to be the same as that on a single particle if the interparticle spacing is not less than three particle diameters. This restriction gives an upper limit for the volume fraction of the particles of 1% to satisfy the diluteness assumption. For turbulent flow, another parameter plays a more significant role. This is the ratio of the aerodynamic response time to the time between collisions (Crowe, 1981). This ratio depends on the particles' loading ratio, the relative velocity between particles and gas, and the gas velocity gradient.

1
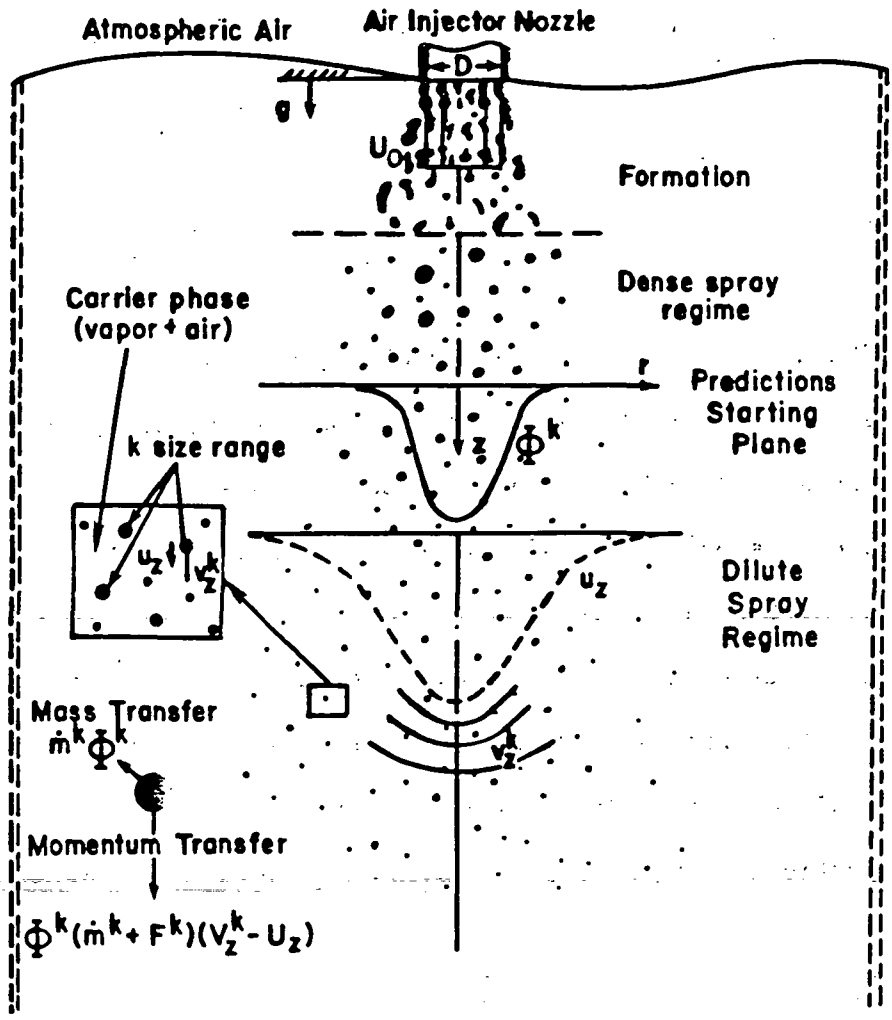
Figure I-I THE FLOW CONSIDERED
(EVAPORATING FREON-II SPRAY)

If this ratio is less than unity, a particle has time to respond to the local

gas velocity field before the next collision so its motion is dominated by

aerodynamic forces and the particle collisions can be neglected. Using this

restriction the particle number density, or the volume fraction, for a dilute

spray can be calculated.

In the dilute spray regime the interactions between droplets is

neglected. This implies that the droplet coalescence or break-up does not

occur. The droplets may exchange mass, momentum, and energy with the gas and

for dilute spray the exchange functions for isolated droplets can be used.

The droplets are classified into finite-size groups and each group is

considered as a distinctive phase. Further, constant properties are assumed

for all the phases to avoid the density fluctuations of the carrier phase at

this stage.

1.2 Previous Work

1.2.1 Fundamentals of Two-Phase Flow

The simplest analytical approach for calculating the properties of dilute

suspensions of two-phase flow is to assume dynamic equilibrium, where the

particles and gas velocities are equal at each point in the flow. The

suspensions can then be considered as a single homogeneous fluid that is

treated exactly as a single-phase flow. The mixture properties are those

based on the continuum mechanics that apply to molecular mixtures. The

infinitely fast interphase transport between the phases is the basic premise

of that approach. The equilibrium assumption is valid for small values of

Stokes number, less than 10^{-1}, and small values of particle/fluid material

density ratio, less than 10^{2}, (DiGiacinto et al., 1982). Stokes number is the

ratio of the particle relaxation time to the characteristic time of the

surrounding fluid. These two restrictions are not satisfied for the flow of gaseous phase laden with liquid droplets or solid particles. Accordingly, the local equilibrium approximation leads to unrealistic results for that type of flow (Shuen et al., 1983). In spite of the inaccuracies in that approach, it has been used by some workers (Shearer et al., 1979; Michaelides, 1984; and Kamimoto and Matsuoka, 1977).

On the other hand, if both the density ratio and the Stokes number are large, the particles will not be able to respond to the changes in the carrier phase. In this case the difference between the velocities of the phases can not be neglected and each phase should be treated separately (Crowe, 1982).

There are two approaches to handle the carrier phase in the separated flow models, depending on the mass loading ratio, which is defined as the mass flow rate of the particles to that of gas. If this ratio is small, less than 0.1, the velocity field of the carrier phase is not affected by the presence of the particles while the motion of the particles is determined by the gas flow properties (Rudinger, 1965). In this case the governing equations of the carrier phase have no extra terms but rather they are identical to the well-known Navier-Stokes equations. This approach is referred to as one-way coupling (DiGiacinto et al., 1982) from gas to particles only and has been used by many workers (Cox and Mason, 1971; Batchelor, 1974; and Boyson and Swithenbank, 1979). On the other hand, if the mass loading ratio is high, the particles may modify the gas flow field significantly. In this case the particles are regarded as source of mass and momentum for the carrier phase. This approach is referred to as two-way coupling (DiGiacinto et al., 1982; and Crowe, 1982) from fluid to particles and vice versa.

There are two main approaches to handle the dispersed phase in the separate two-phase flow models, namely the Lagrangian and the Eulerian approaches. In the Lagrangian approach the dispersed phase is treated by solving Lagrangian equations of motion for the particles with a prescribed set of initial conditions. Once the flow properties of the particles are known, the interface quantities between the two phases can be calculated. In the Eulerian approach the dispersed phase is treated as an interacting and interpenetrating continuum. In that approach the governing equations for the two phases are quite similar to the well-known Navier-Stokes equations. These equations are coupled primarily by three mechanisms, the mass exchange, the displacement of the carrier phase by the volume occupied by particles, and momentum interchange between particles and the carrier phase. Many two-way coupling studies are presented in the literature, based either on the Lagrangian or Eulerian approaches (Elghobashi and Megahed, 1981; Yeung, 1982; Abbas et al., 1981; and Crowe et al., 1977).

Of most importance, the continuum assumption must be justified when using the Eulerian approach. Batchelor (1974), Lumley (1978a), and Marble (1962) have discussed the continuum concept for the dispersed phase. In summary, the particles must be sufficiently small in order that a volume element, small compared to the Kolmogoroff microlength scale, η, contains a large number of particles. Thus a statistical average concerning the behavior of the particles can be made within this volume element. This requires that the average separation distance between the particles is at least one order of magnitude smaller than η. Hinze (1972) stated that the continuum assumption has proven to be applicable also to situations that do not strictly meet that condition. Others (Crowe, 1982; Soo, 1967; and Yeung, 1978) showed that most practical physical systems involving gas-particle mixtures satisfy the

continuum assumption. We may refer, amongst others, to theoretical

investigations by Marble (1970), Buckingham and Siekhaus (1981), Pourahmadi

and Humphrey (1983), Rizk and Elghobashi (1984), and Mostafa and Elghobashi

(1983) who used the Eulerian approach to study different flow conditions of

two-phase flows. Early work based on Lagrangian equations of motion are due

to El-Banhawy and Whitelaw (1980), Mongia and Smith (1978), Shuen et al.

(1983), El-Kotb et al. (1983), and El-Emam and Mansour (1983).

Arguments over the advantages and the disadvantages of Eulerian and

Lagrangian approaches persist in the literature. The Eulerian approach models

can easily incorporate particle diffusion effects since the randomness of the

particulate phase is accounted for by the way of the formulation. This

approach can be extended easily to multidimensional flows. Numerical

instabilities, false diffusion, and large storage requirements are the most

serious disadvantages of that approach. However, the use of advanced digital

computers and the ability to overcome the numerical problems (for example, by

choosing a suitable higher order finite-difference scheme) alleviate most of

these disadvantages. The Lagrangian approach exhibits no numerical diffusion

but the particle dispersion must be incorporated through an empirical

diffusion velocity or more expensive Monte Carlo methods (Chen and Crowe,

1984). Durst et al. (1984) showed that the Lagrangian approach, in cases

where the particle loadings are high, is inferior to the Eulerian approach.

The Lagrangian approach calculations require interpolation between the meshes

since gas and particle properties are strongly coupled. In any case it

requires a toilsome computation for the source terms. If the interpolation

process is too crude, Aggarwal et al. (1983) have shown that errors of the

same order as the diffusion error in the Eulerian approach will be

encountered. Sirignano (1983) argued that the droplet properties should not

be averaged over the numerical cell as suggested by Dukowicz (1980), but rather a linear interpolation should be made. In the present work attention will be restricted to a formulation following the Eulerian approach.

The previous fundamental studies of the various aspects of two-phase flow are concentrated on either the effects of various factors on the flow around a single particle or on the governing equations of the dispersed phase. Fuchs (1964) and Torbin and Gauvin (1959, 1960, 1961) did an extensive survey about the dynamics of single particles. Those studies are very important to fundamentally understand the two-phase flow. Most of the recent publications in this regard will be discussed in section four.

On the other hand, several phenomenological attempts have appeared in the literature to derive equations governing the macroscopic behavior of dispersed two-phase flow. The equations cited most frequently are those of Drew (1971), Kalinin (1970), Whitaker (1973), Gray (1975), Panton (1968), and Soo (1967). Other deriviations include those by Nigmatulin (1967), Owen (1969), Rietema and Van Den Akker (1983), Buevich and Markov (1973), and Jackson and Davidson (1983). The resulting equations differ in various ways such as the formulation for the pressure gradient term, the nature of the momentum, source terms, or the proper coupling between the two fields.

Buevich and Markov (1973) obtained the conservation of mass, momentum and moment of momentum for the two interpenetrating and interacting continua. All the unknowns in the governing equations are expressed in terms of mean stresses acting at the surface of an individual suspended sphere. Crowe (1980) used the control volume, or Reynolds transport theorem approach, to derive the continuity and momentum equations for a flowing vapor with suspended burning, evaporating, or condensing droplets.

Solbrig and Hughes (1975) derived the momentum equations and mechanical constitutive equations that are required to describe transient, two-phase, single-component evaporating and condensing flows. Momentum field balance equations were derived for each phase on the basis of a seriated-continuum approach. A seriated continuum is distinguished from an interpenetrating medium by the representation of interphase friction with velocity differences in the former and velocity gradients in the latter. A two-phase mixture is an example of a seriated continuum, whereas a mixture of gases is an example of an interpenetrating continuum. The seriated continuum also considers embedded stationary solid surfaces such as that which occurs in nuclear reactor cores. There are some undetermined numerical coefficients that appeared in the momentum equations of Solbrig and Hughes (1975). These coefficients must be determined for the different flow regimes and geometry.

Panton (1968) formulated the flow properties for the non-equilibrium two-phase flow of a gas-particle mixture. The conservation equations of continuum fluid mechanics are assumed to apply to the flow field locally, both within the particles and through the gas. Control volumes for each phase are defined and integral forms of the conservation equation are applied. By inspecting the equations, the proper area-averaged properties are defined so that they are meaningful terms in the physical conservation laws. Because the detailed flow is inherently unsteady, it was necessary to take the time average of the equations. Thus, the dependent variables of the the final conservation equations were area-time-averaged properties. New terms, even in laminar flow, appeared in the momentum equations and were called the area-averaged Reynolds stresses. The Reynolds stresses attributed to the fluctuations in the gas velocity occur because of the presence of the particles. Every time a particle passes the point under observation, a fluctuation in the gas velocity

occurs. Panton commented that these unknowns are the price to be paid for the details of the flow.

Delhay (1980) surveyed two-phase flow modeling. He discussed the different types of averaging -- time, area and volume -- in two-phase flow. Also, the different two-phase flow and single fluid modeling were reviewed. Delhay concluded that more work is needed to build the bridge between the Lagrangian behavior of a particle and the Eulerian form of the constitutive terms entering the averaged balance equations.

Drew (1971) derived averaged field equations for two-phase media. He treated the separated surfaces between the two-phase media as transition regions where the material properties have jump discontinuities. Postulating the laws of balance of mass, linear momentum, angular momentum, energy, and an entropy inequality, jump condition laws for each phase were derived. Solving the differential equations and jump conditions, exact expressions for the field quantities involved were found. Drew also defined and related the appropriate average variables for each phase involved. He commented that for any particular problem, his averaged field equations must be supplemented by constitutive equations, which is not a simple task. Ishii (1975) discussed the way of averaging used by Drew (1971), specifically the two integrals over both space and time domains. Ishii commented that it is not quite convincing why these four integrations are necessary to develop meaningful macroscopic field equations. He pointed out that the time and space differential operators in the averaged fields represent finite difference operators in the physical interpretations.

Ishii (1975) presented a detailed discussion on the formulation of various mathematical models of two-phase flows based on the conservation laws of mass, momentum and energy. He considered the local instant formulation and

the time-averaged macroscopic models. He presented the two-fluid model, which is formulated by considering each phase separately. Thus, the model is expressed by two sets of conservation equations of mass, momentum, and energy with interaction terms appearing in the field equations. His formulation has the advantage of treating large and small particles alike, with averaging carried out across the interface. Ishii's formulation simplifies the treatment of the dispersed phase by introducing a duality of discrete nature and distributive representation. The discreteness is accounted for via treating the virtual mass and unsteadiness of flow field of each finite size particle. The distributive nature of the particle cloud is accounted for by taking an elementary volume consisting of a sufficiently large number of particles. Ishii also considered the diffusion model, which is formulated by considering the mixture as a whole. Thus, it is expressed in terms of three mixture conservation equations of mass, momentum, and energy with one additional diffusion equation.

Sha and Soo (1978) discussed the basic concepts for the rigorous formulation of a system of a single-component fluid in two phases. They pointed out that the direct extension of continuum mechanics is inadequate because of the mutually exclusive nature of the phases in a multiphase system. Multiphase mechanics have their own distinct regime with additional inertial and viscous interaction terms, applied to mixtures of phases that are separated by interfaces and are mutually exclusive. This is in contrast to the field equations of mixtures based on continuum mechanics, which directly apply to molecular mixtures where the phases coexist at the same points in space. Boure (1979), Crowe (1978), and No (1982) argued that the equations of Sha and Soo (1978) are inconsistent and not valid even in one-dimensional situations.

In section two, the governing equations of dispersed two-phase flow are presented and compared with other equations in the literature.

1.2.2 Turbulent Evaporating Sprays

Modeling of evaporating and combusting sprays is an extremely difficult problem due to the complex physical and chemical phenomena encountered in this type of two-phase flow. A substantial number of reviews of this problem have appeared in the literature. The recent reviews of Law (1982), Faeth (1977, 1983), Labowski and Rosner (1973), and Sirignano (1983) discussed the previous work on the different phenomena associated with the spray evaporation and combustion problem. The present study will be restricted to evaporating or nonevaporating dilute sprays.

Krestein (1983) has analyzed a simple model of an evaporating spray to predict the probability density function (pdf) of vapor concentration within the spray. The model assumes that the droplets deposit linear streaks of vapor as they traverse the motionless host gas, and that the vapor diffuses radially from these streaks. Since it neglects droplet collisions, saturation, and related effects, the model is applicable primarily to dilute sprays. The results of this analysis can be used to estimate droplet vaporization rates from experimentally measured pdf's of concentration. Therefore the individual-droplet processes could be linked to fluctuating ambient conditions in spray simulation codes.

O'Rourke and Bracco (1980) developed a numerical model for turbulent dense sprays. The model is two-dimensional unsteady and uses atomization experimental results as nozzle exit boundary conditions and a stochastic algorithm to compute droplet events, including collisions and coalescence. Westbrook (1976) presented a numerical solution technique for the spray

equation for a type of stratified charge internal combustion chamber. He neglected the gas entrainment by the droplets and adopted the dilute spray approximations. The gas motion was assumed to be consisted of a rotational swirl with a constant angular velocity. Axial and radial components of the gas velocity were assumed to be identically zero.

Martinelli et al. (1983) used O'Rourke's model after considering a $K-\epsilon$ submodel for gas turbulence to predict the data of Wu et al. (1984). Agreement is good with mean quantities but the computed standard deviation of the drop velocity distribution is generally smaller than the measured one. Although the effects of turbulence on the droplet motion is considered in the model, the direct effects of the droplets on the gas motion are neglected.

Yeul et al. (1982) have since reported measurements in evaporating kerosene sprays from a twin-fluid injector in a co-flowing stream. Measurements of droplet size were undertaken using a laser tomographic light-scattering technique while mean velocities were measured using LDA. They did not measure the turbulence characteristics or the droplet/velocity correlations which are needed for the theoretical models evaluation. Wu et al. (1984) reported LDV measurements for the distribution function of the axial and radial components of the droplet velocity at various radial and axial locations within steady sprays under the conditions of direct fuel injection in internal combustion engines, but at room temperature. The measurements were taken within 300 to 800 nozzle diameters from the nozzle exit.

1.2.3 Turbulence Mathematical Models

Computational models are a very useful tool for a better understanding of the features of the two-phase flow, considering the inability of the

analytical methods and the difficulty of experimental investigations. Vasiliev (1969) reviewed the development of the two-phase flow, relying chiefly on the research that has been done in the Soviet Union. He cited the papers on the governing equations for laminar and turbulent flows as well as those on the effects of the dispersed phase on the turbulence intensity and the spectrum of turbulence. He concluded that the presence of small suspended particles leads to more rapid damping of the turbulent energy under isotropic flow conditions. In the case of large values of density ratio it also causes a noticeable distortion of the turbulence energy spectrum and a decrease of its micro scales in comparison with the case of single-phase flow.

Rakhmatulin (1956) (cited by Vasiliev, 1969) suggested that the motion of the mixture should be treated as an interpenetrating motion of several continua. The equations of motion are written separately for each phase, and the interaction between the phases is taken into account by considering the interaction forces that appear as internal forces for the whole system. The governing equations of Rakhmatulin (1956) were used by Bondarenko and Shaposhnikova (1980) to analyze flow regimes in channels of different shapes. Those equations were also used by Vasil'kov (1976) to predict a turbulent submerged jet containing an admixture of solid particles.

Michaelides (1984) analyzed the gas-solid two-phase pipe flows using the mixing length hypothesis. The mixture was taken to be a homogeneous fluid of variable density across the pipe cross-section. These two assumptions make the solution very restricted to dilute suspensions with comparable densities between the solid and the gas.

Buckingham and Siekhaus (1981) described a K-ϵ turbulence model that allows for effects of particles on turbulence properties. The model is applied to flows containing small solid particles, considering added

dissipation due to particle interactions with the carrier phase in the governing. Buckingham and Siekhaus did not compare the performance of their model with any experimental data. The predictions suggest a damping of the turbulence motions primarily because of inertial effects. Nagarajan and Murgatroyd (1971) presented an analytical model for turbulent two-phase fully-developed pipe flow. They assumed linear shear stress in the radial direction and introduced several phenomenological coefficients in the model. This made their model inapplicable to other two-phase flow problems.

Kramer and Depew (1972) developed a one-dimensional model for a fully developed two-phase turbulent pipe flow. In their solution they expressed the velocity fields in terms of various empirical coefficients and assumed a linear mixing length to express the turbulent correlations. This has again made the application of their model to any other problem very difficult.

Genchev and Karpuzov (1980) have proposed a turbulence model for fluid-particle flows in which the effects of particles on the turbulence transport equations are considered. They assumed that the mean velocity of the particles is equal to the fluid mean velocity and neglected the fluid-particle turbulent correlations existing in the time-averaged equations (Elghobashi and Abou-Arab, 1983). Genchev and Karpuzov predicted a fully developed pipe flow laden with solid particles of density ratio of order 10^3 and volume concentration of order of 10^{-3}. They did not compare their predictions with experimental data to evaluate the capabilities and the limitations of their model.

Danon et al. (1977) described a K-L model for two-phase jets. The length scale (L) was not modified from the value appropriate for a constant density single phase jet; however, a term representing the added dissipation due to the presence of particles was included in the governing equation for K. The

14

model was evaluated using the data of Hetsroni and Sokolov (1971) for a round jet containing oil droplets. The predictions using the basic model were not in good agreement with these measurements. The comparison between the predictions and measurements was improved by multiplying the rates of production and dissipation of K by a coefficient that was a strong function of the void fraction. These authors commented that there is a substantial and unexplained influence of particles on turbulence properties of jets, even at low particle concentrations.

Melville and Bray (1979) described a model for particulate flow, with small interphase slip, employing constant eddy diffusivities for momentum and particle transport. The predictions were evaluated using the measurements of Laats and Frishman (1970a and 1970b) for a round jet containing powders of various sizes.

Pourahmadi and Humphrey (1983) proposed a mathematical model for dilute suspensions of two-phase flow based on the single-phase $K-\varepsilon$ model. They considered the direct effects of the particle's sharing the same control volume with the gas on the governing equations of K and ε. These authors neglected all the third-order correlations without justification and used stokes drag coefficient although the particle Reynolds number is generally greater than unity in two-phase flow. They also used Peskin's formula for the calculations of the particle's Schmidt number. This formula was tested by Elghobashi et al. (1984) for glass particles and produced unrealistic values for the particle's Schmidt number, negative or zero.

Elghobashi and Abou-Arab (1983) proposed a two-equation turbulence model for incompressible dilute two-phase flow which undergoes no phase changes. Using this model, Elghobashi et al. (1984) predicted the turbulent axisymmetric gaseous jet laden with uniform size solid particles. They

15

achieved good agreement with the experimental data of Modarress et al.
(1984). This model has been extended by Mostafa and Elghobashi (1985a) to
include the effects of phase changes.

Shuen et al. (1983) evaluated the performance of the available Lagrangian
methods for predicting the dispersed phase behavior by comparing the results
with measurements of particle-laden jets. They considered only dilute
suspensions of solid particles, and hence concluded that the effects of the
particles on the turbulence quantities are almost negligible. This allowed
them to recommend the use of the conventional K-ε model for two-phase flows
without any modifications. Shuen et al. (1983) indicated that the suggested
method by Gosman and Ioannides (1981) for calculating particle trajectories,
the "stochastic or Monte-Carlo method," in contrast to other methods, provides
good predictions over their data base. In this method the isotropic turbulent
gas velocity field is split into mean and fluctuation. The mean value is
obtained from the solution of the mean equations while the fluctuating one is
estimated from random sampling of a Gaussian distribution of the kinetic
energy of turbulence. The Monte-Carlo method requires selection of
characteristic eddy length and time scales. Shuen et al. (1983), following
Gosman and Ioannides (1981), assumed that the eddies are uniform and their
size is proportional to a turbulent length scale, ℓ_e, given by

$$\ell_e = C_e \, K^{3/2} / \varepsilon \qquad\qquad 1.1$$

Shuen et al. (1983) used the value of 0.16 for the constant C_e, which was
suggested by Gosman and Ioannides (1981) who later changed this value to 0.31
to get a better agreement with the experimental data (Crowe, 1982). Crowe,
(1982) recently argued that the value of C_e should be 0.46 to give a good

agreement with the experimental results. This is unfortunate since Shuen et al. (1983); Gosman and Ioannides (1981); and Crowe, (1982) have used the same experimental data of Snyder and Lumley (1971) to obtain the value of the empirical coefficient C_e.

In conclusion, after the literature on two-phase turbulent flow was examined, it was found that there is still no complete mathematical model of this class of flows comparable with the model of single-phase turbulent flows. The main objective of this study is to develop such a model.

1.2.4 Turbulent Two-Phase Jet Flows

A turbulent nonreacting gaseous jet laden with solid particles or evaporating droplets is a relatively simple flow that allows the study of the interactions between the two phases and the turbulent dispersion of the discrete phase. Most of the previous measurements (Rajani, 1972; Hetsroni and Sokolov, 1971; and Laats and Frishman, 1970a) of the structure of particle-laden jets considered the effects of the dispersed phase on the continuous phase properties. Abramovich (1970) and Goldschmidt and Eskinazi (1966), discussed the effects of the dispersed phase on the structure of a turbulent gaseous jet. They showed that the particle concentration profiles in a two-phase jet are narrower than the gas velocity profiles. This behavior was explained later by Elghobashi et al. (1984).

Levy and Lockwood (1981) and Laats and Frishman (1970a) found that the gas mean velocity profiles in a two-phase jet are narrower than those of the clear jet. Modarress et al. (1984) and Girshovich et al. (1981) further showed that the solid or liquid particle velocity is higher than the gas velocity in the developed region of the jet. Other studies (Al-Taweel and Laundau, 1977; and Laats and Frishman, 1973) showed that the turbulent energy

17

level decreases with the increase of the suspension of particles into a jet. The effect of small droplets of cottonseed of 13 μm average diameter on the flow structure of an axially symmetrical turbulent air jet has been studied by Hetsroni and Sokolov (1971). They found that in the two-phase jet, the velocity spread and the turbulence intensities were reduced in comparison with the single-phase jet. They also found that even at low volumetric droplet loadings, the jet was narrower than single-phase air jet. At a high loading, the jet spread was wider upstream and narrower in the downstream region. The intensity of velocity fluctuations was reduced throughout the jet. Hetsroni and Sokolov (1971) measured time-averaged and fluctuating longitudinal velocities by means of a hot-wire anemometer. The probe was not calibrated in a two-phase flow but the authors stated that the calibration curves obtained in single-phase flow could be used for two-phase flow with minor corrections. Rajani (1972) pointed out the uncertainties regarding the calibration of probes used in dust-laden flows that may lead to an overestimation of the measured quantities. Therefore, their results should be viewed with caution as pointed out by Melville and Bray (1979).

Field (1963) and Subramanian and Ganesh (1982a and 1982b) have provided evidence of the overall effect of solid particles on a dust-laden jet by measuring the rate of ambient air entrainment by the jet. Field considered lycopodium powder of 30 μm size while Subramanan and Ganesh used sand particles of uniform size of 150-180 μm. They found that the entrainment was affected by particle size, density and mass loading ratios, and the dispersed phase initial conditions. Subramanian and Ganesh showed that the presence of particles increases the entrainment rate. Since their measurements are in the developing region ($z/D \leq 7$), where z/D is the axial distance to nozzle diameter ratio, and no nozzle exit conditions are reported, it is difficult to

18

analyze that data.

Hayashi and Branch (1980) measured the concentration profiles of particles in axisymmetric jets. The measurements were made by seeding 1%, 3%, and 5% by weight of 24 μm mean diameter spherical flash ash particles into jets at Mach numbers of 0.2, 0.8, and 1.0. The particle concentration profiles showed that particles concentrate on the axis of the jet at the exit of the nozzle and the profiles are highly influenced by the initial conditions. This observation is expected since the measurements were done in the developing region, which is highly affected by the nozzle exit conditions.

Zuev and Lepeshinskii (1981) studied the two-dimensional steady isobaric two-phase jets. They considered the effects of particle-particle interaction on the governing equations from an analogy with the kinetic theory of gases. They adopted the mixing length hypothesis to close the set of equations. Zuev and Lepeshinskii did not compare the predictions using their model with any experimental data to test their approach. Vasil'kov (1976) added terms that take into account the interaction of the phases to the governing equations of single-phase gas dynamics to predict a turbulent submerged jet containing an admixture of solid particles. He assumed that the radial velocities of the particles are equal to those of the gas and adopted the mixing length hypothesis to close the set of the governing equations. Vasil'kov obtained a reasonable agreement between the predictions using his phenomenological model and the data of Laats and Frishman (1970a and 1970b).

Popper et al. (1974) studied the motion of oil droplets of 50 μm, in a round air jet using LDV. It was found that at the jet axis, the droplet velocities are 5-9% lower than the corresponding velocities in a single-phase air jet. In the developed region the droplet velocities were higher than the air velocity at the same location.

The effects of spherical glass particles of 110 μm average diameter on the flow structure of an axially symmetrical turbulent air jet has been studied by Rajani (1972) for various solid/air loading ratios, from 0 to 1.3 kg/kg. Time-averaged velocity measurements were performed by laser Doppler anemometer (LDA) and the particle concentration measurements by a scattered light technique. Rajani devoted a large part of his work to the development of the experimental techniques, their accuracy, and limitations. Therefore, he reported very limited data, especially for the dispersed phase.

Yuu et al. (1978) examined the distribution of concentrations of the dust particles of the average diameter on a mass basis of 15 and 20 μm in a round jet. The flow was highly dilute, since solid volume fraction in the injected flow was in the range of $0.4 - 2 \times 10^{-6}$. The measurement of particle concentrations was performed with a photoelectric dust counter and the mean velocity was measured with a pitot-static probe. Using the concentration data, they indicated that the particle diffusivity decreases with the increase of the particle inertia and in general it is smaller than that of fluid scalar quantities. Goldschmidt and Eskinazi (1966) measured the concentration of the liquid droplets of the average diameter on a weight basis of 3.3 μm in a two-dimensional jet. They indicated that the droplets' mass tends not to diffuse more than the fluid momentum.

Girshovich et al. (1981) and Laats and Frishman (1973) investigated experimentally the effect of solid particles on both the mean and turbulence axial velocity components of an air jet using LDV techniques. They studied the effect of the circular tube diameter, initial velocities, initial particles/air mass loading ratio, and particle diameters on the jet performance. Laats and his coworkers found less rapid decay of centerline velocity and a reduced velocity spread of the jet with the increase of the

20

solid loading. They also found that the increase in the mean axial velocity and the decrease in the turbulence intensity at the centerline for the carrier phase depend on the loading ratio and the diameter of the particles. Unfortunately Laats and his coworkers did not measure the initial conditions at the nozzle exit and did not report the material density of the particles. This fact renders their data inadequate for the evaluation of turbulence models.

Levy and Lockwood (1981) measured fluid and solid phase mean and fluctuating velocities in a round gaseous jet using LDV techniques. They studied sand particles ranging in size from 215 to 1060 μm with sand to air mass ratios ranging from 1.14 to 3.5. Levy and Lockwood found that, relative to the pure gas phase, the axial turbulence intensity was reduced by introducing particles in the size range of 180-500 μm and was increased when the particles are in the range of 500-1200 μm. But again they did not report the nozzle exit conditions. Modarress et al. (1983) reported much needed experimental data to help understanding the behavior of two-phase turbulent jets and to validate the theoretical models for these flows (Fig. 1-1). They investigated the effects of 50 μm and 200 μm glass beads on the mean air velocity and found that the turbulent stresses for mass loading ratio varies from 0.32 to 0.85. Modarress et al. found that the increase in the centerline mean air velocity and the diminishing of the turbulence quantities are proportional to the loading ratio, the particle diameter, and the initial conditions of each phase.

Shearer et al. (1979) measured the mean velocity, velocity fluctuations, and Reynolds stress of single-phase constant density jets, as well as those of an evaporating spray (Freon-11). Since their measurements were in the region far downstream from the nozzle (170 $\leq$ z/D $\leq$ 510), the flow was highly dilute
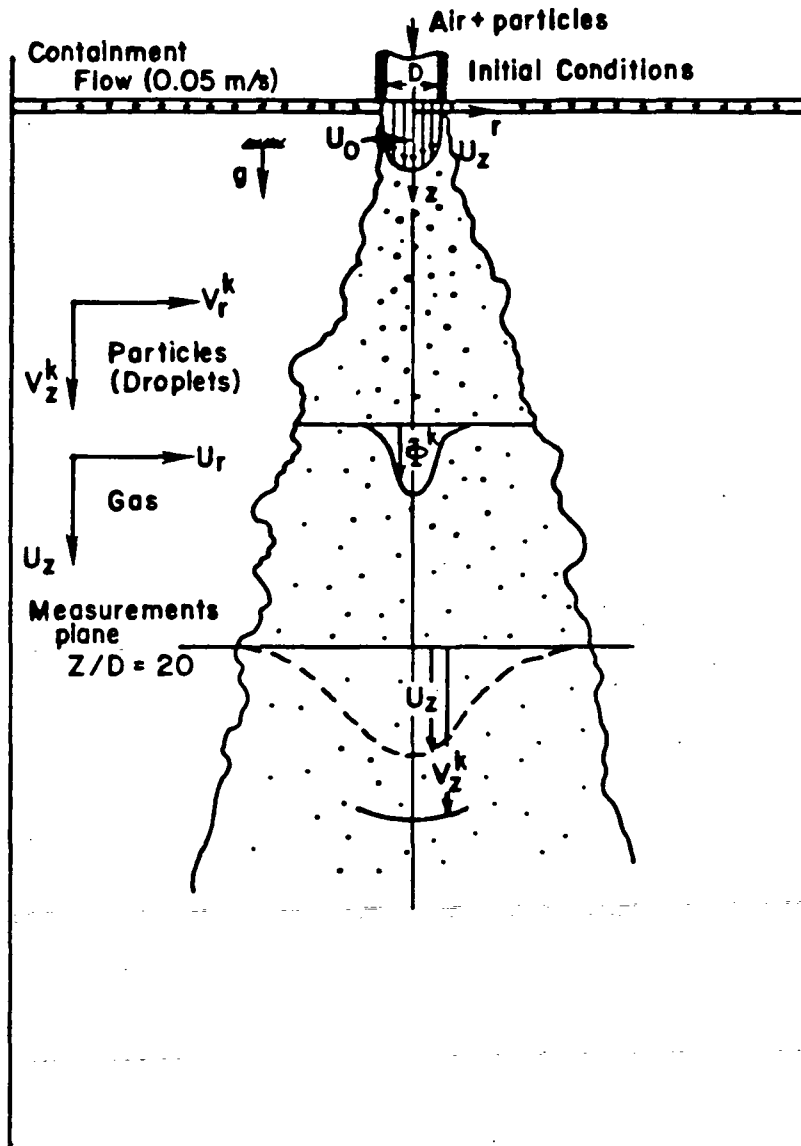
21

Figure 1-2 THE FLOW CONSIDERED (SOLID
          PARTICLES OR METHANOL LIQUID
          DROPLETS)

and the effects of the dispersed phase on the gas properties were very slight. Solomon et al. (1984) measured the flow properties of the carrier phase as well as those of the droplets in a turbulent round jet laden with Freon-11 spray. They considered the dilute portion of the spray ($50 \leq z/D \leq 510$) injected into a still air environment in order to provide data useful for the evaluation of spray models. They measured all the radial profiles of the main dependent variables at 50 nozzle diameters from the exit plane for two mass loading ratios of 7.71 and 15.78. This information is essential for accurately predicting such flow.

The last three experiments (Modarress et al., 1983; Shearer et al., 1979; and Solomon et al., 1984) are used in the this work to test the proposed turbulence model.

1.3 Summary of Approach

The present contribution focuses on developing and testing a two-equation turbulence model for predicting isothermal steady two-phase flows including the effects of phase changes. A set of equations describes the conservation of mass, momentum of each phase, vapor concentration, and kinetic energy of turbulence and its dissipation rate for the carrier fluid. Closure of the time-mean equations is achieved by modeling the existing turbulent correlations up to the third order. The model considers turbulent non-reacting axisymmetric jet flows laden with evaporating droplets or solid particles. This flow regime is a relatively simple flow that allows the study of the interactions between the droplets and the carrier phase, the turbulent dispersion of the droplets. The radial profiles of the main dependent variables are easy to measure in this type of flow, thus it is convenient for the turbulence model's validation.

23

In the following sections, the transport equations governing the mean quantities are presented first of all, followed by the development of the proposed two-equation model. Then the mass and momentum exchange coefficients are evaluated and an expression for the particle's Schmidt number is developed. The work concludes with an evaluation of the model using the recent measurements of Modarress et al. (1983), Solomon et al. (1984), and the measurements of Shearer et al. (1979).

2.0 GOVERNING EQUATIONS OF DILUTE SPRAY

The purpose of this section is to present the basic equations that govern the turbulent dilute vaporizing sprays, and to discuss the problems that their solution poses.

Section 2.1 states the assumptions for this study. Section 2.2 lists the time-dependent equations. The discussion then turns to time-averaged equations in section 2.3. Finally, the problem of closure is discussed in section 2.4.

2.1 Assumptions

It is assumed that no droplet coalescensce or breakup occurs. This implies that the droplets are sufficiently dispersed so that droplet collisions are infrequent. This assumption renders the present study restricted to dilute suspensions only. The initial breakup of liquid sprays or jets is not considered. It is assumed that the initial profiles of volume fractions and velocities are independently specified. Therefore, there is two-way coupling between the droplets and the carrier phase. It is assumed that the droplets of different sizes constitute different continuous phases. This is from the point of view of the "continuum" mechanics of a cloud of droplets, apart from the obvious definition of a multiphase system, a mixture of phases of liquid droplet and gas (Soo, 1967). Therefore, the continuous droplet-size distribution is divided into n intervals; d^k is the average diameter for droplets in the kth diameter range. If d^s and d^L are the smallest and largest droplet diameters, then the sizes are ordered as follows

$$d^s = d^n < d^{n-1} --- < d^1 = d^L \qquad\qquad 2.1$$

Thus, n different diameter ranges constitute correspondingly n dispersed

phases and the evaporated mass with the surrounding gas constitute the carrier

phase.

It was also assumed that the droplets are sufficiently small in order

that a volume element, small compared to the Kolmogoroff microlength scale,

contains such a large number of droplets that a statistical average concerning

the behavior of the droplets can be made within this volume element. It was

further assumed that the droplets remain spherical during their entire

lifetime. This assumption is discussed in detail in section 4.2. Also, it

was assumed that the mean flow is steady and the material properties of the

different phases are constant.

This leads to two sets of transport equations, one set for the droplets

and the other for the carrier phase, which is defined as the atomizing air

plus the evaporated material. These equations are coupled primarily by three

mechanisms, the mass exchange, the displacement of the carrier phase by the

volume occupied by droplets, and momentum interchange between droplets and the

carrier phase. The momentum interchange is due to the aerodynamic forces

exerted on the dispersed phase and the momentum growth resulting from the

relative velocity between the generated vapor and the surrounding gas.

2.2 Time Dependent Equations

As discussed in subsection 1.2.1 many authors derived continuity and

momentum equations for each phase by performing volume averaging (Sha and Soo,

1978; Hinze, 1972; and Jackson and Davidson, 1983) or averaging in space and

time (Panton, 1968; and Drew, 1971). Here the instantaneous, volume-averaged

equations, in Cartesian tensor notations, are presented based on those of

(Crowe, 1980; Hinze, 1972; Harlow and Amsden, 1975; and Jackson and Davidson,

1983).

The continuity equation for the carrier phase is

$$(\rho_1 \Phi_1)_{,t} + (\rho_1 \Phi_1 U_i)_{,i} = \sum_k \dot{m}^k \phi^k \qquad\qquad 2.2$$

The term on the right-hand side of Equation 2.2 represents the rate of change of the added mass or the source term due to the evaporation process from all droplets existing with the carrier phase in the same control volume. This term also represents a sink term in the continuity equation of the droplets (Equation 2.3).

The continuity equation for the kth dispersed phase is

$$(\rho_2 \phi^k)_{,t} + (\rho_2 \phi^k v_i^k)_{,i} = - \dot{m}^k \phi^k \qquad\qquad 2.3$$

The global continuity is

$$\Phi_1 + \sum_k \phi^k = 1 \qquad\qquad 2.4$$

The momentum equations for the carrier phase are

$$(\rho_1 \Phi_1 U_i)_{,t} + (\rho_1 \Phi_1 U_i U_j)_{,j} = - \Phi_1 P_{,i} - \sum_k (F^k \phi^k (U_i - v_i^k)$$

$$- \dot{m}^k \phi^k v_i^k) + \mu_1 (\Phi_1 (U_{i,j} + U_{j,i}))_{,j} \qquad\qquad 2.5$$

The momentum equations for the kth dispersed phase are

$$(\rho_2 \Phi^k v_i^k)_{,t} + (\rho_2 \Phi^k v_i^k v_j^k)_{,j} = -\Phi^k P_{,i} + F^k \Phi^k (U_i - v_i^k) - \dot{m}^k \Phi^k v_i^k$$

$$+ \mu_2 (\Phi^k (v_{i,j}^k + v_{j,i}^k))_{,j} + g_i \Phi^k (\rho_2 - \rho_1) \qquad\qquad 2.6$$

The set of equations (2.2 – 2.6) have $(4k + 5)$ unknowns ($3k$ of droplet velocities (v_i^k), k of droplet volume fractions (Φ^k), 3 carrier phase velocities (U_i), carrier phase volume fraction (Φ_1), and the static pressure (P)) and $(4k + 5)$ equations. So it forms a closed set of equations since the number of unknowns is equal to the number of equations.

Using the continuity equations for the different phases (Equations 2.2 and 2.3), Equations 2.5 and 2.6 as can be rewritten as

$$\rho_1 \Phi_1 U_{i,t} + \rho_1 \Phi_1 U_j U_{i,j} = -\Phi_1 P_{,i} - \sum_k \Phi^k (F^k + \dot{m}^k)(U_i - v_i^k)$$

$$+ \mu_1 (\Phi_1 (U_{i,j} + U_{j,i}))_{,j} \qquad\qquad 2.7$$

$$\rho_2 \Phi^k v_{i,t}^k + \rho_2 \Phi^k v_j^k v_{i,j}^k = -\Phi^k P_{,i} + F^k \Phi^k (U_i - v_i^k) + g_i \Phi^k (\rho_2 - \rho_1)$$

$$+ \mu_2 (\Phi^k (v_{i,j}^k + v_{j,i}^k))_{,j} \qquad\qquad 2.8$$

In the equations above and throughout this work the partial derivatives are represented by a subscript consisting of a comma and an index; e.g., $(\ )_{,t}$

$$\equiv \frac{\partial (\ )}{\partial t}, \quad U_{i,j} \equiv \frac{\partial U_i}{\partial x_j}, \quad U_{i,kj} \equiv \frac{\partial^2 U_i}{\partial x_k \partial x_j}$$

The subscripts 1 and 2 denote, respectively, the carrier fluid and dispersed

phase; the superscript k denotes the kth dispersed phase; U_i is the velocity

component of the carrier fluid; V_i^k is the velocity component of the droplets

in the kth diameter range; ρ and μ are the material density and viscosity; P

is the pressure; Φ is the volume fraction; g_i is the gravitational

acceleration in the i direction; F^k is the interphase friction coefficient,

and $\dot{m}^k$ is the evaporation rate per droplet volume.

Note that the factors Φ_1 and Φ^k lie outside the pressure gradients in

Equations 2.5 and 2.6, contrary to what some authors have proposed for

considering those factors within the gradients (Sha and Soo, 1978). Harlow

and Amsden (1975), Nigmatulin (1979), Solbrig and Hughes (1975) and Boure

(1979) argued that Φ_1 and Φ^k should be outside the pressure gradients as in

Equations 2.5 and 2.6.

The momentum growth term ($\dot{m}^k \Phi^k V_i^k$) in Equations 2.5 and 2.6 represents a

force on the fluid due to the difference between the velocity of vapor leaving

the droplet surface and that of the carrier fluid. If the flow from a droplet

is assumed to be uniform in all directions, then the average velocity of this

flow in any direction is zero. Therefore, the vapor leaves the droplet

surface with a velocity equal to that of the parent droplet (Nigmatulin, 1967;

Solbrig and Hughes, 1975; and Jackson and Davidson, 1983). In this case no

differences should be produced on the momentum equation of the droplets'

Equation 2.8 from those of solid particles (Crowe, 1980).

Solbrig and Hughes (1975) tested the relative importance of the transient

force terms in the momentum equation of solid particles under different flow

conditions. They reached the same conclusion of many other workers (Sha and

Soo, 1978; Soo, 1967; and Hjelmfelt and Mockros, 1966) that the Basset or the

transient term and the virtual mass term in the momentum equations of the

solid particles can be neglected if they are moving in a gaseous media. Therefore those terms are neglected in the present study.

The concentration equation

To avoid the problem of density fluctuations of the carrier phase at this stage, only isothermal flows are considered and vaporization is assumed to be due to the vapor concentration gradient only.

The concentration C is defined as the ratio of the evaporated mass within a control volume to the mass of the carrier phase in the same volume. The instantaneous, volume-averaged concentration equation for the evaporating material is

$$(\rho_1 \phi_1 C)_{,t} + (\rho_1 \phi_1 U_j C)_{,j} = (\rho_1 \delta \phi_1 C_{,j})_{,j} + \sum_k \phi^k \dot{m}^k \qquad 2.9$$

where δ is the molecular mass diffusivity of the evaporating material in air. The source term in Equation 2.9 ($\sum_k \phi^k \dot{m}^k$) represents the evaporated material from the droplets of different sizes.

2.3 Time-Averaged Equations

Introduction of time-averaged quantities. For steady mean flow, the time averaged or mean values of $\overline{U}_i, \overline{V}_i, \overline{P}$ and Φ are defined as the following:

$$\overline{U}_i = \lim_{T \to \infty} \frac{1}{T} \int_0^T U_i dt \quad , \quad \overline{V}_i = \lim_{T \to \infty} \frac{1}{T} \int_0^T V_i dt$$

$$\overline{P} = \lim_{T \to \infty} \frac{1}{T} \int_0^T P dt \quad \& \quad \overline{\Phi} = \lim_{T \to \infty} \frac{1}{T} \int_0^T \Phi dt \qquad 2.10$$

Following common practice, all the quantities are separated into to a fluctuating and a time average component as follows:

$$U_i = \bar{U}_i + u_i \quad , \quad V_i = \bar{V}_i + v_i$$

$$P = \bar{P} + p, \quad \Phi = \bar{\Phi} + \phi$$

$$\& \quad C = \bar{C} + c \qquad\qquad 2.11$$

For brevity, the overbars indicating averaged values will be dropped from all the quantities herein.

The mean continuity equation of the carrier phase. Introduction of Equation 2.11 into Equation 2.2, and subsequent time averaging yields:

$$\rho_1 (\Phi_i U_i)_{,i} + \rho_1 (\overline{\phi_1 u_i})_{,i} = \sum_k \dot{m}^k \phi^k \qquad 2.12$$

The mean continuity equation of the kth phase. Introduction of Equation 2.11 into Equation 2.3, and subsequent time averaging yields:

$$\rho_2 (\Phi^k V_i^k)_{,i} + \rho_2 (\overline{\phi^k v_i^k})_{,i} = - \dot{m}^k \phi^k \qquad 2.13$$

The mean global continuity.

$$\Phi_1 + \sum_k \Phi^k = 1 \qquad\qquad 2.14$$

The mean momentum equations for the carrier phase. Introduction of Equation 2.11 into Equation 2.5, and subsequent time averaging yields:

$$\rho_1(\Phi_1 U_i U_j)_{,j} = -\Phi_1 P_{,i} - \overline{\phi_1 P_{,i}} - \sum_k \phi^k F^k(U_i - V_i^k) + \sum_k \overline{\dot{m}^k \phi^k} V_i^k$$

$$- \sum_k F^k \overline{\phi^k(u_i - v_i^k)} + \sum_k \overline{\dot{m}^k \phi^k v_i^k} + \mu_1\left(\Phi_1(U_{i,j} + U_{j,i}) + \overline{\phi_1(u_{i,j} + u_{j,i})}\right)_{,j}$$

$$- \rho_1\left(\Phi_1 \overline{u_i u_j} + U_i \overline{\phi_1 u_j} + U_j \overline{\phi_1 u_i} + \overline{\phi_1 u_i u_j}\right)_{,j} \qquad\qquad 2.15$$

Multiply Equation 2.12 by U_j, then subtract from Equation 2.15 and rearrange, the result will be

$$\rho_1 \Phi_1 U_{i,j} U_j = -\Phi_1 P_{,i} - \overline{\phi_1 P_{,i}} - \sum_k \phi^k (F^k + \dot{m}^k)(U_i - V_i^k)$$

$$- \sum_k F^k \overline{\phi^k(u_i - v_i^k)} + \sum_k \overline{\dot{m}^k \phi^k v_i^k} + \mu_1\left(\Phi_1(U_{i,j} + U_{j,i})\right.$$

$$\left.+ \overline{\phi_1(u_{i,j} + u_{j,i})}\right)_{,j} - \rho_1\left(\Phi_1 \overline{u_i u_j} + U_i \overline{\phi_1 u_j}\right.$$

$$\left.+ U_j \overline{\phi_1 u_i} + \overline{\phi_1 u_i u_j}\right)_{,j} + \rho_1 U_i \overline{(\phi_1 u_j)_{,j}} \qquad\qquad 2.16$$

The mean momentum equations for the kth phase. Introduction of Equaiton 2.11 into Equation 2.6, and subsequent time averaging yields:

$$\rho_2(\phi^k V_i^k V_j^k)_{,j} = -\phi^k P_{,i} - \overline{\phi^k p_{,i}} + F^k \phi^k(U_i - V_i^k) - \overline{\dot{m}^k \phi^k} V_i^k$$

$$+ F^k \overline{\phi^k(u_i - v_i^k)} - \overline{\dot{m}^k \phi^k v_i^k} + \mu_2\left(\phi^k(V_{i,j}^k + V_{j,i}^k) + \overline{\phi^k(v_{i,j}^k + v_{j,i}^k)}\right)_{,j}$$

$$- \rho_2\left(\phi^k \overline{v_i^k v_j^k} + V_i^k \overline{\phi^k v_j^k} + V_j^k \overline{\phi^k v_i^k} + \overline{\phi^k v_i^k v_j^k}\right)_{,j} + g_i \phi^k(\rho_2 - \rho_1) \qquad 2.17$$

Multiply Equation 2.13 by V_j, then subtract from Equation 2.17 and rearrange, the result will be

$$\rho_2 \phi^k v_{i,j}^k V_j^k = -\phi^k P_{,i} - \overline{\phi^k P_{,i}} + F^k \phi^k (U_i - v_i^k)$$

$$+ F^k \overline{\phi^k (u_i - v_i^k)} - \dot{m}^k \overline{\phi^k v_i^k} + \mu_2 \{ \phi^k (v_{i,j}^k + v_{j,i}^k)$$

$$+ \overline{\phi^k (v_{i,j}^k + v_{j,i}^k)} \}_{,j} - \rho_2 \{ \phi^k \overline{v_i^k v_j^k} + v_i^k \overline{\phi^k v_j^k}$$

$$+ v_j^k \overline{\phi^k v_i^k} + \overline{\phi^k v_i^k v_j^k} \}_{,j} + g_i \phi^k (\rho_2 - \rho_1) + \rho_2 v_i^k \overline{(\phi^k v_j^k)}_{,j} \qquad 2.18$$

The mean concentration equations. Introduction of Equation 2.11 into Equation 2.9, and subsequent time averaging yields:

$$(\rho_1 \Phi_1 U_j C)_{,j} = \{ \rho_1 \delta (\Phi_1 C_{,j} + \overline{\phi_1 c_{,j}}) \}_{,j} + \sum_k \phi^k \dot{m}^k$$

$$- \rho_1 (\overline{\phi_1 c} U_j + C \overline{\phi_1 u_j} + \overline{\phi_1 u_j c} + \overline{\phi_1 u_j} C)_{,j} \qquad 2.19$$

Multiply Equation 2.12 by C, then subtract from Equation 2.19 and rearrange, the result will be

$$\rho_1 \Phi_1 U_j C_{,j} = \{ \rho_1 \delta (\Phi_1 C_{,j} + \overline{\phi_1 c_{,j}}) \}_{,j} + \sum_k \phi^k \dot{m}^k (1 - C)$$

$$- \rho_1 (\overline{\phi_1 c} U_j + C \overline{\phi_1 u_j} + \overline{\phi_1 u_j c} + \overline{\phi_1 u_j} C)_{,j} + \rho_1 C \overline{(\phi_1 u_j)}_{,j} \qquad 2.20$$

In Equations 2.12 to 2.20 the overbars indicate Reynolds averaged correlations.

2.4 The Problem of Closure

In order to close the system of equations, the turbulent correlations in Equations 2.12 - 2.20 must be modeled in terms of the time-averaged quantities and some turbulence quantities that are governed by the laws prescribed by a "turbulence model." Examination of the literature on the mathematical models of two-phase flows shows that most of the existing models are based on ad hoc modifications of the single-phase turbulence kinetic energy and length-scale equations. As a result, those models fail to predict the physical behavior of two-phase flows. The next section, 3, describes a two-equation turbulence model suitable for dilute vaporizing sprays.

3.0 A TWO-EQUATION TURBULENCE MODEL

3.1 Introduction

The objective of this section is to develop a general and economical turbulence model for free bounded dilute vaporizing sprays.

The first task is to select the type of model that is to be employed. Thus, in Section 3.2, the necessity to consider a model that employs transport equations for both the energy and the scale of turbulence will be pointed out. Starting with the instantaneous two-phase momentum equations for an isothermal flow, the transport equations for the turbulence kinetic energy and its dissipation rate for the carrier phase are obtained in Section 3.3. Closure of the proposed set of transport equations is achieved by modeling the turbulent correlations up to a third order in Section 3.4. The modeled equations in the Cartesian tensor notations are presented in Section 3.5. Finally, the modeled equations in the cylindrical coordinates are presented in Section 3.6.

3.2 Choice of Model Type

As discussed in Subsection 1.2.3, the previous attempts to model the dilute suspensions of two-phase flow to account adequately for major exchanges of momentum and mass between phases has not yet been established, even for dilute systems containing particles smaller than the Kolmogorov length scale. Few investigators have tried to consider the effects of the particulate phase on the turbulence structure (Nagarajan and Murgatroyd, 1971; and Genchev and Karpuzov, 1980) but they introduced many phenomenological approximations and coefficients that render their schemes are applicable to more general flow conditions and configurations. Melville and Bray (1979) and Michaelides (1984) have employed the mixing length hypothesis to handle the

gas solid two-phase flow in free jet and fully-developed pipe flows respectively. This approach is limited to flows where turbulence structure changes at a slow rate in the main flow direction. However, the empirical constants involved vary from one flow situation to another and are thus valid for restricted flow regions only. Danon et al. (1977) employed a one equation model (K equation) to consider the effects of particles on the turbulence quantities. The deficiencies of that model to obtain accurate predictions of two-phase turbulent jet flows necessitated that they multiply the production and the dissipation of K by coefficients that are dependent on particle size and concentration. The encouraging results obtained by Elghobashi and Abou-Arab (1983), Pourahmadi and Humphrey (1983), and Buckingham and Siekhaus (1981) suggest that higher levels of closure are required to predict shearing two-phase flow accurately. The model will be based on the two-equation (K-ε) model of turbulence for single-phase flows with universal constants (Launder et al., 1972).

3.3. The Exact Equations for K and ε

3.3.1 The Turbulence Kinetic Energy Equation (K)

The equation governing the mean kinetic energy $(K = 1/2 \; \overline{u_i u_i})$ of turbulence is obtained by substituting with the mean and fluctuating values instead of the local values in the instantaneous momentum equation of the carrier fluid (Equation 2.7), then multiplying by u_i, and finally time-averaging.

The resulting K equation reads:

$$\left(\Phi_1 U_\ell \overline{(u_i u_i}/2) \right)_{,\ell} = \left(- \Phi_1 U_{i,\ell} \overline{u_i u_\ell} - U_{i,\ell} \overline{\Phi_1 u_i u_\ell} \right)$$

$\qquad$ Convection $\qquad\qquad\qquad$ (I) Production

$$-\frac{1}{\rho_1}\left(-\overline{\Phi_1 P_{,i} u_i} + \overline{P_{,i}\phi_1 u_i} - \overline{\phi_1 u_i P_{,i}} + \rho_1\overline{\Phi_1 u_i u_\ell u_{i,\ell}} + \rho_1\overline{\phi_1 u_i u_\ell u_{i,\ell}}\right)$$

(II) Turbulent Diffusion

$$-\left(U_\ell\overline{u_i\phi_1 u_{i,\ell}} + U_\ell U_{i,\ell}\overline{\phi_1 u_i}\right)$$

(III) Production and Transfer

$$+\frac{1}{\rho_1}\sum_k\left(F^k + \dot{m}^k\right)\left(\overline{\phi^k u_i}(v_i^k - U_i) + \overline{\phi^k u_i(v_i^k - u_i)} + \overline{\phi^k u_i(v_i^k - u_i)}\right)$$

(IV) Extra Dissipation (ε_p)

$$+\left(\nu_1\overline{u_i((u_{i,\ell} + u_{\ell,i})\Phi_1)}\right)_{,\ell} + \left(\nu_1\overline{u_i(\phi_1(U_{i,\ell} + U_{\ell,i}))}\right)_{,\ell} + \nu_1\overline{u_i(\phi_1(u_{i,\ell} + u_{\ell,i}))}_{,\ell}$$

(V) Viscous Diffusion   (VI) Extra Viscous Diffusion
     and Dissipation   and Dissipation

3.1

3.3.2 The Turbulence Energy Dissipation Rate Equation (ε)

The exact equation for the dissipation rate per unit volume

$\left(\varepsilon = \nu_1\overline{(u_{i,j} u_{i,j})}\right)$ is derived by differentiating the instantaneous equation

(2.7) with respect to x_i, then multiplying throughout by $\nu_1 u_{i,j}$, and finally

time averaging. The exact equation of ε thus obtained is

$$\left(\Phi_1 U_\ell \varepsilon_{,\ell}\right) = \left(-2\nu_1\overline{u_{i,j} u_{i,\ell}}(\Phi_1 U_\ell)_{,j} - 2\nu_1\overline{u_{i,j} u_{\ell,j}\Phi_1}U_{i,\ell} - 2\nu_1\overline{(\Phi_1 u_\ell)_{,j} u_{i,j}}U_{i,\ell}\right.$$

Convection   (I) Production by the Mean Motion

$$-2\nu_1\overline{u_{i,j} u_{i,\ell}(\Phi_1 U_\ell)_{,j}} - 2\nu_1\overline{\phi_1 u_\ell u_{i,j}}U_{i,\ell j} - 2\nu_1\overline{u_{i,j} u_\ell(\Phi_1 U_{i,\ell})_{,j}}$$

$$+\left(-2\nu_1\overline{u_{i,j} u_{i,\ell}(u_\ell\Phi_1)_{,j}} - 2\nu_1\overline{u_{i,j} u_{i,\ell}(u_\ell\phi_1)_{,j}}\right)$$

(II) Production by Self-Stretching of
          Vortex Tubes

$$+ \ [-2\nu_1 \overline{\phi_1 u_{i,j} u_{i,\ell j} u_\ell} \ - \ 2\nu_1 \overline{\phi_1 u_{i,j} u_{i,\ell j} u_\ell}]$$

(III) Turbulent Diffusion

$$+ \ [-2\nu_1 \overline{\phi_1 u_{i,j}} (U_\ell U_{i,\ell})_{,j} \ - \ 2\nu_1 \overline{u_{i,j} \phi_{1,j}} U_\ell U_{i,\ell} \ - \ 2\nu_1 U_\ell \overline{\phi_1 u_{i,j} u_{i,\ell j}}]$$

(IV) Production and Transfer

$$+ \ \frac{1}{\rho_1} \ [-2\nu_1 \overline{u_{i,j} (P_{,i} \phi_1)}_{,j} \ - \ 2\nu_1 \overline{u_{i,j} (\phi_1 P_{,i})}_{,j} \ - \ 2\nu_1 \overline{u_{i,j} (\phi_1 P_{,i})}_{,j}]$$

(V) Spatial Transport by Pressure (fluctuation and mean)

$$+ \ \frac{-2\nu_1}{\rho_1} \ \sum_k (F^k + \dot{m}^k) \ [\overline{u_{i,j} [\phi^k (U_i - v_i^k)]}_{,j} + \overline{u_{i,j} [(u_i - v_i^k)\phi^k]}_{,j} + \overline{u_{i,j} [\phi^k (u_i - v_i^k)]}_{,j}]$$

(VI) Extra Dissipation

$$+ \ 2\nu_1 \nu_1 \overline{u_{i,j} [(u_{i,\ell} + u_{\ell,i})\phi_1]}_{,j\ell}$$

(VII) Viscous Diffusion and Destruction

$$+ \ [2\nu_1 \nu_1 \overline{u_{i,j} [\phi_1 (U_{i,\ell} + U_{\ell,i})]}_{,j\ell} + 2\nu_1 \nu_1 \overline{u_{i,j} (\phi_1 (u_{i,\ell} + u_{\ell,i}))}_{,j\ell}] \qquad 3.2$$

(VIII) Extra Viscous Diffusion and Destruction

The terms in the K and ϵ equations, (3.1) and (3.2), are classified into groups enclosed by large curved brackets; each group is labeled according to its particular contribution to the conservation of the transported quantity. The turbulent correlations in Equations 3.1 and 3.2 that include the fluctuation of the volume fraction, ϕ, or ϕ^k, or their gradients are due to the presence of the particles in the same control volume with the carrier

38

phase; setting these correlations to zero, ϕ_1 to unity and ϕ^k to zero will reduce Equations 3.1 and 3.2 to their familiar counterpart for single-phase flows.

3.4 Closure of the Proposed Set of Transport Equations

The proposed model is restricted to high Reynolds number flows of dilute vaporizing sprays. Therefore, the viscous diffusion in all the governing equations is neglected due to its relatively small magnitude as compared with the turbulent diffusion. Due to the diluteness assumption of the suspension all fourth-order correlations containing the volume fraction fluctuations such as $\overline{\phi_1 u_i u_\ell u_{i,\ell}}$ $\overline{u_{i,j} u_{i,\ell} (u_\ell \phi_1)_{,j}}$ and $\overline{\phi_1 u_{i,j} u_{i,\ell j} u_\ell}$ are neglected due to their relatively small values. The continuity equation of single-phase flow is used in the modeling approximations of some of the turbulent correlations.

3.4.1 Closure of the Continuity Equation of the Carrier Phase

The second term on the LHS of Equation 2.12 represents a mass flux contribution to the turbulent diffusion of the carrier phase. Following Hinze (1972), Melville and Bray (1979) and Elghobashi and Abou-Arab (1983), a gradient-type diffusion is assumed for this correlation given by:

$$\overline{\phi_1 u_i} = - \varepsilon_f \phi_{1,i} \qquad\qquad 3.3$$

where ε_f is the mass eddy diffusivity of the turbulent flow of the carrier phase. This quantity can be related to the momentum eddy diffusivity (ν_t) as the following:

$$\frac{\varepsilon_f}{\nu_t} = \frac{1}{\sigma_c} \qquad\qquad 3.4$$

where σ_c is the effective Schmidt number for the carrier phase. It may be expected to be constant of value 0.7 in line with the average levels of effective Schmidt number reported for a number of free shear flows (Launder, 1976; and Spalding, 1971).

The momentum eddy diffusivity of the carrier phase is related to fluid kinetic energy (K) and the rate of dissipation (ϵ) of K by:

$$\nu_t = c_\mu K^2/\epsilon \qquad\qquad 3.5$$

The value of c_μ in general is 0.09 but it can be a function of suitable flow parameters to extend the range of applicability of the K-ϵ model. For example, in axisymmetric jet flows which are considered in this work, those parameters are the deceleration of the velocity at the axis of the jet (Equation 3.36) and the jet width (Equation 3.37).

Corrsin (1974) discussed the limitations of the simple gradient hypothesis for modeling turbulent diffusion in turbulence. He pointed out that this model may lead to inexact results if the size of the energy-containing eddies is much smaller than the distance over which the gradient of the considered quantity varies appreciably.

Lumley (1975) tried to overcome this problem by proposing a model for the turbulent flux of passive scalar in inhomogenous flows. But since Lumley's model is not well tested yet, the simple gradient hypothesis will be used in the present work due to its fruitful results in many types of flows (Lunder et al., 1972).

3.4.2 Closure of the Continuity Equation of the kth Phase

Similar to Equation 3.3 the correlation $\overline{\phi^k v_i^k}$ on the LHS of Equation 2.13

is modeled as

$$\overline{\phi^k v_i^k} = -\varepsilon_h^k \phi_{,i}^k \qquad\qquad 3.6$$

ε_h^k is the mass eddy diffusivity of the turbulent flow of the droplets. An expression to obtain this quantity in terms of its counterpart for the carrier phase and the droplets' Schmidt number σ_p^k is developed in section 5. The droplets' Schmidt number is defined as

$$\sigma_p^k = \varepsilon_h^k / \varepsilon_f \qquad\qquad 3.7$$

3.4.3 Closure of the Momentum Equations of the Carrier Phase

Here, the modeling of the turbulent correlations needed to close the momentum equations (2.16) are presented. The correlations of two scalars containing the volume fraction in the momentum and concentration equations such as $\overline{\phi_1 c}$, $\overline{\phi_1 p}$ or $\overline{\phi_1 c u_j}$ are neglected. This approximation is based on the following: 1) the lack of understanding of the nature of those correlations, thus the modeling which is supported by the experimental data (Lumley, 1978b) is not available, and 2) their relatively small values compared to the turbulent diffusion terms (Buckingham and Siekhaus, 1981; and Launder, 1976).

The correlation $\overline{u_i u_j}$ in Equation 2.16 represents the transfer of momentum by the turbulent motion. The oldest proposal for modeling this correlation is that of Boussinesq (cited by Launder, 1976):

$$\overline{u_i u_j} = -\nu_t (U_{i,j} + U_{j,i}) + \frac{2}{3} \delta_{ij} K \qquad\qquad 3.8$$

The term involving the Kronecker delta, δ_{ij}, is necessary to make the

expression applicable also to normal stresses (when i = j). The expression (3.8) has been severely criticized by some workers, and it should not be used without caution. The use of that expression is justified on the basis of an approximate local equilibrium. If the addition of the droplets causes the turbulence of the carrier phase to adjust more slowly to the mean velocity field, or if it introduced additional mechanisms for generation of turbulent energy, the expression (3.8) will be a poor approximation. Melville and Bray (1979) argued that neither of these effects will happen if the mass loading ratio is less than unity. The other approach is to solve a transport equation for $\overline{u_i u_j}$, which in turn contains higher order correlations that require modeling. To be consistent with the present level of closure the present study will use (Equation 3.8).

The correlation $\overline{\phi_1 u_i u_j}$ will be modeled by adapting Launder's proposal (1976) that gives

$$\overline{\phi_1 u_i u_j} = - c \ (K/\varepsilon) \ [\overline{u_i u_\ell (u_j \phi_1)_{,\ell}} + \overline{u_j u_\ell (u_i \phi_1)_{,\ell}}] \qquad 3.9$$

where c is a constant of value 0.1.

The correlation $\phi^k (u_i - v_j^k)$, which appears in the momentum equations of both the carrier phase and the droplets, can be written as

$$\overline{\phi^k (u_i - v_i^k)} = \overline{\phi^k u_i} - \overline{\phi^k v_i^k} \qquad 3.10$$

The second term on the RHS of Equation 3.10 was discussed previously. The first term is modeled as

$$\overline{\phi^k u_i} = - \varepsilon_f \phi^k_{,i} \qquad 3.11$$

42

The last correlation to be modeled in the momentum equations of the carrier phase is $\overline{_1 u_{i,j}}$, which appears multiplied by $_1$, and will therefore be neglected due to its relatively small value.

3.4.4 Closure of the Momentum Equations of the kth Phase

Similar to the carrier phase treatment the correlations $\overline{\phi^k p_{,i}}$ and $\overline{\phi^k(v^k_{i,j} + v^k_{j,i})}$ in Equation 2.18 are neglected. The two correlations $\overline{\phi^k v^k_i}$ and $\overline{\phi^k(u_i - v^k_i)}$ have already been discussed. The only two correlations still to be modeled are those of the forms $\overline{v^k_i v^k_j}$ and $\overline{\phi^k v^k_i v^k_j}$. Similar to the carrier phase, the correlation $\overline{v^k_i v^k_j}$ is modeled as

$$\overline{v^k_i v^k_j} = - v^k_p(v^k_{i,j} + v^k_{j,i}) + \frac{2}{3} \delta_{ij} K^k_p \qquad 3.12$$

where $\qquad K^k_p = \frac{1}{2} \overline{v^k_i v^k_i} \qquad 3.13$

The momentum eddy diffusivity of the droplets in the size range k (v^k_p) is related to its counterpart for the mass as the following:

$$\epsilon^k_h / v^k_p = 1/\sigma_v \qquad 3.14$$

where σ_v is a coefficient of value 0.7 as given by Melville and Bray (1979). Again, ϵ^k_h is determined in section 5. The correlation $\overline{\phi^k v^k_i v^k_j}$ is modeled similar to Equation 3.9 as

$$\overline{\phi^k v^k_i v^k_j} = c_\phi(K/\epsilon) \; (\overline{v^k_i v^k_\ell} \overline{(v^k_j \phi^k)}_{,\ell} + \overline{v^k_j v^k_\ell} \overline{(v^k_i \phi^k)}_{,\ell}) \qquad 3.15$$

3.4.5 Closure of the Vapor Concentration Equation

As discussed previously the correlations $\overline{\phi_1 c_{,j}}$, $\overline{\phi_1 c}$ and $\overline{\phi_1 c u_j}$ in Equation 2.20 are neglected compared with $\overline{c u_j}$ or $\overline{\phi_1 u_j}$. An investigation of the behavior of $\overline{c u_j}$ suggests that it can be modeled similar to Equation 3.3 as

$$\overline{c u_j} = - \varepsilon_f C_{,j} \qquad\qquad 3.16$$

3.4.6 Closure of the Turbulence Kinetic Energy Equation

The exact equation of the turbulence kinetic energy K for the carrier fluid is given by Equation 3.1. The terms are grouped according to their physical contribution to the conservation of K. The modeling of the turbulent correlations appearing in the K equation (14 correlations) are presented in this section. $\overline{\phi_1 u_i u_\ell u_{i,\ell}}$ is neglected since it is a fourth order correlation. The correlations $\overline{u_i u_\ell}$, $\overline{\phi_1 u_i}$, $\overline{\phi_1 u_i u_\ell}$ and $\overline{\phi^k u_i}$ in Equation 3.1 were discussed in subsection 3.4.2.

The pressure diffusion terms ($\overline{u_i p_{,i}}$ and $\overline{\phi_1 p_{,i} \phi_1}$) in Equation 3.1 are neglected, following the Imperial College group and the recommendations of Hinze (1975), and because very little is known about it (Launder, 1976).

The turbulent diffusion correlation $\overline{u_i u_\ell u_{i,\ell}}$ can be written as

$$[u_\ell (1/2\ u_i^2)]_{,\ell} \qquad\qquad 3.17$$

which modeled as

$$[(\nu_t / \sigma_k) K_{,\ell}]_{,\ell} \qquad\qquad 3.18$$

where σ_k is an empirical diffusion constant of order one.

The correlation $\overline{\phi_1 u_i u_{i,\ell}}$ can be written as $[\overline{\phi_1 (1/2u_i^2}]_{,\ell}$, which can be neglected due to its relatively small value compared with $[\overline{u_\ell (1/2u_i^2)}]_{,\ell}$.

Following Elghobashi and Abou-Arab (1983), the correlation $\overline{u_i (v_i^k - u_i)}$ is modeled as

$$\overline{u_i (v_i^k - u_i)} = - K \left\{ 1 - \int_o^\infty ((\Omega_1 - \Omega_R)/\Omega_2) \ E(\omega) \ d\omega \right\} \qquad 3.19$$

where ω is the harmonic frequency of turbulence and $E(\omega)$ is the Lagrangian energy spectrum function of the carrier phase. Ω_1, Ω_2, and Ω_R are functions of the carrier and dispersed phases properties, the droplet diameter, and the harmonic frequency. They are discussed in detail in subsection 4.1.

The correlation $\overline{\phi^k u_i (v_i^k - u_i)}$ is modeled as

$$\overline{\phi^k u_i (v_i^k - u_i)} = - c_\phi (\frac{K}{\epsilon}) \overline{(v_i^k - u_i) u_i} \ \left\{ \overline{(u_\ell \phi^k)}_{,\ell} + \overline{((v_\ell^k - u_\ell) \phi^k)}_{,\ell} \right\}$$

$$= - c_\phi (\frac{K}{\epsilon}) \overline{(v_i^k - u_i) u_i} \ \overline{(v_\ell^k \phi^k)}_{,\ell} \qquad 3.20$$

The extra viscous diffusion and dissipation, two terms in group VI in Equation 3.1, are neglected due to their relatively small magnitudes as compared with the other similar terms (see Daly and Harlow, 1981, and Launder et al., 1976; Launder et al. 1975).

Neglecting the viscous diffusion, the last correlation to be modeled in the K equation, $\overline{\mu_1 u_i ((u_{i,\ell} + \mu_{\ell,i}) \phi_1)}_{,\ell}$ represents the dissipation rate of K. When the local Reynolds number of turbulence is large the dissipative motions can be assumed to be isotropic, therefore

$$\overline{v u_i ((u_{i,\ell} + u_{\ell,i}) \phi_1)}_{,\ell} \ \tilde{\sim} - \phi_1 \epsilon \qquad 3.21$$

45

3.4.7 Closure of the Turbulence Energy Dissipation Rate Equation

The exact equation of the dissipation rate of turbulence energy, ε, for the carrier fluid is given by Equation 3.2. The terms are also grouped similar to the K equation.

Tennekes and Lumley (1972) have shown, based on an order-of-magnitude analysis, that the terms involving mean strain rates in Equation 3.2, groups (I) and (IV), are negligible at high turbulent Reynolds number compared with the production by self-stretching of vortex tubes. Therefore, groups (I) and (IV) are neglected in this study.

The correlation $2\nu_1\phi_1\overline{u_{i,j}u_{i,\ell j}u_\ell}$, which accounts for the diffusion of ε by velocity fluctuations, is handled as the following:

$$2\nu_1\overline{u_{i,j}u_{i,\ell j}u_\ell} = (\nu_1\overline{u_{i,j}u_{i,j}u_\ell})_{,\ell}$$

$$= (\overline{\varepsilon\, u_\ell})_{,\ell}$$

$$= -\left[(\nu_t/\sigma_\varepsilon)\varepsilon_{,\ell}\right]_{,\ell} \qquad\qquad 3.22$$

Group (V) represents the diffusional transport of ε by pressure fluctuations. Also, it contains a term that represents a transfer due to the mean pressure gradient, $2\overline{u_{i,j}(\phi_1 P_{,i})}_{,j}$. Following Rodi (1971), the present study neglects the pressure diffusion terms (group V).

The viscous diffusion terms, part of group (VII) and group (VIII), are neglected due to their relatively small values compared with the turbulent diffusion.

The first term in group (II) expresses the generation rate of vorticity

fluctuations through the self-stretching action of turbulence. Rodi (1971), and Hanjalic and Launder (1972) have argued that this term should be considered in conjunction with group (VII), representing the decay of the dissipation rate ultimately through the action of viscosity. At a high turbulent Reynolds number, these two terms are of opposite sign, however, and their difference necessarily remains finite. Following Rodi (1971), the terms are collectively approximated as follows:

$$- 2\nu_1 \overline{u_{i,j} u_{i,\ell} (u_\ell \phi_1)}_{,j} - 2\nu_1^2 \overline{u_{i,j} (u_{i,\ell} + u_{\ell,i}) \phi_1)}_{,j\ell}$$

$$= (c_{\varepsilon1} P_k / \varepsilon - c_{\varepsilon2} \phi_1) \frac{\varepsilon^2}{K} \qquad\qquad 3.23$$

where P_k is the total production of K [group (I) and (III) in Equation 3.1], and $c_{\varepsilon1}$ and $c_{\varepsilon2}$ are constants of value 1.43 and 1.92 respectively.

The last correlations to be modeled in ε equation are those of group (VI), which represent the extra dissipation due to the relative velocity between the phases. They are modeled collectively as one term which is given by

$$- c_{\varepsilon3} \varepsilon_p \ \varepsilon/K$$

where ε_p (term IV in Equation 3.1) is the extra dissipation of K. The constant $c_{\varepsilon3}$ was optimized by Elghobashi et al. (1983) for a two-phase jet flow. The value of this constant is 1.2.

3.5 Modeled Transport Equations in the Cartesian Tensor Notations

Using the modeling approximations discussed in subsection 3.4, the

transport equations in the modeled form are obtained. Those equations are given in Appendix B.

3.6 Modeled Transport Equations in the Cylindrical Coordinates

The flows considered in this work are

a) axisymmetric (without swirl),

$$V_\theta^k = U_\theta = 0, \quad \frac{\partial}{\partial\theta} \text{ (time-averaged quantites)} = 0, \qquad 3.24$$

b) of the boundary-layer type,

$$V_z^k > V_r^k, \ U_z > U_r \ , \ \frac{\partial}{\partial r} \gg \frac{\partial}{\partial z} \ . \qquad 3.25$$

The present study adopts the notations commonly used for the boundary layer flows: z, r, θ for the coordinates; U_z, V_r, V_θ for the velocity components of the carrier phase; V_z^k, V_r^k, V_θ^k for the velocity components of the droplets of class k.

Using expressions 3.24 and 3.25, the modeled transport equations for the mean and turbulent quantities presented in Appendix B can be expressed in cylindrical polar form. This can be done in a straightforward manner by the methods of tensor calculus as exposed in Synge and Schild (1978), for instance.

The mean continutiy equation of the carrier phase is

$$\rho_1(\Phi_1 U_z)_{,z} + \frac{\rho_1}{r}(r\Phi_1 U_r)_{,r} - \rho_1(\frac{\nu_t}{\sigma_c}\Phi_{1,z})_{,z} - \frac{\rho_1}{r}(r\frac{\nu_t}{\sigma_c}\Phi_{1,r})_{,r}$$

$$= \sum_k \dot{m}^k \Phi^k \qquad 3.26$$

The mean continuity equation of the kth group is

$$\rho_2(\phi^k v_z^k)_{,z} + \frac{\rho_2}{r}(r\phi^k v_r^k)_{,r} - \rho_2(\frac{v_p^k}{\sigma_c}\phi^k_{,z})_{,z} - \frac{\rho_2}{r}(r\frac{v_p^k}{\sigma_c}\phi^k_{,r})_{,r} = -\dot{m}^k\phi^k .$$

3.27

The mean global continuity is

$$\Phi_1 + \sum_k \phi^k = 1$$

3.28

The mean momentum equation for the carrier phase in the axial (z) direction

$$\rho_1\Phi_1 U_z U_{z,z} + \rho_1\Phi_1 U_r U_{z,r} = -\Phi_1 P_{,z} - \sum_k \phi^k(F^k+\dot{m}^k)(U_z-V_z^k)$$

$$+ \frac{1}{r}(\Phi_1\rho_1 r v_t U_{z,r})_{,r} + \rho_1 U_{z,r}(\frac{v_t}{\sigma_c}\Phi_{1,r}) + c_\phi\rho_1 \frac{1}{r}(\frac{K}{\epsilon} r v_t U_{z,r}(\frac{v_t}{\sigma_c}\Phi_{1,r})_{,r})_{,r}$$

3.29

The mean momentum equation for the carrier phase in the radial (r) direction is

$$\rho_1\Phi_1 U_z U_{r,z} + \rho_1\Phi_1 U_r U_{r,r} = -\Phi_1 P_{,r} - \sum_k \phi^k(F^k+\dot{m}^k)(U_r-V_r^k)$$

$$- \sum_k \dot{m}^k \frac{\sigma_p^k}{\sigma_c}P\phi^k_{,r} - \sum_k F^k \frac{v_t}{\sigma_c}(1-\sigma_p^k)\phi^k_{,r}$$

$$+ \rho_1 \frac{v_t}{\sigma_c}\Phi_{1,r}U_{r,r} + \frac{\rho_1}{r}(\frac{v_t}{\sigma_c}rU_r\Phi_{1,r})_{,r} - \frac{2}{3}\frac{\rho_1}{r}(rK\Phi_1)_{,r}$$

49

$$+ c_\phi \frac{\rho_1}{r} (\frac{4}{3} \frac{K^2}{\epsilon} r (\frac{\nu_t}{\sigma_c} \Phi_{1,r}),_r),_r \qquad \qquad 3.30$$

The mean momentum equation for the kth phase in the axial (z) directon is

$$\rho_2 \Phi^k V_z^k V_{z,z}^k + \rho_2 \Phi^k V_r^k V_{z,r}^k = - \Phi^k P,_z + F^k \Phi^k (U_z - V_z^k)$$

$$+ \frac{1}{r}(\Phi^k r \rho_2 \sigma_v \nu_p^k V_{z,r}^k),_r + \rho_2 V_{z,r}^k (\nu_p^k \Phi^k,_r) + c_\phi \rho_2 \frac{1}{r} (\frac{K}{\epsilon} r \nu_p^k V_{z,r}^k (\nu_p^k \Phi^k,_r),_r),_r$$

$$+ (\rho_2 - \rho_1) g \Phi^k \qquad \qquad 3.31$$

The mean momentum equation for the kth phase in the radial (r) direction is

$$\rho_2 \Phi^k V_z^k V_{r,z}^k + \rho_2 \Phi^k V_r^k V_{r,r}^k = - \Phi^k P,_r + F^k \Phi^k (U_r - V_r^k)$$

$$+ \dot{m}^k \frac{\sigma_p^k}{\sigma_c} \Phi^k,_r + F^k \frac{\nu_t}{\sigma_c} (1 - \sigma_p^k) \Phi^k,_r$$

$$+ \rho_2 \frac{\nu_p^k}{\sigma_c} \Phi^k,_r V_{r,r}^k + \frac{\rho_2}{r} (\frac{\nu_p^k}{\sigma_c} r V_r^k \Phi^k,_r),_r - \frac{2}{3} \frac{\rho_2}{r} (r K_p^k \Phi^k),_r$$

$$+ c_\phi \frac{\rho_2}{r} (\frac{4}{3} r \frac{K}{\epsilon} K_p^k (\frac{\nu_t}{\sigma_c} \Phi_{1,r}),_r),_r \qquad \qquad 3.32$$

The mean concentration equation is

$$\rho_1 \Phi_1 U_z C,_z + \rho_1 \Phi_1 U_r C,_r = \frac{1}{r} (\rho_1 r \Phi_1 \frac{\nu_t}{\sigma_c} C,_r),_r$$

$$+ \sum_k \Phi^k \dot{m}^k (1-C) + \rho_1 C,_r (\frac{\nu_t}{\sigma_c} \Phi_{1,r}). \qquad \qquad 3.33$$

50

The turbulence kinetic energy equation (K) is

$$\rho_1\Phi_1 U_z K_{,z} + \rho_1\Phi_1 U_r K_{,r} = \rho_1\Phi_1 \nu_t U_{z,r} U_{z,r} - \frac{4}{3}\rho_1 c_\phi\left(\frac{\nu_t}{c_\mu}\right)\left(\frac{\nu_t}{\sigma_c}\Phi_{1,r}\right)_{,r} U_{r,r}$$

$$+ \rho_1 c_\phi\left(\frac{K}{\epsilon}\right)\nu_t\left(\frac{\nu_t}{\sigma_c}\Phi_{1,r}\right)_{,r} U_{z,r} U_{z,r} - \sum_k K\Phi^k(F^k+\dot{m}^k)(1-\int_o^\infty(-\frac{\Omega_1-\Omega_R}{\Omega_2})E(\omega)d\omega)$$

$$+ \sum_k (F^k+\dot{m}^k)[(U_r-V_r^k)(\nu_P^k\Phi^k_{,r}) - c_\phi\left(\frac{\nu_t}{c_\mu}\right)(\nu_P^k\Phi^k_{,r})_{,r}(1- \int_o^\infty(-\frac{\Omega_1-\Omega_R}{\Omega_2})E(\omega)d\omega)]$$

$$+ \frac{1}{r}\left(\rho_1\Phi_1\frac{\nu_t}{\sigma_k}rK_{,r}\right)_{,r} - \rho_1\Phi_1\epsilon , \qquad\qquad 3.34$$

The turbulence energy dissipation rate equation (ϵ) is

$$\rho_1\Phi_1 U_z \epsilon_{,z} + \rho_1\Phi_1 U_r \epsilon_{,r} = c_{\epsilon1}\frac{\epsilon}{K}\rho_1\Phi_1\ [\nu_t U_{z,r}U_{z,r} - \frac{4}{3}\frac{c_\phi}{\Phi_1}\left(\frac{\nu_t}{c_\mu}\right)\left(\frac{\nu_t}{\sigma_c}\Phi_{1,r}\right)_{,r} U_{r,r}$$

$$+ \frac{c_\phi}{\Phi_1}\left(\frac{K}{\epsilon}\right)\nu_t\left(\frac{\nu_t}{\sigma_c}\Phi_{1,r}\right)_{,r} U_{z,r}U_{z,r}] - c_{\epsilon3}\frac{\epsilon}{K}[\sum_k (F^k+\dot{m}^k)(\Phi^k K(1- \int_o^\infty(-\frac{\Omega_1-\Omega_R}{\Omega_2})E(\omega)d\omega)$$

$$- (U_r - V_r^k)(\nu_P^k\Phi^k_{,r}) + c_\phi\left(\frac{\nu_t}{c_\mu}\right)(\nu_P^k\Phi^k_{,r})_{,r}(1- \int_o^\infty(-\frac{\Omega_1-\Omega_R}{\Omega_2})E(\omega)d\omega)]$$

$$+ \frac{1}{r}\left(\rho_1 r\Phi_1\frac{\nu_t}{\sigma_\epsilon}\epsilon_{,r}\right)_{,r} - c_{\epsilon2}\rho_1\Phi_1\frac{\epsilon^2}{K} . \qquad\qquad 3.35$$

The constants of the turbulence model

The constants in Equations 3.26 to 3.35 are two sets: one is identical to

that of the single-phase K-ε model and the other belongs to the two-phase

model. The former is well established and it was not changed here. The

latter is new ($c_{\epsilon 3}$, σ_c) and has been obtained from one set of data (Elghobashi

et al., 1984). The coefficients of the single-phase model and the optimized

values of the new coefficients are given in Table 3.1.

Table 3.1 Coefficients of the Turbulence Model

σ_c	σ_k	c_μ	σ_ϵ	c_ϕ	$c_{\epsilon 1}$	$c_{\epsilon 2}$	$c_{\epsilon 3}$	σ_v
0.7	1	Eq.(3.36)	1.3	0.1	1.44	Eq.(3.38)	1.2	0.7

$$c_\mu = 0.09 - 0.04f_1 ; \qquad\qquad 3.36$$

$$f_1 = \left| 0.5R \; \frac{\frac{dU_{z,c}}{dz} - \left| \frac{dU_{z,c}}{dz} \right|}{U_{z,c} - U_{z,\infty}} \right|^{0.2} . \qquad 3.37$$

$U_{z,c}$ and $U_{z,\infty}$ are the axial velocities of the fluid at the jet centerline and

the ambient stream respectively, R is the local jet width (Launder et al.,

1972).

The constant $c_{\epsilon 2}$ in Table 3.1 is given by

$$c_{\epsilon 2} = 1.92 - 0.0067 \; f \qquad\qquad 3.38$$

The quantities Ω_1, Ω_2, Ω_R and $E(\omega)$, which are involved in the integration

terms in Equations 3.34 and 3.35 will be discussed in subsection 4.1. The

evaporated mass per unit time and unit droplet volume ($\dot{m}^k$) is calculated in

4.3. The interphase friction coefficient (F^k) is evaluated in subsection 4.4. The last quantity in Equations 3.26 to 3.35 that should be calculated is the momentum eddy diffusivity of the droplets (ν_p^k). This quantity is calculated in section 5.

4.0 SINGLE PARTICLE BEHAVIOR IN A TURBULENT FLOW

In this section some turbulent correlations that are needed in the turbulence model closure are obtained. First the equation of motion of a single particle in a turbulent flow will be discussed, then Chao's (1964) solution for that equation will be presented, and finally the turbulent correlation between the fluid velocity and the relative slip velocity will be obtained.

4.1 Transport Behavior of a Single Particle

Tchen (1947) extended the Basset-Boussinesq-Oseen (BBO) equation for the unsteady Stokes motion of a spherical particle in a stagnant fluid to that of a particle in a moving fluid that reads:

$$\frac{4\pi a^3}{3} \rho_2 \dot{v} = \frac{4\pi a^3}{3} \rho_1 \dot{u} - \frac{2\pi a^3}{3} \rho_1 (\dot{v} - \dot{u}) - 6\pi\mu_1 a (v - u)$$

$$- 6\pi\mu_1 a \cdot \frac{a}{\sqrt{\pi\nu_1}} \int_{\infty}^{t} \frac{\dot{v}(t_1) - \dot{u}(t_1)}{\sqrt{t - t_1}} dt_1$$

$$- \frac{4\pi a^3}{3} g (\rho_2 - \rho_1) . \tag{4.1}$$

In Equation 4.1 u(t) is the velocity of the fluid in the neighborhood of the particle, but far enough to be unaffected by it; v(t) is the velocity of the particle; ρ_1 and ρ_2 are, respectively, the density of fluid and the density of the particle; a is the particle radius; g is the acceleration of gravity; and μ_1 and ν_1 are, respectively, the dynamic and kinematic viscosities of the fluid. The dot denotes $(\frac{d}{dt} + v \frac{d}{dx})$. The physical meaning of the different terms of Equation 4.1 are discussed by many workers (Fuchs, 1964; Hinze, 1975). As a summary, the first term on the right hand side (RHS) of Equation

4.1 is added to BBO equation on the basis of intuitive consideration by Tchen (1947) to account for the unsteady motion of the fluid or its pressure gradient. The second term is the inertia force due to relative acceleration of the virtual mass attached to the particle; the third term is the Stokesian drag; the fourth term is often referred to as the "Basset" force, which results from the relative acceleration between the particle and the fluid; and the last term is the gravity force. The importance of each term in Equation 4.1 under different flow conditions and the various approximations for handling that equation is explored by Hjelmfelt and Mockros (1966). They found that for high density ratios (e.g., those greater than 10^3) all the terms on the RHS of Equation 4.1 are unimportant except for the drag term. For the sake of generality, however, all the terms will be retained in the present analysis.

Corrsin and Lumley (1956) argued that the first term on the RHS side of Equation 4.1, which Tchen included to represent the force created by the pressure gradient in the fluid, should be evaluated via the full Navier-Stokes equation. Accordingly they proposed that Equation 4.1 should be replaced by:

$$\frac{4\pi a^3}{3} \rho_2 \frac{dv_i}{dt} = \frac{4\pi a^3}{3} \rho_1 \left(\frac{\partial u_i}{\partial t} + u_j \frac{\partial u_i}{\partial x_j} - \nu_1 \frac{\partial^2 u_i}{\partial x_j^2} \right)$$

$$- \frac{2\pi a^3}{3} \rho_1 \left(\frac{dv_i}{dt} - \frac{\partial u_i}{\partial t} - v_j \frac{\partial u_i}{\partial x_j} \right)$$

$$- 6\pi \mu_1 a \, (v_i - u_i)$$

$$6\pi \mu_1 a \, \frac{a}{\sqrt{\pi \nu_1}} \int_\infty^t \frac{\left(\frac{dv_i}{dt} - \frac{\partial u_i}{\partial t} - v_j \frac{\partial u_i}{\partial x_j} \right) dt_1}{\sqrt{t - t_1}} .$$

$$- \frac{4\pi a^3}{3} g (\rho_2 - \rho_1) \qquad\qquad 4.2$$

Maxey and Riley (1983) derived an equation of motion for a solid particle in a turbulent flow. They considered the Faxen terms to account for the unsteady effects on Stokes drag law. For particles of size smaller than the Kolmogoroff length scale, η, Hinze (1975) argued that the following two conditions can be satisfied:

a) $\quad \dfrac{a^2}{\nu_1} \dfrac{\partial u_1}{\partial x_1} \ll 1 \qquad\qquad 4.3$

b) $\quad \dfrac{v_1}{\nu_1} \dfrac{\partial u_1 / \partial x_1}{\partial^2 u_1 / \partial x_1^2} \gg 1 \qquad\qquad 4.4$

Thus, if the conditions 4.3 and 4.4 are satisfied, then the viscous stress term in Equation 4.2 and the Faxen terms on Maxey and Riley's equation can be neglected. Therefore, in the case of particles with a diameter less than the Kolmogoroff length scale, all the equations of Corrsin and Lumley, and Maxey and Riley, become identical to Equation 4.1.

Chao (1964) considered Equation 4.1 with the two restrictions 4.3 and 4.4 to obtain the connection between some transport properties of a particle and those of its surrounding fluid. Neglecting the gravity force and applying such restrictions, Equation 4.1 reads as follows:

$$\dot{v}_i - \beta \dot{u}_i + \alpha\beta(v_i - u_i) + \beta\left(\frac{3\alpha}{\pi}\right)^{1/2} \int_{-o}^{t} \frac{(\dot{v}_i - \dot{u}_i)dt_1}{(t-t_1)} = 0 \qquad\qquad 4.5$$

in which $\alpha = 3\nu_1/a^2 \qquad\qquad 4.6$

$$\beta = \frac{3\rho_1}{2\rho_2 + \rho_1} \qquad\qquad 4.7$$

Chao (1964) applied the Fourier transform of the velocity component $u_i(t)$ as defined by

$$\tilde{u}_i(\omega) = \int_{-\infty}^{\infty} u_i(t) \exp(-i\omega t) dt \qquad 4.8$$

and similarly for $\tilde{v}_i$. Unlike $\tilde{u}_i$, $\tilde{v}_i$ is not only a function of ω, but also a function of the physical parameters α and β.

The Fourier transform solution of Equation 4.8 with $t_o = -\infty$ gives

$$\tilde{v}_i = \frac{[\alpha + \sqrt{\frac{3\alpha\omega}{2}}] + i[\omega + \sqrt{\frac{3\alpha\omega}{2}}]}{[\alpha + \sqrt{\frac{3\alpha\omega}{2}}] + i[\frac{\omega}{\beta} + \sqrt{\frac{3\alpha\omega}{2}}]} \tilde{u}_i \qquad 4.9$$

By introducing the energy spectrum function $E(\omega)$, a relation is obtained between the intensity of the particle turbulent motion and that of the surrounding fluid:

$$\frac{\overline{v_i^2}}{\overline{u_i^2}} = \int_0^{\infty} \frac{\Omega_1}{\Omega_2} E(\omega) d\omega \qquad 4.10$$

where $\Omega_1 = (\frac{\omega}{\alpha})^2 + \sqrt{6}(\frac{\omega}{\alpha})^{3/2} + 3(\frac{\omega}{\alpha}) + \sqrt{6}(\frac{\omega}{\alpha})^{1/2} + 1$; $\qquad 4.11$

$$\Omega_2 = \beta^{-2}(\frac{\omega}{\alpha})^2 + \sqrt{6}\,\beta^{-1}(\frac{\omega}{\alpha})^{3/2} + 3(\frac{\omega}{\alpha}) + \sqrt{6}(\frac{\omega}{\alpha})^{1/2} + 1 ; \qquad 4.12$$

The Lagrangian frequency function $E(\omega)$ is in general affected by the presence of the particles. In the low frequency range (inertial subrange), the modulation of the Lagrangian frequency function of the carrier fluid by

the particles can be neglected (Al-Taweel and Landau, 1977). Thus, in the

present work the Lagrangian frequency function is given by (Hinze, 1975)

$$E(\omega) = (\frac{2}{\pi}) (\frac{\tau_L}{1+\omega^2 \tau_L^2}) ,$$ 4.13

where ω ranges from 1 to 10^4 (sec^{-1}).

The local Lagrangian integral time scale τ_L is calculated from (Mostafa and Elghobashi 1984b):

$$\tau_L = 0.233 \ K/\epsilon$$ 4.14

Chao proceeded his solution by defining a relative velocity ω_i between the particle and the local gas velocity as

$$\omega_i = v_i - u_i$$ 4.15

This value, when substituted into Equation 4.1, again with $t_o = -\infty$, followed by the Fourier transformation and solving for ω_i, gives

$$\tilde{\omega}_i = \frac{-(1-\beta)i\omega}{[\alpha\beta + \beta(\frac{3\alpha\omega}{2})^{1/2}] + i[\omega + \beta(\frac{3\omega}{2})^{1/2}]} \tilde{u}_i$$ 4.16

The first term in the denominater of Equation 4.16, $\alpha\beta$, was written wrongly (as α only) by Chao (1964) and Soo (1967). Hetsroni and Sokolov (1971) handled the incorrect form of Equation 4.16 to study the effect of the dispersed phase on the fluid turbulence energy spectrum. Using that erroneous equation Hetsroni and Sokolov obtained Equation 29 (in their article), which relates the turbulence intensity of a two-phase flow to that of a single

phase. If Equation 4.16 is used in the analysis of Hetsroni and Sokolov, their Equation 29 will give equal turbulence intensities for the single- and two-phase flows. Although Hetsroni and Sokolov's theoretical analysis gives good qualitative results, it has no basis and therefore should not be taken seriously.

Chao (1964) obtained the ratio between mean square relative velocity to that of the surrounding fluid:

$$\frac{\overline{\omega_i^2}}{\overline{u_i^2}} = \int_0^\infty \frac{\Omega_R}{\Omega_2} E(\omega) d\omega \qquad\qquad 4.17$$

where

$$\Omega_R = [(1-\beta)\omega/\alpha\beta]^2 \qquad\qquad 4.18$$

This solution applies to dilute suspensions, where there is no interactions between the particles.

Elghobashi and Abou-Arab (1983) considered Chao's solution to get the turbulent correlation $\overline{u_i(u_i-v_i)}$ that is needed in their turbulence model. This quantity is given by

$$\overline{u_i(u_i - v_i)} = -\frac{1}{2} \overline{u_i^2} (1 - \int_0^\infty \frac{\Omega_1 - \Omega_R}{\Omega_2} E(\omega)d\omega) \qquad\qquad 4.19$$

This correlation will be used to close the time-mean equations in the present work.

4.2 Droplet Shape

4.2.1 Theoretical Analysis

It is well known that the change in droplet shape affects not only the interfacial area and drag force but also the evaporation rate. Most of the

59

theoretical studies (Krestein, 1983; O'Rourke, 1981; Mostafa and Elghobashi, 1983) for liquid droplet-gas flow have been based on the assumption of spherical droplets. This assumption must be justified, especially if the droplet is suspended in a turbulent flow.

The shape of a liquid droplet moving in a continuous phase is determined by the forces acting along the surface of the droplet. At any time the net force is the balance of the pressure, gravity, buoyancy, drag, and inertial forces of the exterior fluid. At the fluid-fluid interface there will be an equilibrium of normal forces. The forces acting inward are due to the dynamic stresses and static head of the exterior fluid and interfacial tension. Those acting outward are due to the dynamic stress and static head of the interior fluid. If the droplet is spherical, all the forces will lie on a radial line and the interfacial tension force will be the same on all parts of the surface.

For a liquid droplet moving in a gaseous flow, a study is presented here of the physical factors that might be expected to control the spherical shape. Those factors are as follows:

1. <u>Surface tension</u> -- This force is a consequence of the net inward attraction exerted on the surface molecules by those which are lying deeper within the droplet over the prevailing force in the gas outside. This increment in total pressure, across the interface, Δp, at a certain point on the droplet surface is given, in general, by

$$\Delta P = \gamma(1/a_1 + 1/a_2)$$
4.20

where γ is the surface tension of the liquid-air interface (N/m). In the special case of a spherical droplet, $a_1 = a_2 = a$, and then

2. <u>Internal hydrostatic pressure</u> -- There exists within the droplet a vertical pressure gradient of exactly the sort found in any mass of fluid at rest in a gravitational field. In the limit of large droplets, the difference in hydrostatic pressure between top and bottom of a droplet ($2\rho_2 ga$) becomes quite important in controlling droplet shape.

3. <u>The relative velocity between the droplet and the gaseous phase</u> -- The fluid dynamic pressure exerted because of the relative velocity between the gaseous phase and the droplet tends to cause a distortion in the spherical shape. The effect of this inertial force ($1/2\rho_1(U-V)^2$) increases as the Reynolds number does. As the Reynolds number is increased, droplet oscillation (unsteady state distortion in shape) will set in; ultimately as Re increases droplet breakup will occur.

4. <u>Internal circulation</u> -- Due to the vortical motion, there is a centrifugal reaction that varies as the square of the circulation velocity (Oliver and Chung, 1982). Many workers (Beard, 1976; Pruppacher and Beard, 1970) reported that in the case of a water droplet (of diameters less than 1 mm) falling at terminal velocity, internal circulation has negligible effect on distortion.

After stating the factors that might be expected to control the shape of a liquid droplet suspended in a moving gas, a study of the order of magnitude of each factor is necessary. The equation for the shape was given by Laplace's formula (McDonald, 1954) for the mechanical equilibrium of an interfacial surface, which can be written at the droplet's equator as:

$$\gamma(\frac{1}{a_1} + \frac{1}{a_2}) = \frac{2\gamma}{a} + (\rho_2 - \rho_1)ga + \frac{1}{2}\rho_1(U-V)^2 \qquad 4.22$$

The first term on the RHS of Equation 4.22 is the spherical curvature

pressure, the second is the hydraulic head, and the third is the differential

dynamic pressure. From the above equation it can be seen that as long as the

spherical pressure $(2\gamma/a)$ is dominant, a variation in surface tension is

unimportant. In Table 4.1 the comparative values of the three terms in

Equation 4.22 are calculated for 100 μ methanol and Freon-11 droplets (the

materials used in the present study) moving in air with a relative velocity of

5 m/s. Also, the dimensionless groups; defined by Equations 4.23a, 4.24 and

4.26 are given in Table 4.1. The physical corresponding properties of

methanol and Freon-11 are given in Appendix A.

Table 4.1 The Forces Acting Along the Surface of
Liquid Droplets and the Corresponding
Dimensionless Groups.

	$\frac{2\gamma}{a}$ N/m^2	$(\rho_2 - \rho_1)ga$ N/m^2	$\frac{1}{2}\rho_1(U-V)^2$ N/m^2	$Re = \frac{\rho_1(U-V)d}{\mu_1}$	$We = \frac{\rho_1(U-V)^2 d}{\gamma}$	$Et = \frac{g(\rho_2-\rho_1)d^2}{\gamma}$
Methanol	872	0.4	14.73	32.72	0.135	0.0036
Freon-11	300	0.744	14.73	32.72	0.39	0.02

Table 4.1 shows that, for liquid droplets of diameters less than

100 μ and for the two different materials, the surface-pressure increment is

large compared with the minute hydrostatic pressure differences within the

droplet, or compared with the small aerodynamic pressures. Hence, these

liquid droplets do simply assume the shape implying minimum surface free-energy, thus accounting for their well-known spherical form.

Because of the need to answer the question of whether internal circulations should be important in the droplet shape problem, the upper limit to the centripetal force acting on the droplet surface due to the internal circulation will be estimated here. Pruppacher and Beard (1970) reported that for a water droplet falling at terminal velocity, the velocity at the equator was found to be about 1/100 of the droplet's terminal velocity. For a relative velocity of 5 m/s, the maximum velocity at the equator is about 0.05 m/s. The centripetal force per unit area acting on the small lamina of the internal boundary layer can be calculated. This lamina of radial distance can be assumed to be equal to one tenth of the distance from the droplet surface to the internal stagnation point. Thus, for a droplet of 100 μm diameter, this distance is about 1.5 μm. Since the centrifugal reaction resulting from the vortical motion varies as the square of the circulation velocity, the centripetal force per unit area acting on the internal lamina of the droplet is found to be about 0.8 N/m^2. Thus, the order of magnitude of the centrifugal pressure gradient appears to warrant neglect of internal circulation compared to the other parameters.

4.2.2 Experimental Observations

Many researchers have investigated the different factors affecting the droplet shape and the flow field inside and outside liquid droplets moving in a continuous phase (gas or other liquid). Wellek et al. (1966) investigated the effects of various properties, droplet size, and droplet velocity on droplet shape for forty-five dispersed liquid droplets falling through stationary liquid continuous phases. The maximum ratio between the viscosity

of the dispersed and continuous phases was that of ethylene glycol (droplet) and hexane (liquid system). This ratio was about 47. Empirical relations involving the Weber number, We, Eotvos number, Et, and viscosity ratio were obtained. These relations enable the prediction of the eccentricity of nonoscillating droplets over a wide range of Reynolds numbers (6.0 to 1354). This number is given by

$$Re = \frac{\rho_1 (U-V)d}{\mu_1}$$ 4.23a

One of their relations is:

$$R = \frac{a_1}{a_2} = 1.0 + 0.091 \, We^{0.95}$$ 4.23b

where the Weber number is given by

$$We = \frac{\rho_1 (U-V)^2 d}{\gamma}$$ 4.24

and $R = \frac{a_1}{a_2}$ is the ratio of the length of the minor to the major axis of the droplet. From Table 4.1 for a 100 μ Freon-11 droplet moving with a relative velocity 5 m/s in air at the atmospheric conditions (Re = 32.73 and We = 0.39), R = 1.037, which could be assumed a spherical shape. Garner and Lane (1959) measured the distortion of liquid droplets falling in gases. They reported the following linear relationship:

$$R = 1 + 0.13 \, Et$$ 4.25

where the Eotvos E is given by

$$Et = \frac{g(\rho_2 - \rho_1)d^2}{\gamma}$$

4.26

For the Freon-11 droplet with conditions summarized in Table 4.1, R is equal to 1.003. Winnikow and Chao (1965) investigated the behavior of droplets falling in water at Reynolds numbers ranging from 138-971. Their conclusion about the deformation of nonoscillating droplets was that the droplets are spherical up to Et = 0.2 Since Equation 4.23 gives the distortion ratio in terms of the Weber number which is a function of the aerodynamic pressure, Equation 4.23 is recommended for the calculation of the spherical shape limits for present droplets in a moving gas. Pruppacher and Beard (1970) studied the deformation of water droplets falling at terminal velocity in air of 20°C at sea level pressure, and nearly water saturated by a wind tunnel means. They concluded that droplets with an equivalent diameter smaller than 280 μm equivalent to Reynolds number Re = 25 had no detectable deformation from spherical shape. Droplets of sizes d < 400 μm Re < 200 were slightly deformed into an oblate spheroid (R = 1.02).

Beard (1976) also analyzed all the available theoretical and experimental data on droplets falling in gases to derive a reliable method for obtaining the terminal velocity and shape of a water droplet at any level in the atmosphere. He concluded that droplets with diameters < 1 mm (Re < 300) are essentially spherical. He also reported that the effects of a varying surface tension and internal viscosity were shown to have a negligible influence on the shape and terminal velocity of a falling droplet of diameters up to 1 mm.

Now, it is clear that the assumption of a spherical shape for methanol or Freon-11 droplets of diameters up to 100 μm moving with a relative velocity up to 5 m/s (or Re = 32.72) is realistic based on the previous force analysis and

the experimental evidence of the other researchers.

4.3 Mass Transfer

There are many aerodynamic parameters that dominate the process of evaporation of a spray injected into a moving airstream. Relative velocity and free stream turbulence are the most important parameters.

First, the evaporation of a spherical droplet, motionless relative to an infinite, uniform medium is considered in section 4.3.1. Then the evaporation rate of a moving droplet in a gaseous medium is covered in section 4.3.2. Finally, the effect of free stream turbulence on the evaporation rate is discussed in subsection 4.5.

4.3.1 Quasi-Stationary Evaporation of Droplets Motionless Relative
to Media

One of the earliest investigations of evaporation in stagnant gases was made in 1877 by Maxwell (cited by Fuchs, 1959) who solved the steady-state conservation equations of mass and energy in the gas phase under the following assumptions:

1. Spherical droplet

2. Incompressible droplet fluid and surrounding fluid

3. Spherical symmetry: forced and natural convection are neglected. This reduces the analysis to one dimension.

4. The droplet fluid is of a single component.

5. Constant pressure process

6. Both droplet fluid and surrounding fluid are mutually immiscible, and there is no chemical reaction.

7. No spray effects: the droplet is isolated and immersed in an infinite environment.

8. The system involves only purified fluids (there is no surface-active material).

9. Diffusion being rate-controlling: the rate of evaporation is completely determined by the rate of diffusion of the vapor in the medium.

10. Constant and uniform droplet temperature: this implies that there is no droplet cooling or heating.

11. Constant gas phase transport properties.

12. Saturation vapor pressure at droplet surface: this is based on the assumption that the phase-change process between liquid and vapor occurs at a rate much faster than those for gas-phase transport. Therefore, the vapor at the surface is produced at the saturation pressure corresponding to the droplet surface temperature T_s.

In the case of stationary evaporation, the rate of diffusion of the vapor of the droplet across any spherical surface with radius r and concentric with the droplet is constant and expressed by the equation:

$$I_o = 4\Pi r^2 \rho_l \ \delta \frac{dC_r}{dr} \qquad \text{Kg/s} \qquad\qquad 4.27$$

where C_r is the concentration of the evaporated material at radius r and δ is the diffusivity of that material. Integrate Equation 4.27 with the following boundary conditions:

$$C_r = C \quad \text{at} \quad r = \infty \qquad\qquad 4.28$$

$$C_r = C_L \quad \text{at} \quad r = a \qquad\qquad 4.29$$

This gives Maxwell's equation:

$$I_o = 4\Pi a\, \delta\, (C - C_L) \qquad 4.30$$

Strictly speaking, the evaporation of a droplet cannot be a stationary process since the radius and hence the rate of evaporation is constantly decreasing. Fuchs (1959) pointed out that when $C_L \rho_1 \ll \rho_2$, the evaporation can be regarded as quasi-stationary; i.e., one can assume that the rate of evaporation at a given moment is expressed by Equation 4.30. Since

$$I_o = \frac{dm}{dt} \qquad 4.31$$

where t is the time and $m = 4/3\Pi a^3 \rho_2$ is the mass of the droplet, Equation 4.30 can be rewritten in the form:

$$\frac{da^3}{dt} = \frac{2\delta}{\rho_2}\, (C_L - C) \qquad 4.32$$

or

$$\frac{dS}{dt} = \frac{8\Pi\delta}{\rho_2}\, (C_L - C) \qquad 4.33$$

where $S = 4\Pi a^2$ is the surface area of the droplet. Integration of these equations gives:

$$a_o^2 - a^2 = \frac{2\delta}{\rho_2}\, (C_L - C_\infty)t \qquad 4.34$$

$$S_o - S = \frac{8\Pi S}{\rho_2}\, (C_L - C_\infty)t \qquad 4.35$$

68

where a_o and S_o are the initial radius and surface of the droplet. The surface of the droplet is therefore a linear function of time.

The assumption of equilibrium between the liquid and its vapor at the droplet interface suggests that the diffusive resistance of the gas to evaporation is large compared with the interfacial resistance. This is considered to be a good assumption under all conditions, except at very low gas pressures or for droplets whose size is in the order of the mean free path of the gas molecules (about 0.1 micron). Thus, equilibrium has been assumed in most analysis dealing with evaporation of droplets.

4.3.2 Influence of the Stefan Flow on the Rate of Evaporation

Observe that Equation 4.30 was derived neglecting the radial convection transport due to bulk flow of the gases away from the droplet. Unlike natural and forced convection that can be neglected in a spherical case, radial convection is always present, although its effects are small at low evaporation rates.

Stefan at 1881 (cited by Fuchs, 1959) was the first to note the importance of radial convection. To maintain full pressure in the medium together with the partial vapor pressure gradient of the vapor, there must be an equal and opposite partial gas pressure gradient of the remaining components of the medium. Owing to the presence of the second gradient the gas diffuses to the droplet surface, but because of the impermeability of the latter the total gas flux towards the surface should equal zero. Hence, the hydrodynamic flow of the medium compensates the diffusion of the gas. From this discussion it follows that the rate of this flow m^1 is governed by the equation:

$$\delta^1 \frac{dC^1}{dr} = m^1 C^1 \qquad \qquad 4.36$$

where C is the concentration and $\delta^1 = \delta$ the diffusion coefficient of the surrounding gas. Since

$$C + C^1 = 1 \qquad \qquad 4.37$$

or

$$\frac{dC^1}{dr} = -\frac{dC}{dr} \qquad \qquad 4.38$$

and the total flux of vapor has diffusion and hydrodynamic components, Equation 4.27 is replaced by

$$I_o = 4\Pi\rho_1 r^2 \left(\delta \frac{dC_r}{dr} - C_r m^1\right) \qquad \qquad 4.39$$

$$= 4\Pi\rho_1 r^2 \delta \left(\frac{1}{1-C} \frac{dC_r}{dr}\right) \qquad \qquad 4.40$$

Just as Equation 4.27 leads to Maxwell's equation, so Equation 4.40 gives:

$$I_o = 4\Pi\rho_1 \ a \ \delta \ \ell n \ (1+B); \qquad \qquad 4.41$$

where the transfer number B is given by

$$B = \frac{C_L - C}{1 - C_L} \qquad \qquad 4.42$$

The evaporation rate per droplet volume (ṁ) is given by

$$\dot{m} = I_o / \frac{4}{3} \Pi a^3 = \frac{12 \ \rho_1 \ \delta}{d^2} \ \ell n \ (1+B) \qquad \qquad 4.43$$

70

4.3.3 Quasi-Stationary Evaporation of Droplets Moving Relative to the Media

The greatest practical interest centers on the evaporation of droplets moving relative to the medium under the influence of gravity, inertia, etc. This problem can be reduced to the calculation of the rate of evaporation from a spherical droplet ventilated by a gas stream.

Following the majority of the workers in the field of evaporation of droplets moving relative to the medium, the convection effects on the evaporation rate can be expressed by

$$I = I_o f = I_o Sh \qquad\qquad 4.44$$

where Sh is the Sherwood number and f is the wind coefficient. This denotes the increase in the rate of evaporation due to the relative movement of the medium.

Using Equations 4.43 and 4.44 one can write:

$$\dot{m} = \frac{12\delta\rho_1}{d^2} \ell n \ (1+B) \ Sh \qquad\qquad 4.45$$

Using the principle of dimensionless analysis one can show that Sh is a function of Re and Sc. At the same time the majority of the theoretical and experimental work in the field of evaporation of droplets expressed that function by

$$Sh = 2 + \beta_1 Re^{1/2} Sc^{1/3} \qquad\qquad 4.46$$

where the Sherwood number is given by

$$Sh = \dot{m} \ / \pi \ d \ \delta (C_L - C) \qquad\qquad 4.47$$

and the Schmidt number is given by

$$Sc = \nu_1 / \delta \qquad\qquad 4.48$$

The first accurate measurements of the rate of evaporation of droplets suspended in a stream were those of Frossling 1938 (cited by Fuchs, 1959). This extremely careful work has served as a model for all subsequent work in this field. The experiments were carried out at 20° using droplets of water, aniline and nitrobenzene, and spheres of napthalene with a = 0.1 - 0.9 mm suspended from glass fibers of radius 25 μm. The droplets were placed 20 cm above the exit of a vertical aerodynamic tube of 10 or 20 cm in diameter. The Reynolds number was varied over the range of 2.3 - 1280 and the Schmidt number range was 0.7 - 2.7. The rate of evaporation was determined by periodically photographing the droplet with sevenfold magnification. The temperature fluctuation of the air stream did not exceed ± 1%. The determination of the rates of evaporation of droplets of organic substances in still air was carried out in a closed cylindrical vessel 5 cm in diameter, the walls being covered with active charcoal. Frossling examined the effects of different factors that might affect the accuracy of the results such as imperfectly spherical droplets, turbulence, compressibility of the air, nonideality of the vapor, and the counter flow effects and indicated that they are less than the experimental error (≤ ± 1%). His experiments confirm the accuracy of Equation 4.46 with an experimental value β_1 = 0.552.

The fundamental experiments of Ranz and Marshall (1952) were done at room temperature on benzene and water droplets with a = 0.06 - 0.11 cm. The

droplets that suspended from the capillary end of a microburette of radius 30 - 50 µm were ventilated by dry air from below. The study was restricted to a Reynolds number range of 0 to 200. Evaporation rates were determined by measuring the rate of feed through a burette necessary to maintain a constant droplet diameter. Ranz and Mar hall's results also confirm the accuracy of Equation 4.46 with an experimental value of β_1 = 0.6.

Ahmadzadeh and Harker (1974) summarized the previous experimental data on the evaporation from liquid droplets. All the experimental data in the range of Re < 1000 give the value of β_1 = 0.55 - 0.6.

Kinzer and Gunn (1951) used water droplets of a = 5 - 70 µm at 0 - 40°C and 10 - 100% relative humidity and employed instantaneous photography to measure the evaporation rate. The droplets fell freely in a tube of square cross-section. For droplets of a = 0.02 - 0.5 mm the experiments were conducted in tubes 200 m long. Insulated metal rings were placed horizontally along the axis of the tube at equal intervals. The droplets emerged from a capillary connected to the terminal of a battery and became charged when they broke away. Kinzer and Gunn measured the rate of fall of the droplets by passing them through a ring, thus creating an electric impulse that is amplified and recorded on a moving tape. Since the decrease of terminal velocity with time fall gave the rate of mass loss, they determined the rate of evaporation as a function of the rate of the droplet fall. They also measured the rate of fall and the evaporation rate by a photographic technique. For Re = 100 - 1600 their results were fitted by Equation 4.46 with β_1 = 0.46. When Re < 0.9, the constant β_1 rises from zero to a maximum value of approximately 0.92 at Re = 4 and then gradually falls to the abovementioned value of 0.46 at Re = 100. This result contradicts the data of other workers, where β_1 has a value in the Re region of 1-100 equal to or less

than the value at greater Re.

Galloway and Sage (1967) have reviewed the available information concerning the effects of the molecular properties of the fluid, conditions of flow, and level of turbulence on the evaporation rate from spheres. At normal conditions and an intermediate range of Reynolds number, Equation 4.46 with β_1 = 0.6 represents the standard curve for all other date.

Yuen and Chen (1978) investigated the evaporation of liquid droplets at high temperatures. The data on water and methanol droplets (porous spheres) evaporating into the flow of air with the temperature of the latter within 150 – 960°C was obtained in an air tunnel. The experiments were carried out for the Reynolds number range from 200 to 2000.

Yen and Chen pointed out that for low temperatures their results are identical with the standard curve of Equation 4.46 with the same coefficient as that of Frossling.

Prakash and Sirignano (1980) studied the liquid droplet vaporization in a hot convective gaseous environment. They developed a new gas-phase viscous, thermal, and species concentration boundary layer analysis using an integral approach. The gas-phase analysis was coupled with a liquid-phase analysis for the internal motion and heat transfer. The coupled equations were solved for different hydrocarbon fuels in air at 1000°K and 10 atm. They concluded that the heat flux into the liquid phase should be considered in such analysis. The temperature distribution inside the droplet is nonuniform for most of the droplet lifetime. The Ranz-Marshall correlation seems to agree well when the heat flux into the liquid phase is taken into account by modifying the heat of vaporization. If the droplet has the same temperature as the surrounding gas at the droplet generator exit, the heat flux into the liquid phase can be neglected, and in this case the Ranz-Marshall correlation does not need any

modifications.

Now after the discussion of the previous experimental work on the evaporation of liquid droplets suspended in a moving stream, it is clear that Equation 4.46 as:

$$Sh = 2 + 0.55 \ Re^{1/2} \ Sc^{1/3} \qquad\qquad 4.49$$

This equation along with Equation 4.45 will be used in the turbulence model to calculate the evaporated mass from the droplets to the surrounding gas.

4.4 Drag Coefficient

The drag coefficient of spherical solid particles, nonevaporating droplets, and evaporating droplets is discussed in this section.

4.4.1 Drag Coefficient of a Solid Particle

All the solutions with low inertia terms, Stokes and Oseen, are valid for very low Reynolds numbers. The Stokes solution, which ignores completely the inertia terms, is valid for $Re < 1$; Oseen considered the Navior-Stokes equation with very limited inertia terms, but the drag coefficient is unchanged. For a moderate Reynolds number $1 < Re < 200$, there are a lot of experimental results for the drag coefficient and the plot of these data versus the Reynolds number is called the standard drag curve. The recommended drag coefficient on a solid sphere in steady motion as the best approximation for this curve is given by Clift et al., 1978

$$C_{DS} = (24/Re) \left[1 + 0.135 \ (Re)^{0.82-0.05w} \right] \qquad 0.01 < Re < 20 \qquad 4.50$$

$$C_{DS} = (24/Re) \left[1 + 0.1935 (Re)^{0.6305} \right] \qquad 20 < Re < 200 \qquad 4.51$$

where $w = Log_{10} Re$ and the particle Reynolds number is calculated from

$$Re = \rho_1 \, |\vec{U} - \vec{V}| \, d/\mu_1 \qquad 4.52$$

$$\vec{U} = \sqrt{U_z^2 + U_r^2} \qquad 4.53$$

$$\vec{V} = \sqrt{V_z^2 + V_r^2} \qquad 4.54$$

4.4.2 Drag Coefficient of a Nonevaporating Droplet

To satisfy the continuity of tangential shear stress across the liquid-gas interface, a slight amount of internal motion seems certain to develop. This internal circulation of the liquid droplet decreases the boundary layer thickness of the exterior flow and may reduce the drag coefficient.

Pruppacher and Beard (1970) studied the internal circulation and shape of a water droplet, which can be considered as a nonevaporating droplet falling at terminal velocity in air at 20°C at sea level pressure, and nearly water saturated. They concluded that the maximum surface velocity, at the equator, of a droplet was found to be about 1/100 of the droplet's terminal velocity. Due to this vanishingly small value, one can expect that the flow structure around a nonevaporating liquid droplet falling in air will be approximately the same as that for a solid particle, hence the drag coefficient will be the same. Beard and Pruppacher (1969) measured the drag on water droplets falling in water saturated air at terminal velocity in a wind tunnel for Reynolds numbers between 0.2 and 200. They concluded that for this Reynolds number range the drag on water droplets is in good agreement with that for the drag on solid spheres measured or calculated by many other researchers. Beard

(1976), depending upon all the available theoretical and experimental data, concluded that droplets with diameters < 1 mm (Re < 300) are essentially spherical and the drag may be closely approximated by the drag on a rigid sphere. Ingebo (1956) investigated the drag coefficient for liquid droplets and solid spheres accelerating in air stream using a high-speed camera technique. Accelerations of the order of 20,000 m/s^2 were considered. The sphere diameter range was from 20 to 120 microns. To ensure the spherical shape for the liquid droplets (isooctane, water, and trichloroethylene), the Reynolds number was in the range 6 < Re < 400. The main purpose of Ingebo's work was the study of the effects of the rate of acceleration, the liquid status and the evaporation rate on the drag coefficient. His main conclusion was that the unsteady-state drag coefficients are different than the steady-state values, but when the acceleration rates were low, the unsteady-state drag coefficients were in agreement with steady-state values of previous investigations. The interesting result is Ingebo's conclusion that the drag coefficient for slowly evaporating droplets, nonevaporating droplets, and solid spheres are the same.

Rivkind et al. (1976) solved the Navier-Stokes equations for the flow of fluid inside and outside a spherical droplet using the method of finite differences. They considered the variables Re, μ_2/μ_1 and ρ_2/ρ_1 as controlling parameters of the problem. The drag coefficients of the droplets were investigated for $0 < \mu_2/\mu_1 < \infty$ and 0.5 < Re < 100. They concluded that the density ratio has virtually no effect on flow characteristics. According to their numerical results, they proposed that the drag coefficient of the droplet can be defined in terms of the drag coefficients of the solid sphere (C_{DS}) and of the gas bubble (C_{Db}) at the same Re by the formula

$$C_D = \frac{\mu_2 C_{DS} + \mu_1 C_{Db}}{\mu_1 + \mu_2} \qquad\qquad 4.55$$

Rivkind and Ryskin (1976) extended their previous work to consider the circulating flow inside and outside the droplet up to Re = 200. They again recommended Equation 4.55 for the calculation of the drag coefficient of a liquid droplet moving in gaseous flow. By calculating the drag coefficient of water and methanol droplets moving in atmospheric air with a Reynolds number up to 200, it was found that the difference between the values produced by Equation 4.55 and those of a solid particle (Clift et al., 1978) is only 3%.

Hamielec and Johnson (1962) used the error distribution method to predict the velocity profiles and terminal velocities for solid and fluid spheres moving in viscous media under the influence of gravity. The error distribution or Galerkin method is based on choosing a polynomial for the stream function that satisfies all the boundary conditions together with an integral form of the Navier-Stokes equation. By this method, Hamielec and Johnson predicted reasonably accurate velocity profiles and terminal velocities for circulating droplets and bubbles. Hamielec et al. (1963) modified the work of Hamielec and Johnson (1962) to account for the finite interfacial interface with trial stream functions. They predicted velocity profiles for viscous, laminar, and imcompressible flow around droplets, bubbles and solid spheres. The drag coefficients, flow separation angles, and forced convection transfer rates were calculated and compared with experimental data for solid spheres, circulating droplets, and bubbles of some other workers. They obtained good agreement up to Re = 100. Hamielec et al. (1963) tried to correlate the available experimental data for the drag coefficient of liquid droplets falling in water using a viscosity-ratio correction factor. This relation is given by:

$$C_D = \frac{3.05}{Re^{0.74}} \left(\frac{783\mu_R^2 + 2142\mu_R + 1080}{(60 + 29\mu_R)(4 + 3\mu_R)} \right)$$ 4.56

$$10 < Re < 100$$

where $\mu_R = \mu_2/\mu_1$

In the present study the drag coefficient of a water droplet moving in atmospheric air was compared with a Reynolds number in the range (10 < Re < 100) using Equation 4.55 and 4.56 with the experimental data of Beard and Pruppacher (1969). It was found that the values produced by Equation 4.55 are 3% less than the corresponding experimental values while those produced by Equation 4.56 are 17% less. Therefore, Equation 4.55 is recommended for the calculation of the drag coefficient of a moving nonevaporating droplet in a media with comparable viscosity to that of the droplet.

Nakano and Tien (1967) also used Galerkin's method to investigate the effect of increasing the internal Reynolds number (0 < Re < 50) or, more accurately, the flow behavior within the fluid sphere by including inertia terms for both phases. Changes in the internal Reynolds number had little effect on the external streamlines or on overall drag. Thus, they got almost the same results as Hamielec and his coworkers.

Now, based on the previous theoretical and experimental work, it is clear that the effect of internal circulation and low evaporation rate on the drag coefficient of a liquid droplet moving in a gaseous stream is negligible. This drag coefficient can be considered from the standard drag curve of a flow over a solid sphere.

4.4.3 Drag Coefficient of an Evaporating Droplet

Hamielec et al. (1963) studied numerically the effect of mass transfer

from a spherical particle at Reynolds numbers 1, 40, and 100 on the drag coefficient. In all cases they showed that radial mass efflux decreases friction drag and increases the pressure drag slightly. Due to the bulk flow of vapor from the droplet surface, the boundary layer thickness decreases. Thus, the velocity gradient or the surface shear stress decreases, so a reduction in the friction drag is predicted. The slight increase in the pressure drag may be attributed to the blowing effects on the angle of boundary layer separation. On the other hand, Kassoy et al. (1966) have shown that at low Reynolds number, the drag of a sphere at constant free stream temperature decreases with decrease in temperature of the sphere. This is attributed to the changes in the surrounding fluid properties that might be more pronounced in the case of evaporation. Yuen and Chen (1976) have noted that the changes in the composition of the gases near the droplet surface are important and would tend to reduce the drag of an evaporating droplet since the viscosity of most vapors is lower than the viscosity of air at the same temperature. The effects of the temperature and concentration gradients due to evaporation on the dependence of drag coefficient on Reynolds number are accounted for by using the free stream density and the 1/3 rule for the dynamic viscosity (Yuen and Chen, 1976).

Eisenklam et al. (1967) investigated experimentally the evaporation rates and drag coefficients for evaporating and burning droplets of various fuels freely falling in atmospheric air at temperatures of up to 1000°C, or burning in cold oxygen atmospheres. They correlated the experimental data for the drag coefficient C_D using the formula

$$C_D = C_{DS}/(1 + B) \qquad\qquad 4.57$$

The experimental data covers the Reynolds number range 0.005 - 15. The correlation 4.57 was suggested by results from boundary layer theory and an analogy with droplet heat transfer, for which case a similar correlation was already in existence.

For intense mass transfer, such as when the droplet is burning, the evaporation is expected to reduce film drag due to a thickening of the boundary layer, and if the droplet is burning, the form drag is expected to be reduced by the "filling in" of the wake by products of combustion. Further effects are the alteration of the position of boundary layer separation and the steep variations in properties due to the large temperature and concentration gradients associated with intense mass transfer.

Yuen and Chen (1976) used Eisenklam's experimental data, along with their own data that extended the Reynolds number range to about 500, to develop an alternative correlation. They defined a reference Reynolds number

$$Re_r = Re_\infty \, \mu_\infty / \mu_r \qquad\qquad 4.58$$

where μ_r is the viscosity of a reference mixture at the temperature

$$T_r = T_L + (T_\infty - T_L)/3 \qquad\qquad 4.59$$

and containing a vapor mole fraction (χ_r) given by

$$\chi_r = \chi_L + (\chi_\infty - \chi_L)/3 \qquad\qquad 4.60$$

The subscripts L and ∞ denote, respectively, the conditions at the droplet's surface and far away from it. Their correlation for the drag coefficient is

then given by the rule that states that if

$$C_{DS} = F(Re_\infty)$$ 4.61

is the standard drag coefficient curve for solid spheres as a function of free stream Reynolds number, then

$$C_D = F(Re_r)$$ 4.62

will be the drag coefficient of an evaporating spherical droplet.

Dukowicz (1984) calculated numerically the drag coefficient of evaporating droplets in the Stokes flow regime. He tested Yuen and Chen (Equation 4.62) and Eisenklam (Equation 4.57) correlations in the low Reynolds number range. Dukowicz (1984) and Sirignano (1983) recommended the use of Yuen and Chen's correlation for the calculation of the drag coefficient of an evaporating spherical droplet.

4.5 Effect of Free Stream Turbulence on Drag and Evaporation Rate

The flow conditions about the particle, especially the free stream turbulence intensities, may cause large variations in the drag coefficients from those values given by the standard drag curve. Zarin and Nicholls (1971) reported that at Re < 200, they have observed little or no change in C_{DS} compared to the C_{DS}'s measured at lower turbulence intensities ($\simeq$ 1%).

In general, the motion of a droplet in a turbulent flow depends upon the characteristics of the droplet and of the turbulent flow. Droplets with small size or small realization time (τ_p) compared with the turbulence time scale (τ_L) respond to the fluctuating motion of the carrier fluid. If $\tau_p > \tau_L$, very little fluctuation in the droplet velocity can be seen (Clift

et al., 1978). In this case the effect of turbulence is then to modify the flow field around the droplet, so that the drag may be affected.

In the present study the value of the ratio τ_p/τ_L is expected to be less than unity, and thus the effect of the free stream turbulence on the drag coefficient should be very small. Experimental evidence supports this assumption. For example, Clift et al. (1978) reported that the effect of the free stream turbulence in the range of droplet Reynolds number $10 < Re < 50$ is less than 5% (Figure 10.11 in that reference).

Regarding the evaporation rates, for $Re < 50$ and for turbulence intensity less than 20%, the experimental data (Clift et al., 1978) showed a very small increase in the evaporation rate. Therefore, in the present study the drag coefficient and the evaporation rate will be mainly functions of the Reynolds number only and not in terms of the turbulence intensity around the particle.

5.0 EDDY DIFFUSIVITY OF A SINGLE PARTICLE

5.1 Introduction

Eulerian mathematical models of particle-laden turbulent flows require knowledge of the statistics of particle motion in order to calculate the particle response to fluid turbulence. Specifically, a reliable expression is needed for calculating the Schmidt number, defined as the ratio of particle diffusivity to fluid point diffusivity for heavy particles. So far, such an expression is unavailable in the literature.

Tchen (1947) studied the diffusion of a rigid particle carried by a turbulent flow. Hinze (1975) indicated that Tchen's assumption that the fluid element should continue to contain the same discrete particle at any time is hardly to be satisfied. Such an assumption cannot be valid if the ratio between the material densities of the particle and fluid is large. In this case the particle will be associated with more than one eddy along its path which is termed the overshooting phenomena. Soo (1956), Friedlander (1957), Chao (1964), and Gouesbet et al. (1984) solved Tchen's equation under the assumption of no overshooting. For asymptotic times of dispersion, that assumption implies a particle Schmidt number of unity which is physically incorrect.

Peskin (1971) studied the particle diffusivity under the condition of overshooting but restricted his analysis to small distances between the discrete particle and the "originally surrounding fluid." As a result, Peskin's formula predicts values of particle Schmidt number very close to unity. Some other workers (Reeks, 1977, and Nir and Pismen, 1978) investigated the particle diffusivity under the condition of overshooting but restricted their study to the Stokes flow regime, which is hardly to be satisfied for suspended heavy particles in a gaseous media.

Csanady (1963) studied the differences between the diffusion of the fluid points and heavy solid particles in the atmosphere. He attributed the appreciable reduction of the dispersion rates of the heavy solid particles to the rapid travel across the turbulence eddies. Meek and Jones (1973) statistically analyzed the heavy particle behavior for a constant relative velocity between the particle and its surrounding gas in homogeneous turbulence. They obtained expressions for the particle dispersion coefficient and its Lagrangian autocorrelation.

In this section a reliable expression for the calculation of the lateral diffusivity of heavy particles suspended in a homogeneous turbulent field is provided. The physical parameters that control the particle behavior in a turbulent flow is discussed. Two widely used theories (Csanady, 1963, and Meek and Jones, 1973) for the calculation of the statistical properties of heavy particles in terms of those of the surrounding fluid are reviewed. The empirical coefficient in Csanady's theory is determined via a comparison with the experimental data. Finally, Meek and Jones' theory is examined and an empirical coefficient is introduced and evaluated via a comparison with the experimental data.

5.2 Physics of Particle Dispersion

The behavior of a single spherical particle suspended in a homogeneous isotropic turbulent field depends on the properties of both the particle and the turbulent flow. The first parameter that controls the particle dispersion is the ratio of the particle size to the Kolmogorov, length scale, η. If this ratio is small the particle dispersion will be influenced by the entire spectrum of eddy sizes and will follow the turbulence fluctuations of the carrier fluid. If, on the other hand, that ratio is greater than unity, the

particle will follow the slow large-scale turbulent motions of the fluid
(Alonso, 1981). In this case the main effect of the turbulence on the
particle is to modify the flow field around it, so that its drag may be
affected.

A more general parameter is the ratio between the particle relaxation
time, τ_p, inversely proportional to the particle's inertia, and the fluid
Lagrangian integral time scale, τ_L, is the controlling parameter of the
particle response to the turbulence fluctuations. If the ratio $\tau_p/\tau_L < 1$, the
particle will be able to respond to the entire spectrum of fluid motion and
the ratio between the root mean square fluctuating velocity of the particle to
that of a fluid point is almost unity. On the other hand if $\tau_p/\tau_L > 1$ the
particle will respond very slowly to the fluctuating fluid motion.

If there is an appreciable relative mean velocity between the particle
and the surrounding fluid, the particle will move about from eddy to eddy,
whereas a fluid point would remain in the same eddy throughout the lifetime of
that eddy. This is what Yudine (1959) called the "crossing trajectories
effect." Yudine (1959) considered the physical consequences for finite free-
fall velocities on the heavy-particle diffusion. He formulated upper and
lower limits for the changes in the dispersion coefficient due to the heavy
particles free fall velocity, f.

Taylor (1921) postulated a theory describing the statistical dispersion
of fluid points in a stationary homogeneous turbulent flow. His result
relates the mean lateral square fluid point displacement, $\overline{Y^2}$, to the mean
square fluctuating velocity, $\overline{u^2}$, and to the Lagrangian velocity correlation
coefficient, $R_L (\tau)$, according to:

$$\overline{Y^2} (t) = 2 \, \overline{u^2} \, \int_0^t \int_0^T R_L(\tau) \, d\tau dT \qquad 5.1$$

The correlation coefficient is defined by

$$R_L(\tau) = \frac{\overline{u(t)\ u(t + \tau)}}{\overline{u^2}}$$

5.2

Taylor (1921) defined a turbulent diffusivity by

$$\epsilon_f(t) = \frac{1}{2}\frac{d}{dt}\overline{Y^2}(t)$$

5.3

$$= \overline{u^2}\ {}_0\!\int^T R_L(\tau)\ d\tau$$

5.4

$$= \overline{u^2}\ \tau_L$$

5.5

Snyder and Lumley (1971) showed that Taylor's theory is equally applicable for the dispersion of alien particles, provided that the velocities are interpreted as particle velocities, and that the Lagrangian time scale, τ_L, is interpreted accordingly. Snyder and Lumley (1971) and Wells and Stock (1983) measured the dispersion of heavy particles in a grid-generated turbulent flow. They reported the decrease of the particle integral time-scale and the rapid decrease of the particle velocity correlation with increasing τ_p.

Calabrese and Middleman (1979) photographically measured the degree of radial dispersion of medium-size particles emanating from a point source in the turbulent core of a fully developed vertical pipe flow of water. They defined the medium-size particles by $\eta < d < L_f$, where d and L_f are the particle diameter and Lagrangian length scale respectively. They were able to calculate the radial mean-square particle displacement directly to find that both heavy and buoyant particles experienced a decrease in mean-square

displacement due to the crossing-trajectory effects.

5.3 Csanady's Theory

Csanady (1963) considered the differences between the diffusion of the
fluid points and heavy particles in the atmosphere. He proposed a functional
form for $\overline{u(o)\,u(t)}$, where $u(t)$ is the fluctuating velocity of the air,
consistent with similar shapes for Eulerian and Lagrangian fluid point
correlations. Thus, Csanady was able to construct two relations for the
particle dispersion coefficient parallel to and normal to the direction of the
particle terminal velocity. Lumley (1978a) showed that Csanady's model gives

$$\frac{\varepsilon_h}{\varepsilon_f} = \frac{1}{(1 + \beta_h^2\, f^2/u^2)^{1/2}} \quad , \quad \beta_h = 4/3 \qquad\qquad 5.6$$

$$\frac{\varepsilon_v}{\varepsilon_f} = \frac{1}{(1 + \beta_v^2\, f^2/u^2)^{1/2}} \quad , \quad \beta_v = 2/3 \qquad\qquad 5.7$$

where ε_f is the asymptotic diffusivity for the fluid. The subscripts h and v
correspond respectively to horizontal and vertical dispersion of the particle
associated with long times relative to the integral time scale of the
turbulence. Lumley stated that the value of β_h is much less well determined
than that of β_v and the value of β_h should be determined via a comparison with
well defined experimental data.

In the present work the value of β_h is determined by comparing the
prediction using Equation 5.6 with the experimental data.

C-2

5.4 Meek and Jones' Theory

Meek and Jones (1973) considered the motion of a heavy particle in a homogeneous turbulent air flow. The particle motion was viewed from a reference frame in which the average fluid velocity is zero. They started with the definition of the particle velocity autocorrelation, which can be expressed in terms of a normalized particle energy spectrum, $E_{p,ii}(\omega)$:

$$R_{p,ii}(\tau) = \int_{\infty}^{\infty} E_{p,ii}(\omega) \cos(\omega\tau) \, d\omega \qquad\qquad 5.8$$

where ω is the circular frequency.

Soo (1956) obtained an expression relating $E_{p,ii}(\omega_o)$ to its fluid counterpart, $E_{ii}(\omega)$, from the solution of the simplified particles equation of motion and under the assumption of zero free-fall. This expression is given by

$$E_{p,ii}(\omega_o) = Q_{ii}(\omega_o) \, E_{ii}(\omega), \qquad\qquad 5.9$$

where $Q_{ii}(\omega_o)$ is the particle response function defined as:

$$Q_{ii}(\omega_0) = \frac{\overline{u_{ii}^2}}{\overline{v_{ii}^2}} \left[\frac{1}{1 + (\frac{\omega^2}{\alpha_1^2})} \right] , \qquad\qquad 5.10$$

where $\quad \alpha_1 = \dfrac{18 \, \mu_1}{\rho_2 d^2} \, ;$ $\qquad\qquad\qquad\qquad$ 5.11

d and ρ_2 are the particle diameter and density respectively and μ_1 is the dynamic viscosity of the surrounding fluid. The Lagrangian frequency function, $E_{ii}(\omega)$, can be approximated by various semiempirical forms. Hinze

(1975) pointed out that the use of an exponential form for the fluid's Lagrangian velocity autocorrelation provides reasonable agreement with the experimental data. The associated energy spectrum is

$$E_{ii}(\omega) = \frac{\tau_{L,ii}}{\pi (1 + \omega^2 \tau_{L,ii}^2)}$$ 5.12

Meek and Jones (1973) indicated that the use of a response function derived for zero free-fall velocity, f_i, requires some adjustment of 5.8 to account for non-zero free-fall and the subsequent movement of the particle from one eddy to another. They suggested that the nonezero free-fall velocity spectrum $E_{p,ii}(\omega)$, be expressed in terms of the zero free-fall velocity spectrum, $E_{p,ii}(\omega_o)$, according to:

$$E_{p,ii}(\omega) = E_{p,ii}(\omega_o)/Z ;$$ 5.13

where $Z = [1 + (f_i/v_i)^2]^{1/2}$. 5.14

Using the above assumptions, the particle velocity autocorrelation can be written as

$$R_{p,ii}(\tau) = \frac{1}{1 - \xi_{ii}} [e^{-\tau/\tau_{ii}} - \xi_{ii} e^{-\tau/\xi_{ii}\tau_{ii}}],$$ 5.15

where $\xi_{ii} = \frac{1}{\alpha_1 \tau_{L,ii}}$; 5.16

$$\tau_{ii} = \tau_{L,ii}/Z .$$ 5.17

The ratio of the fluctuating velocity variances is given by Soo (1956) as:

$$\left(\frac{\overline{v^2}}{\overline{u^2}}\right) = \frac{1}{1 + \xi_{11}} , \qquad 5.18$$

while the mean square particle displacement, $\overline{Y_p^2(t)}$, in the radial direction is

$$\overline{Y_p^2(t)} = \frac{\overline{v^2} \, t \, \tau_{11}}{1 - \xi_{11}} \left[(1 - e^{-t/\tau_{11}}) - \xi_{11}^2 (1 - e^{-t/(\xi_{11}\tau_{11})}) \right] . \qquad 5.19$$

The particle eddy diffusivity is given by

$$\varepsilon_h(t) = \frac{\overline{v^2} \, \tau_{11}}{1 - \xi_{11}} \left[(1 - e^{-t/\tau_{11}}) - \xi_{11}^2 (1 - e^{-t/(\xi_{11}\tau_{11})}) \right] . \qquad 5.20$$

The corresponding fluid point eddy diffusivity is given by

$$\varepsilon_f(t) = \overline{u^2} \tau_{L,11} (1 - e^{-t/\tau_{11}}) \qquad 5.21$$

Thus, the particle Schmidt number $\left(\sigma_p = \dfrac{\varepsilon_h}{\varepsilon_f} \right)$ is given by:

$$\sigma_p(t) = \frac{\varepsilon_h(t)}{\varepsilon_f(t)} = \frac{1}{(1 - \xi_{11})^2 Z} \left[(1 - e^{-t/\tau_{11}}) - \xi_{11}^2 (1 - e^{-\tau/(\xi_{11}\tau_{11})} \right] \qquad 5.22$$

For long times relative to the integral time scale of turbulence

$$\sigma_p = \frac{\varepsilon_h}{\varepsilon_f} = \frac{1}{Z} , \qquad 5.23$$

where Z is given by (5.13).

Peskin (1974) argued that a heavy particle initially coincident with the fluid point naturally lags behind that fluid point as a result of inertia. The fluid points encountered by the heavy particle are not statistically equivalent and would only be so in a turbulent field with infinitely large space and time Eulerian correlation scales. Finite correlation scales imply that the fluid point encountered by the heavy particle as it lags behind the original coincident point are not statistically identical. Accordingly, the heavy particle dispersion or diffusivity is determined by the Eulerian space-time correlation. Peskin stated that Meek and Jones failed to account for the most important effects of the space-time correlation of the turbulent flow on the particle motion. The linear relation (Equation 5.9) between the particle energy spectrum and the fluid Lagrangian spectrum implies that the effects of the space-time correlation are completely neglected.

Meek and Jones (1974) in their reply to Peskin (1974) argued that the good agreement between their predictions and the experimental data of Snyder and Lumley supports their solution, especially in homogeneous turbulence. To achieve this agreement, they used Equation 5.19 and the fluid and particle data of Snyder and Lumley (Equation 5.28 and Table 1 in Meek and Jones' article, 1973). Using their equation and table, the present study can not reproduce their Figure 2, especially for the solid glass particles.

5.5 Modifications of Meek and Jones' Theory:

As pointed out by Peskin (1974), the Eulerian space-time correlation $R_E(y(\tau) - x(\tau))$, where $y(\tau)$ and $x(\tau)$ are the Lagrangian fluid and the particle positions, should be considered in the analysis of heavy particle dispersion instead of the Lagrangian autocorrelation. To do so the solution should be restricted to a very short distance $(y(\tau) - x(\tau))$ between the

particle and the fluid, otherwise the equations will be formidable. Peskin imposed this restriction but his solution predicts values of a particle's Schmidt number very close to unity even for a heavy particle. Yudine (1959) in his discussion of the physical parameters controlling the heavy particle diffusion pointed out that the dispersion process is controlled mainly by the terminal velocity, f. He stated that the dispersion process depends upon the terminal velocity in three ways: (1) the terminal velocity determines the vertical displacement of the center of dispersion of the particle; (2) because the terminal velocity is a certain measure of inertia, the particle does not follow completely the high frequency fluctuations of turbulent fluid velocity; and (3) if it has appreciable terminal velocity, a particle will fall from one eddy to another, whereas a fluid point would remain in the same eddy throughout the lifetime of the eddy. Yudine concluded that, for large f, the dispersion coefficient takes on an asymptotic form inversely proporational to f.

Meek and Jones (1973) pointed out that the inertial effects can be significant especially when $f_i < v_i$. The inertial effects increase the particle Lagrangian time scale compared to that of the fluid if there is no crossing trajectories.

Csanady (1963) accounted for the crossing trajectory effect on a heavy particle dispersion by including in his analysis the quantity f_i/u_i and the ratio between the Lagrangian to Eulerian integral time scales, β_h.

Due to the close similarity between the two theories of Csanady and Meek and Jones and based upon the previous discussion it is clear that the parameters that should be considered in a heavy particle diffusion analysis are the terminal velocity and a coefficient simulating the ratio between the Lagrangian to Eulerian integral time scales. Therefore the following

modification to the Z factor (Equation 5.14) is proposed:

$$Z = (1 + \alpha_h f_i^2 / \overline{v_i^2})^{1/2} , \qquad\qquad 5.24$$

where α_h is an empirical coefficient to be determined via comparison with the experimental data.

To determine β_h in Equation 5.6 and α_h in Equation 5.24 the predictions will be compared using both Csanady's theory and the modified theory of Meek and Jones with the experimental data of Snyder and Lumley (1971) and Wells and Stock (1983). Since the two theories have been developed for stationary, homogeneous turbulence, the data should satisfy these two conditions. Experimental evidence suggests that grid-generated turbulent flows approximate the stationary requirements and corrections can be made for the inhomogeneity (Pismen and Nir, 1979).

5.5.1 Snyder and Lumley's Experiment

Snyder and Lumley (1971) performed an experiment in which a single spherical solid particle was injected into a turbulent flow generated by a grid. They considered particles of various sizes and densities ranging from light particles that closely follow the fluid fluctuations to heavy particles that experienced both inertia and crossing-trajectory effects. The particles were injected above the gird at a distance of 20 grid spacing. They measured the particles' Lagrangian autocorrelations at x/M = 73 as well as the mean square displacement, $\overline{Y_p^2}$, of the particles as they were individually convected through the wind tunnel. Turbulence measurements were made and the turbulence energy decay was given by

$$\frac{\overline{U^2}}{\overline{u^2}} = 42.4 \ (\frac{x}{M} - 16) \hspace{5cm} 5.25$$

where U is the mean axial velocity (6.55 m/s) and x/M is the ratio of the

axial distance to the mesh size (2.54 cm). They also reported the rate of the

energy dissipation, ε, along the centerline of the wind tunnel (see Table

5.1).

Table 5.1. Energy Dissipation Rate (ε) of Snyder and Lumley (1971)

x/M	41	64	73	107	138	171
ε cm^2/s^3	5430	1610	1160	480	266	165

Table 5.2 lists the relevant characteristics for the particles studied by
Snyder and Lumley.

Table 5.2. Particle characteristics for the
data of Snyder and Lumley (1971)

	hollow glass	corn pollen	glass
density, ρ g/cm^3	0.26	1.0	2.5
diameter, d μm	46.5	87.0	87.0
drift velocity, f cm/s	1.67	19.8	44.2

Snyder and Lumley estimated the Lagrangian time scale, τ_L, at one station

only (x/M = 73) by considering the light particle results as representative of

Lagrangian correlations. In comparison with Snyder and Lumley's data, the

variation of τ_L along the wind tunnel axis should be estimated from the

measured turbulence quantities. τ_L can be obtained from the relation (Hinze,

1975)

$$\tau_L = \frac{2}{C} \overline{u^2}/\varepsilon \qquad\qquad 5.26$$

The ratio between the Lagrangian and Eulerian time scales, as given in Equation 5.26, depends on the local flow conditions and cannot be considered as constant. Hinze (1975) pointed out that the experimental data show that the value of the constant C varies between 3 and 10 depending on the Reynolds number, thus (5.26) reads

$$\tau_L = C' \overline{u^2}/\varepsilon, \qquad\qquad 5.27$$

where C' varies from 0.2 to 0.66.

On the other hand, Calabrese and Middleman (1979), using Taylor's theory, obtained the following expression:

$$\tau_L = \frac{5}{12} = 0.625 \overline{u^2}/\varepsilon \qquad\qquad 5.28$$

Berlemont et al. (1982) considered the closure relations of the K-ε model and obtained

$$\tau_L = 0.2 \overline{u^2}/\varepsilon \qquad\qquad 5.29$$

In the present work the coefficient C' in Equation 5.27 will be determined from the dispersion data of the light particle (hollow glass) or the particles with zero terminal velocity that are considered as representative of Lagrangian correlations. Using Equations 5.18, 5.19 and 5.26 for the hollow glass particles, $\overline{Y_p^2}$ is obtained and plotted in Figure 5.1

with an optimized value of C' = 0.35. Figure 5-1 also compares the prediction using Meek and Jones' theory and its modified form with the experimental data for the mean-square displacement of the corn pollen and the glass particles. It is clear from this figure that Meek and Jones' theory does not provide good agreement with the experimental data. With the present modification of Meek and Jones' theory the present study predicts the experimental data for the particles with different diameters and densities in Figure 5-1. This agreement is obtained with $\alpha_h = 0.3$.

Figure 5-2 shows a comparison between the theoretical and the experimental data for the Lagrangian autocorrelations for the different particles. The correlations decrease faster for the heavier particles (high drift velocity compared with the turbulence intensity) due to the crossing trajectory effects. It is also clear that the value of $\alpha_h = 0.3$ produces good agreement with the data for the autocorrelations.

5.5.2 Wells and Stock's Experiment

The effects of "crossing trajectories" and inertia on the dispersion of particles suspended in a field of grid-generated turbulence were investigated experimentally by Wells and Stock (1983). The flow conditions and grid size and shape were very similar to those used by Snyder and Lumley (1971) except that the main direction of the flow was horizontal instead of vertical. The particles were glass spheres, with a diameter of 5 or 57 μm and a density of 2.45 gm/cm^3. The particles were charged by a corona discharge then injected on the centerline of the flow. The test section was subjected to an electric field, which provides a coulomb force to the particles to balance the gravitational force. In this way, the drift velocity could be changed. The particle concentration and velocity were measured with a laser-Doppler
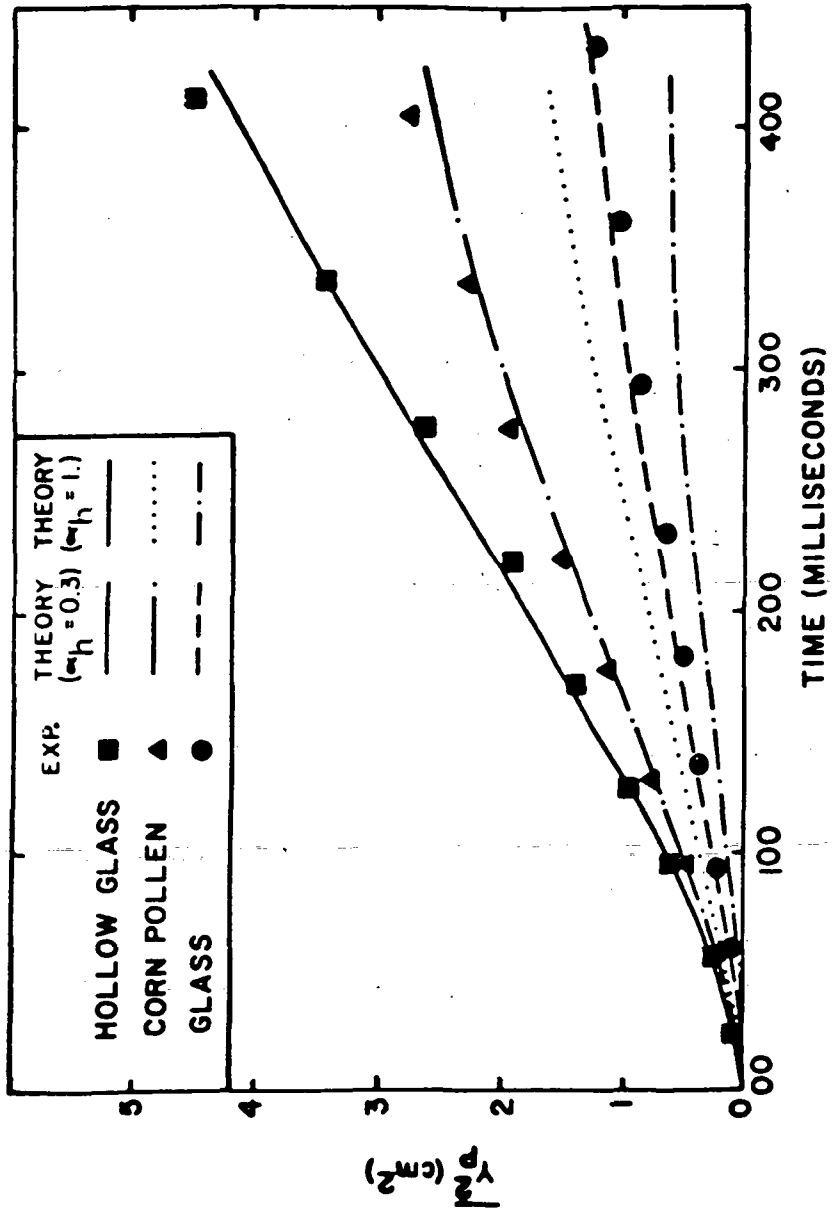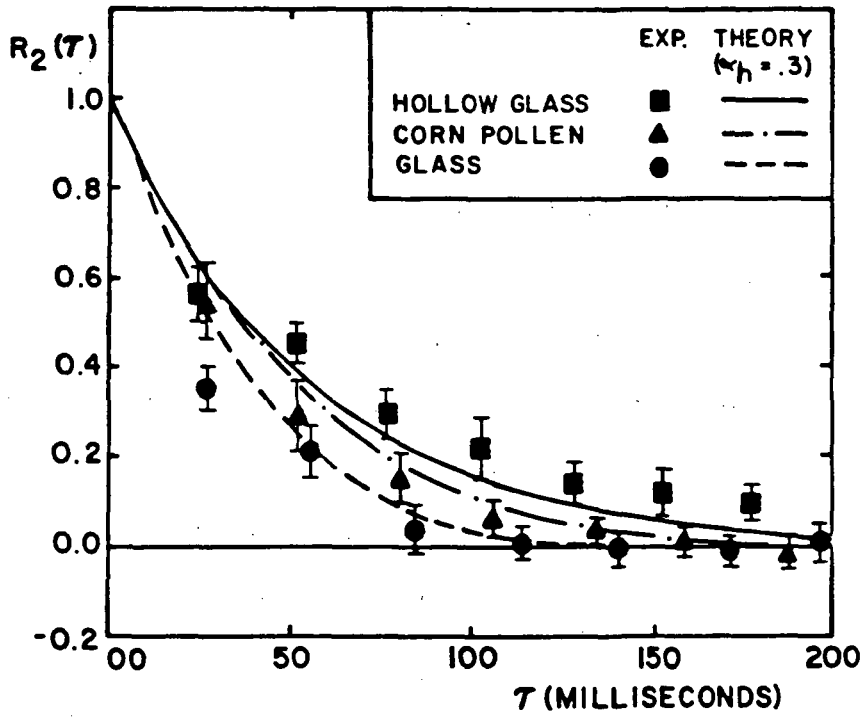
FIGURE 5-1 PARTICLE DISPERSION

FIGURE 5-2 LAGRANGIAN AUTOCORRELATIONS
FOR THE DIFFERENT PARTICLES

anemometry system. The data were reduced to yield the particle mean-square displacement.

The measured turbulence intensity, $\dfrac{\overline{u^2}}{\overline{u^2}}$, and dissipation rate of kinetic energy, ϵ, were used to calculate τ_L . Equation 5.27 was used with C' = 0.5 to reproduce the experimental data for the particles with $f_i = 0$ as shown in Figures 5-3 and 5-4. Figure 5-3 shows $\overline{Y_p^2}$ versus x/M for 5 μm particles with two values for the terminal velocity: zero and 25.8 cm/s. The two figures show good agreement between the predictions and the experimental data using α_h = 0.3 that was optimized for Snyder and Lumley's data.

Figure 5-3 displays the distribution of the Schmidt number, σ_p, against f_i/u_i. This figure compares the prediction using 5.24 with α_h = 0.3, Csanady's model (Equation 5.6), Snyder and Lumley's data, and Wells and Stock's data. The diffusivity ratio for the experiments of Snyder and Lumley and Wells and Stock were obtained using Equation 5.3 at different times or x/M. The agreement between this work and the experimental data is very good. The solid line in figure 5-5 was obtained using a value of β_h in Equation 5.6, equal to 0.55.

Comparison of the modified form of the Meek and Jones' theory (Equation 5.24) and that of Csanady (Equation 5.6) shows both similarities and differences (Mostafa and Elghobashi, 1985b). In Csanady's work, the only two parameters controlling the dispersion of a heavy particle in a turbulent flow are (f/v) and β_h. In that way the ratio f/u is considered as a measure of the crossing-trajectories effects, together with the associated continuity effect. In the present work, the ratios (f/u) and (v/u), and α_h are the controlling parameters. The ratio v/u is a direct measure of the inertia effect on the dispersion process as discussed by Meek and Jones and other
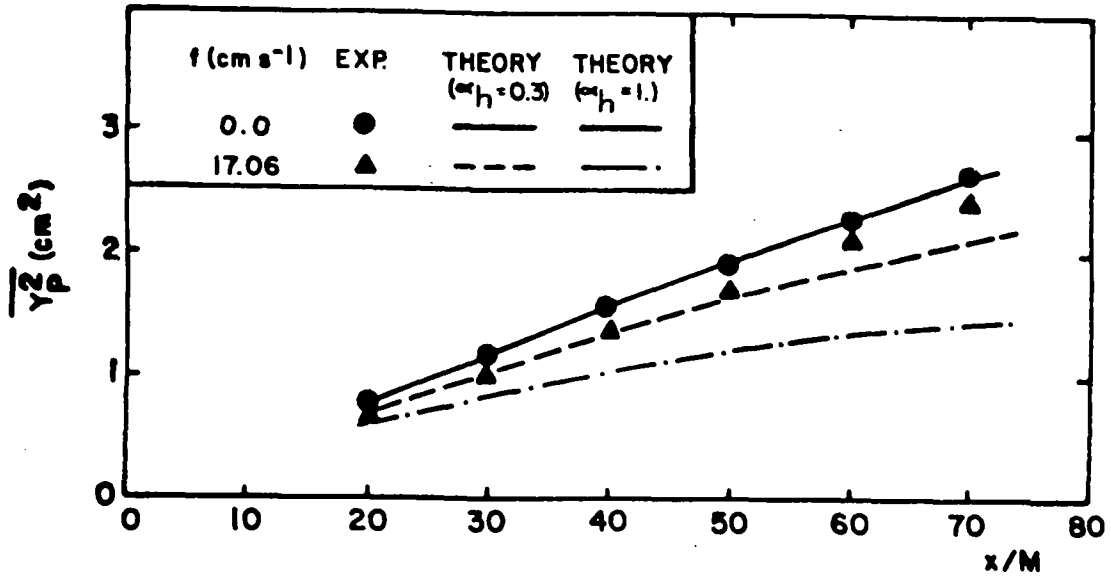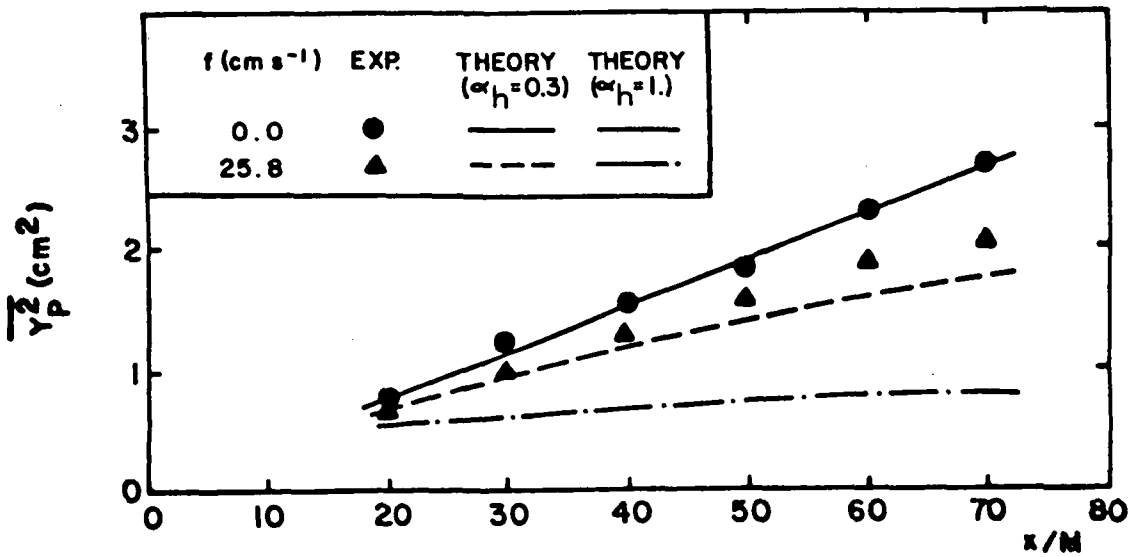
FIGURE 5-3 PARTICLE DISPERSION, 5μ PARTICLES
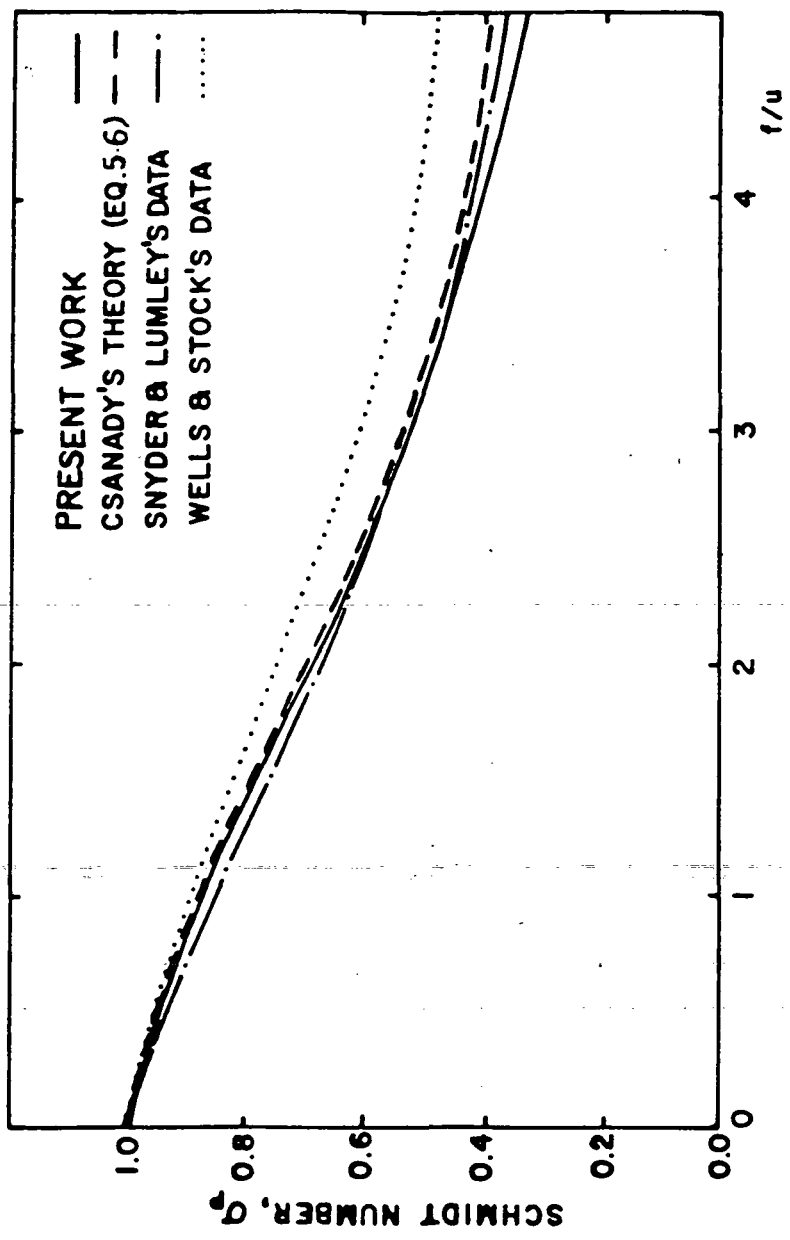
FIGURE 5-4 PARTICLE DISPERSION, 57μ PARTICLES

101

FIGURE 5-5 PARTICLE SCHMIDT NUMBER

workers (see Hinze, 1975) and it has a significant effect, especially when $f/v < 1$.

5.5.3 The Final Expression for Particle's Schmidt Number

The expression for calculating the Schmidt number of a heavy particle suspended in a turbulent flow (Equations 5.23 and 5.24) has been developed assuming that the drift velocity is constant or is large enough to make the Eulerian space-time correlation approximated by the Lagrangian autocorrelation (Peskin, 1974, and Reeks, 1977). Therefore the developed expression can be used for suspended particles in a turbulent flow if the relative mean velocity is assumed to be constant during a period of time $t \geq \tau_L$. At dispersion time greater than the Lagrangian time scale of turbulence, that expression is given by

$$\sigma_p^k = [1 + 0.3 (\vec{U} - \vec{V}^k)^2 / \overline{(v^k)^2}]^{-1/2} \qquad 5.30$$

$$(\frac{\overline{v^k}}{\overline{u^2}})^2 = \frac{1}{1 + \tau_p^k / \tau_L}, \qquad 5.31$$

$$\tau_p^k = \frac{\rho_2 (d^k)^2}{18 \mu_1}, \qquad 5.32$$

$$\tau_L = 0.35 \overline{u^2} / \epsilon \qquad 5.33$$

The coefficient 0.35 in Equation 5.33 is the optimized value using the experimental data of Snyder and Lumley (1971).

6.0 NUMERICAL SOLUTION OF THE EQUATIONS

We have now available a turbulence model and a number of experimental target values for free jet flows. The present section shows how the model will reproduce these target values.

To apply the model, a solution method and boundary conditions are needed. The first part of this section disucsses the of finite-difference technique used in solving the differential equations. The second part disucsses the solution procedure and the boundary conditions.

6.1 The Equations to be Solved

At this point, the reader may welcome a brief reminder of what constitutes the prediction method applied in this section.

This method employs the mean equations of continuity and momentum for each phase, the global continuity equation, the concentration equation, and the K and ε equations. Thus, the equations to be solved are $(6 + 3 k)$ in number; they are for the dependent variables U_z, U_r, V_z^k, V_r^k,

P, Φ_1, Φ^k, K and ε.

6.2 Solution Method

The governing equations are solved simultaneously with the finite-difference method that Spalding (1979) has developed for laminar two-dimensional parabolic dispersed-flow problems with interphase slip (GENMIX-2P). Since the governing equations are parabolic in nature, the method integrates by marching forward, i.e., downstream, starting at an initial cross-section where the profiles for all dependent variables must be specified. The GENMIX-2P computer code is generated from the GENMIX computer code (Spalding, 1978), after excluding the effects of mass transfer, chemical

reaction, and turbulence then adding two new subroutines. These two subroutines are COMP2P and ADJ2P, which set up and solve the finite difference equtions for the dispersed phase variables. All the necessary information about GENMIX is documented (Spalding, 1978) and need not be repeated here. Therefore, we will restrict the description here to the treatment of the dispersed phase and how it is coupled with the carrier phase in the solution procedure.

6.2.1 The Computational Mesh

The computer code GENMIX-2P employs the stream function ψ of the carrier phase as a cross-stream variable that is defined as

$$\Psi = \int_0^r \rho_1 \Phi_1 U_z r dr \quad .$$

6.1

The governing equations are transformed into a coordinate system based on the axial distance, z, and a normalized stream function, ω_n, defined as

$$\omega_n = \frac{\Psi - \Psi_I}{\Psi_E - \Psi_I} \quad ,$$

6.2

where Ψ_I and Ψ_E are the values of the stream function at the inner and outer boundaries of the flow. s measures the distance from an arbitrarily assigned starting point that is often taken as the starting point of the marching integration along the inner boundary of the grid. Lines of constant z are normal to the I boundary. ω_n is assigned the value 0.0 along the I boundary of the grid. It's value then increases monotonically with distance from that boundary, rising to the value 1.0 at the outer boundary of the grid.

The flow field of interest is subdivided into cells and each cell is

105

treated as a control volume. For the carrier phase, these cells are formed by the intersection of the constant z and ω_n lines as shown in Figure 6-1.

6.2.2 Finite Difference Equations (FDE) of the Dispersed Phase

The finite-difference equations for the carrier and dispersed phases are formed from the differential forms by integration over the control volumes of the carrier phase as shown in Figure 6-2. In this figure UP denotes upstream station and DN stands for downstream. TE_i is the tangent of the constant ω_n line just above the grid point i, but it is not distinguished from the angle or its sine. α_i is the inclination of the streamlines of the dispersed phase at $i \sim i + 1$ interface. For simplicity, in this section only, one class of particles will be considered. Therefore, the superscript k will be replaced by the subscript 2 to represent the dispersed phase. α_i equals TE_i plus an increment allowing for cross-flow, which takes account of local $\rho_1 \Phi_1 U_z$. Therefore, it represents the tangent of the streamline angle, but it is not distinguished from the angle or its sine. S_i is the outlet flow area of the ith control volume and $\Delta z = z_D - z_U$.

For the variables $\Phi_2|_i$ and $V_z|_i$ the control volumes over which integration of the equations is carried out are those of $U_z|_i$ of the carrier phase. For $V_r|_i$ the control volume is the one bounded by $i + 1, i$ at the upstream and downstream stations. Let Q represents any variable of the dispersed phase such as V_z, V_r or α and Φ_2. The result of integrating the equations can be most conveniently expressed as follows,

$$Q_i = \frac{A_i Q_{i+1} + B_i Q_{i-1} + C_i}{D_i} \qquad 6.3$$

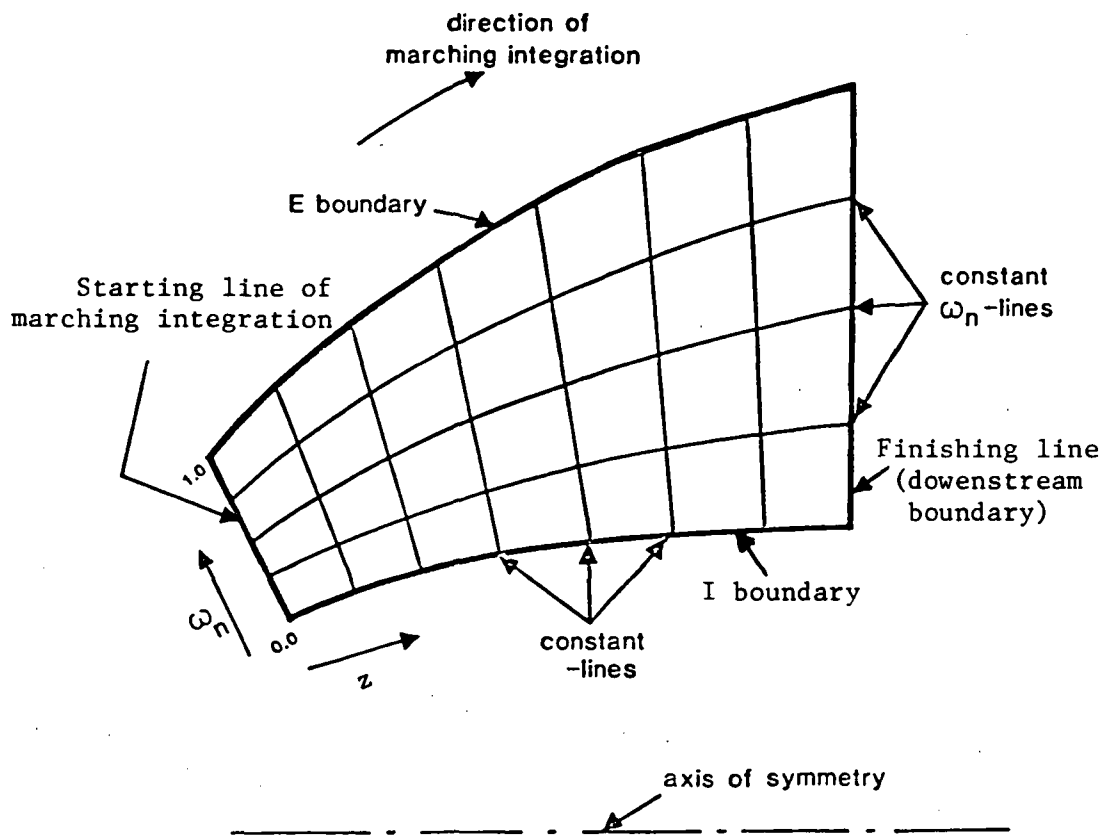The A_i and B_i coefficients represent the effects of transport of the dispersed

Figure 6-1 ILLUSTRATION OF THE z-ω COORDINATE SYSTEM
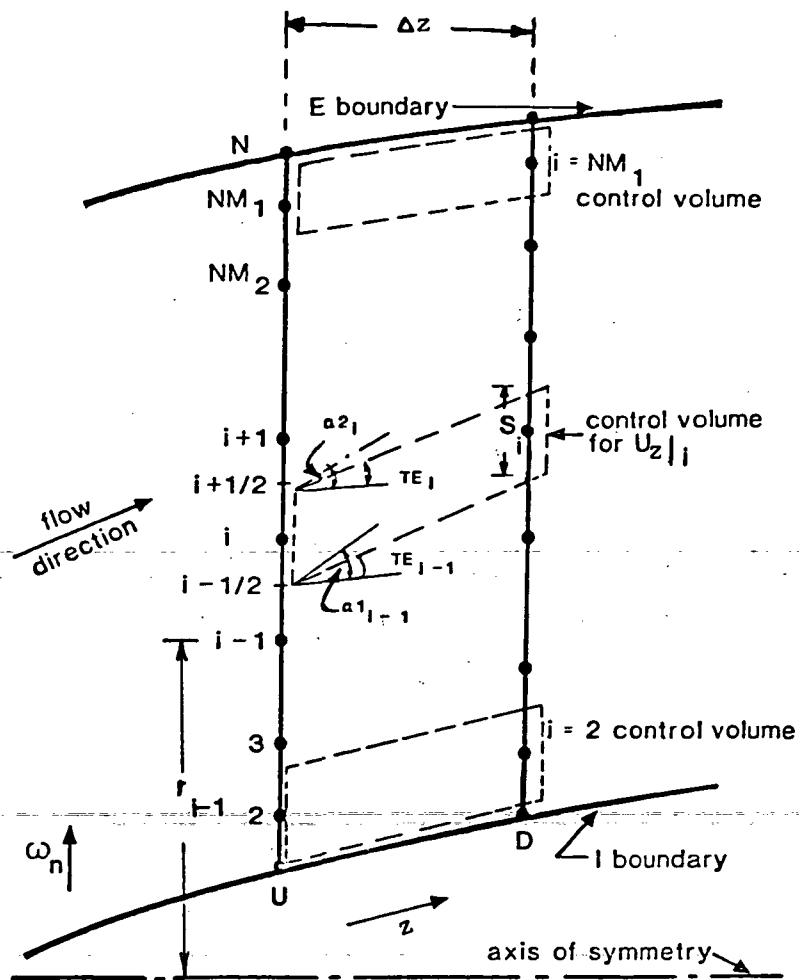
Figure 6-2 ILLUSTRATION OF THE CONTROL VOLUMES USED
FOR THE DERIVATIONS OF THE FINITE DIFFERENCE EQUATIONS

phase across constant ω_n lines. The coefficient C_i represents the effects of upstream convection from the different sources. These sources result from the pressure gradient, the gravity force, the interphase friction in the case of V_z and V_r, and the different turbulent correlations that result from the presence of the particles. The coefficient D_i represents the effect of outflow from the control volume. In the following the forms of the coefficients A_i, B_i, C_i and D_i for the variables $\alpha2$ ($=V_r/V_z$), V_z and ϕ_2 are presented:

For $\alpha2$:

$$A_i = \max \left[0, (DF\alpha - 0.5\ CON\alpha)_{i+3/2}, -CON\alpha_{i+3/2}\right]V_z|_{i+3/2} \quad \text{,} \qquad 6.4$$

$$B_i = \max \left[0, (DF\alpha + 0.5\ CON\alpha)_{i+1/2}\right]V_z|_{i+1/2} \quad \text{,} \qquad 6.5$$

$$C_i = \rho_2(\phi_2 SV_z V_z)|^U_{i+1/2}\alpha_i|^U + (P_i - P_{i+1})r_{i+1/2}\Delta z$$

$$\phi_2|_{i+1/2} - g_r(\rho_2 - \rho_1)\phi_2|_{i+1/2}\ VOL + FU_z\phi_2|_{i+1/2}\alpha_i VOL \quad \text{,} \qquad 6.6$$

$$D_i = [\rho_2\phi_2 SV_z|^U_{i+1/2} + A_i/V_z|_{i+3/2} + B_i/V_z|_{i+1/2} +$$

$$\phi_2 F|_{i+1/2}VOL]\ V_z|_{i+1/2} \quad \text{,} \qquad 6.7$$

where VOL is the total volume of the cell and,

$$CON\alpha_{i+3/2} = \rho_2\Delta z\ (r\phi_2 V_z)|_{i+1}\ (\alpha2 - TE)_{i+1} \quad \text{,} \qquad 6.8$$

$$DF\alpha_{i+3/2} = -[F\nu_t/\sigma_c(1 - 1/\sigma_p)\phi_{2,r}]_{i+1/2}/V_z|_{i+1}VOL$$

$$- \rho_2 \Delta z \; r_{i+1} \; [\nu_p/\sigma_c \; \Phi_{2,r}]_{i+1} \; (1 - TE/\alpha 2)_{i+1}$$

$$+ \rho_2 \Delta z \; r_{i+1} \Phi_2 |_{i+1} \; [\overline{v^2} + \nu_p V_{z,r} TE]_{i+1} / \alpha 2_{i+1} |_{i+3/2}$$

$$- \rho_2 \Delta z \; r_{i+1} \; [\nu_p/\sigma_c \; (\Phi_{2,r} - \Phi_{2,z} TE)]_{i+1}$$

$$+ \rho_2 \Delta z \; c_\phi \; \{rK/\varepsilon \; (\nu_t/\sigma_c \Phi_{2,r}),_r \; [2\overline{v^2} - \nu_p V_{z,r} TE]\}_{i+1}^+ \qquad 6.9$$

$$+ \dot{m} \; \Delta z \; r_{i+1} \; \sigma_p \; \sigma_c \Phi_2 / V_z |_{i+1}$$

For V_z:

$$A_i = \max \; [0, (DFV - 0.5 \; CONV)_{i+1/2} \; , \; - CONV_{i+1/2}] \; , \qquad 6.10$$

$$B_i = \max \; [0, \; (DFV + 0.5 \; CONV)_{i-1/2}] \; , \qquad 6.11$$

$$C_i = \rho_2 [S \Phi_2 V_z V_z]_i^U - (P_D - P_U) \; [\Phi_2 S]_i^U - \qquad 6.12$$

$$g_z (\rho_2 - \rho_1) \; VOL \; \Phi_2 |_i + [F \Phi_2 U_z]_i \; VOL \; , \qquad 6.13$$

$$D_i = \rho_2 [S \Phi_2 V_z]_i^U + A_i + B_i + [F \Phi_2]_i \; VOL \; , $$

where

$$\qquad 6.14$$

$$CONV_i = \rho_2 \Delta z \; [r \Phi_2 V_z]_{i+1/2} \; (\alpha 2 - TE)_i \; , $$

110

$$DFV_i = - \Delta z \, (r\Phi_2)_{i+1/2} \, [\nu_p \sigma_v]_{i+1/2}/(r_{i+1} - r_i)$$

$$+ \, (\overline{v^2} \, TE)_{i+1/2}/V_z|_i] \, - \Delta z \rho_2 [r\nu_p(\Phi_{2,r} - \Phi_{2,z} TE)]_{i+1/2}$$

$$+ \, \Delta z \rho_2 c_\phi \, [rK/\epsilon \, (\nu_p \Phi_{2,r})_{,r} \, (\nu_p V_{z,r})]_{i+1/2} \, . \tag{6.15}$$

For Φ_2:

$$A_i = \max \, [0, \, (DF\Phi - 0.5 \, CON\Phi)_{i+1/2} \, , \, - \, CON\Phi_{i+1/2}] \, , \tag{6.16}$$

$$B_i = \max \, [0, \, (DF\Phi + 0.5 \, CON\Phi)_{i-1/2}] \, , \tag{6.17}$$

$$C_i = \rho_2 \, [SV_z\Phi_2]_i^U \, , \tag{6.18}$$

$$D_i = \rho_2 \, [SV_z]_i + A_{i-1} + B_{i+1} + \overset{Dz(\dot{m}S)_i}{} \, . \tag{6.19}$$

where

$$CON\Phi_i = \rho_2 \, \Delta z \, (rV_z)_{i+1/2} \, (\alpha 2 - TE)_i \, , \tag{6.20}$$

$$DF\Phi_i = \rho_2 \, \Delta z \, (r\nu_p/\sigma_p)_{i+1/2} \, [1/(r_{i+1} - r_i) -$$

$$TE_i/Dz] \, {}^{(1 - \Phi_2|_{i+1}^U/\Phi_2|_{i+1})} \, . \tag{6.21}$$

Note that the A_i and B_i formulae (6.4, 6.5, 6.10, 6.11, 6.16 and 6.17) are hybrid in nature to account for high lateral convection (see Spalding, 1978). $\overline{v^2}$ in Equations 6.9 and 6.15 is calculated from Equation 4-10.

111

The equation set generated by Equation 6.3 for the different nodes at any station is solved by using the Tri-Diagonal Matrix Algorithm (TDMA) to obtain the dependent variable Q_i at the different nodes (see Roache, 1972).

At the beginning of the calculations, Φ_1 is unknown. Thus, the COMP2P subroutine uses a guess-and-correct procedure for Φ_1 or Φ_2. The procedure of correcting Φ_1 or Φ_2 takes place in the subroutine ADJ2P. There are three procedures for correcting Φ_1: direct substitution, computed under relaxation, and use of pressure corrections. In the direct substitution procedure the computed values of Φ_1 are used as the guessed ones for the start of the new solution loop. The disadvantage of this procedure is the possible non-convergence, when the changes are large. The advantages of this method are its simplicity and the consequent economy. This method can be expected to work satisfactorily when Φ_2 values are small ($\Phi_2 < 10^{-3}$).

The computed under-relaxation method starts the next iteration loop with Φ_1 given by

$$\Phi_1 = \Phi_1^* + \zeta(\Phi_1 - \Phi_1^*), \qquad\qquad 6.22$$

where the * denotes old values and ζ is an under-relaxation factor, conveniently taken as: $\zeta \simeq \Phi_1|_{old}$. The under-relaxation factor is expected to be slight for dilute suspension, i.e., this method reduces to the direct substitution method.

The pressure corrections method devises and solves a pressure correction equation driven by errors: $(1 - \Phi_2 - \Phi_1)$. This method is suitable for large values of Φ_2, which are outside the scope of the present study.

6.3 The Solution Procedure

The steps to obtain the solution at a given axial location are:

1. Guess the downstream ϕ_1 distribution (from the upstream values).

2. Solve for U_z downstream: obtain r'^s and $U_r'^s$.

3. Solve for K and ϵ to obtain the eddy diffusivities.

4. Calculate the local dimensionless quantities, Re^k, Sc^k, and Sh^k. Then obtain the mass transfer rate; $\dot{m}^k$, hence the sink terms in the mass conservation equation for each group or the total source term in the continuity equation for the carrier phase.

5. Obtain the downstream diameter distribution from the upstream values and the local evaporated mass.

6. Calculate the size range for each group from knowing the largest and smallest droplet diameters, and the number of sizes to be considered (it could be different from the upstream value).

7. Label the droplets according to their local diameters and the size ranges for each group.

8. Obtain p(r) from the gas-phase lateral momentum equation.

9. Solve for downstream (V_r^k/V_z^k), V_z^k and ϕ_z^k and get $\phi_1 \cdot \phi^k$'s

10. Compare the new ϕ_1 with the guessed ϕ_1^*.

11. Make corrections and repeat steps 1-7 until the solution converges before marching to the next station.

In general, two iterations are needed at each station to achieve convergence.

6.4 The Boundary Conditions

The parabolic flows considered in this report require the prescription of three boundary conditions for each dependent variable. At the predictions starting plane the profiles of all the dependent variables must be specified

from the experimental data. At the axis of symmetry ($r = 0$) all the radial gradients are set to zero, in addition to the vanishing radial velocity. The jet boundaries are determined via the adjustment of the entrainment rate and the specification of the radial gradient of U_z to fixed small value. Just outside these boundaries the values of the other dependent variables will be those corresponding to the ambient conditions. For example, all V_z's and ϕ_2 are equal to zero there.

In the next section the results presented are obtained using 40 lateral nodes to span the flow domain between the centerline of the jet and its outer edge. Grid-dependence tests were conducted with 30, 40, and 50 lateral nodes and different axial step sizes and it was concluded that the 40 node grid results are virtually grid-independent.

7.0 RESULTS

First, a turbulent round gaseous jet laden with monosize solid particles
is considered. This flow allows the study of the interaction between the two
phases and the particles dispersion due to the turbulence without the
complexity of mass transfer. The predictions are compared with the data of
Modarress et al. (1984) in section 7.1. Since no experimental data exists for
an evaporating spray in the developing region (z/D < 20), the model is
considered to predict an idealized flow of a turbulent round jet laden with
multisize evaporating methanol droplets in section 7.2. Two more cases are
considered in sections 7.3 and 7.4. Both of these two cases are for a Freon-
11 spray issuing from an air atomizing nozzle where experimental data are
available. The first flow is that of Shearer et al. (1979) where the data are
available at distances equal to or greater than 170 nozzle diameters. The
second flow is that of Solomon et al. (1984) where the data are available at
distances equal to or greater than 50 nozzle diameters. In both cases the
predictions are compared with the measurements. Table C-1 (Appendix C)
summarizes the different cases considered in this study.

7.1 The Flow of Modarress et al. (1984)

Modarress et al. (1984) reported much needed experimental data to help
understand the behavior of two-phase turbulent jets and validate their
theoretical models. They investigated the effects of 50 μm and 200 μm glass
particles on the mean air velocity and the turbulent stresses at two different
mass loading ratios, 0.32 and 0.85. Figure 1-2 shows a sketch of the two-
phase turbulent jet considered by Modarress et al. (1984). Air carrying
uniform-size glass particles issues vertically downwards from a cylindrical
pipe of diameter D, 0.2 m. The jet is enclosed in a cylindrical container

with a diameter equal to 30 D to avoid ambient disturbances. An air stream of low velocity surrounds the nozzle and extends to the container wall to provide the required entrained mass by the jet, thus preventing the occurrence of internal circulation in the measurements region. Table C-2 (Appendix C) lists the experimental conditions at 0.1 D downstream of the pipe exit. These values represent the initial conditions for the dependent variables required in the numerical calculations.

In what follows the predicted distributions are compared with the measured distributions of the mean velocities, volume fractions of the two phases, turbulence intensity and shear stress of the gaseous phase and the jet spreading rate. Figures 7-1 and 7-2 show the effects of the particles; mass loading ratio (X_0 = 0.32 versus 0.85) on the mean velocities for 50 μ particles (Case 1 and 2). Figures 7-2 and 7-3 show the effects of the particles; diameter (50 μ versus 200 μ) at almost the same loading ratio (0.8) on the mean velocities of the two phases. First the main effects of the particles on the carrier phase velocity are discussed, then the behavior of the particles' velocity and volume fraction at the different mass loading ratios are discussed.

Figures 7-1 to 7-3 show the radial profiles of the mean axial velocities of the two phases at z/D = 20, normalized by the corresponding mean centerline velocity of the single-phase jet, $U_{z,c.s}$. The flow conditions are those of Cases 1, 2 and 3 in Table C-2 (Appendix C). Also shown is the mean velocity profile of the turbulent single-phase jet having the same Reynolds number (14100) at the pipe exit.

It can be seen from these figures that the mean velocity of the carrier phase is highly affected by the presence of the particles in the inner region, especially at the jet centerline (30% higher than that of the single phase for
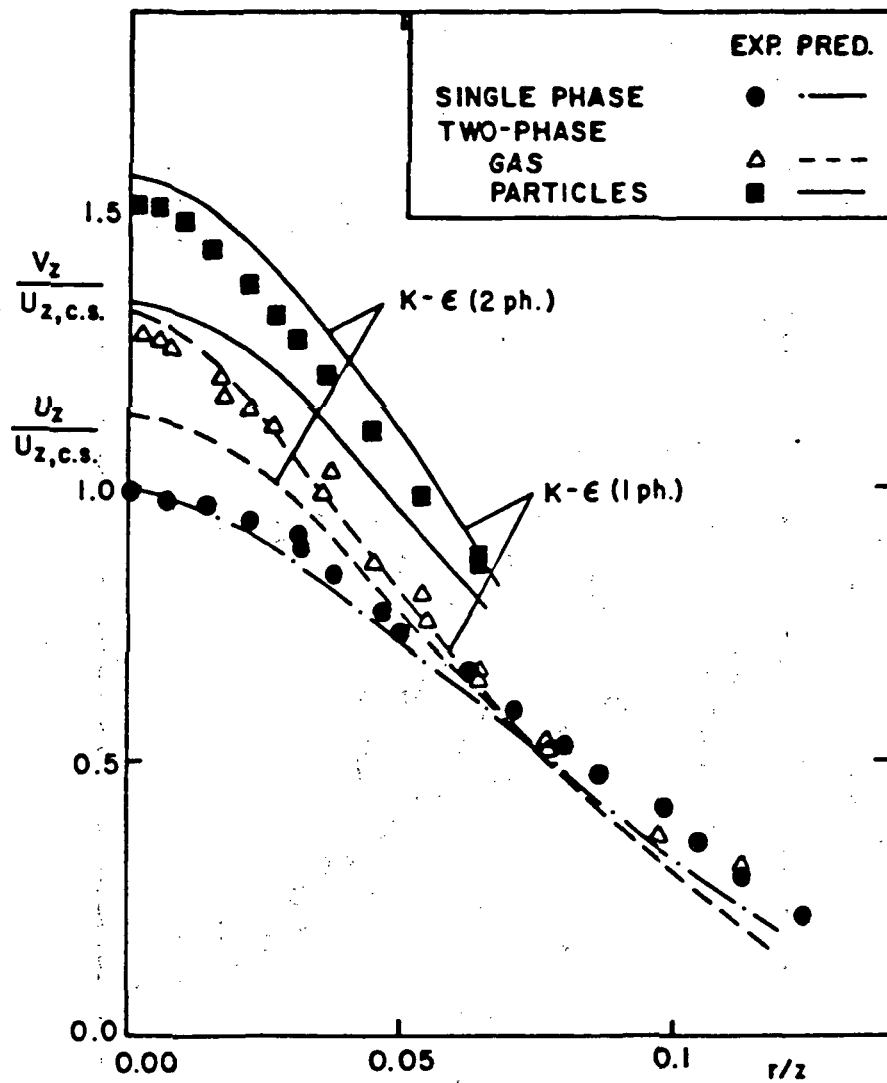
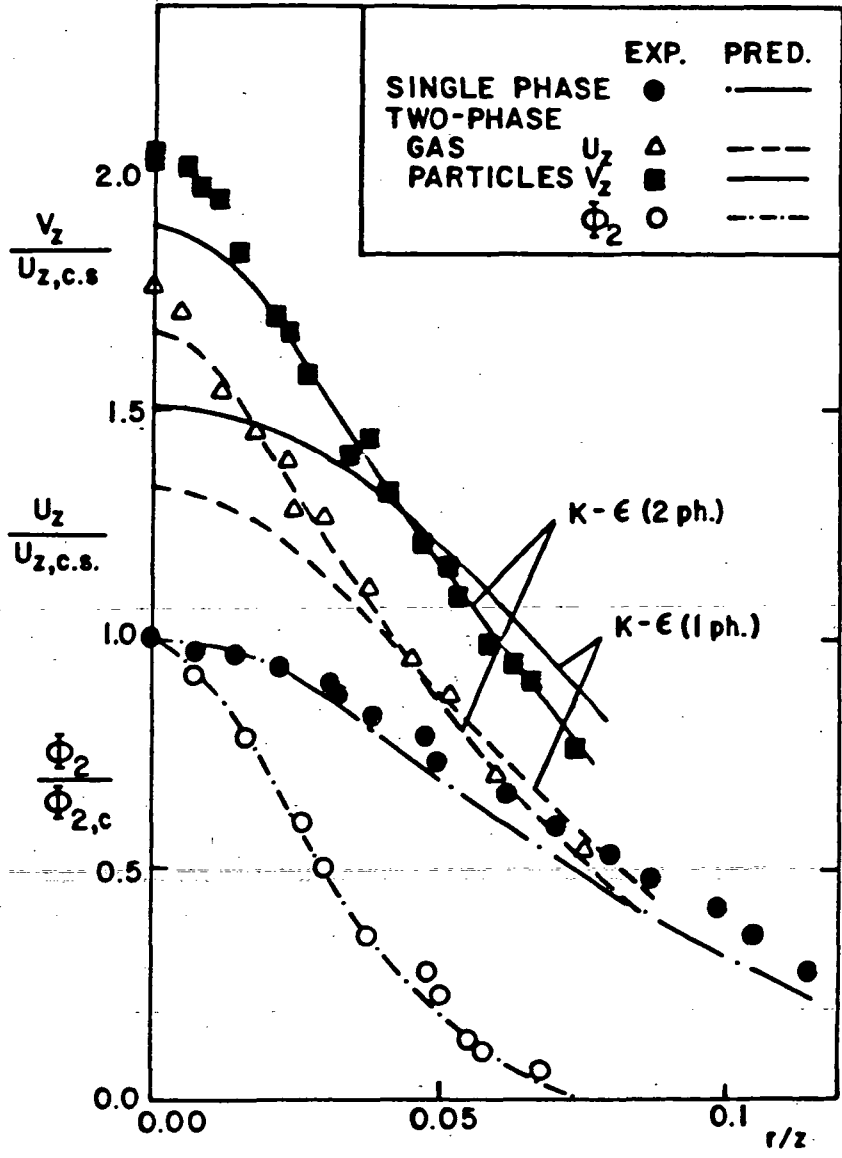FIGURE 7-1 RADIAL DISTRIBUTION OF THE MEAN AXIAL VELOCITIES AT z/D = 20 (CASE I)

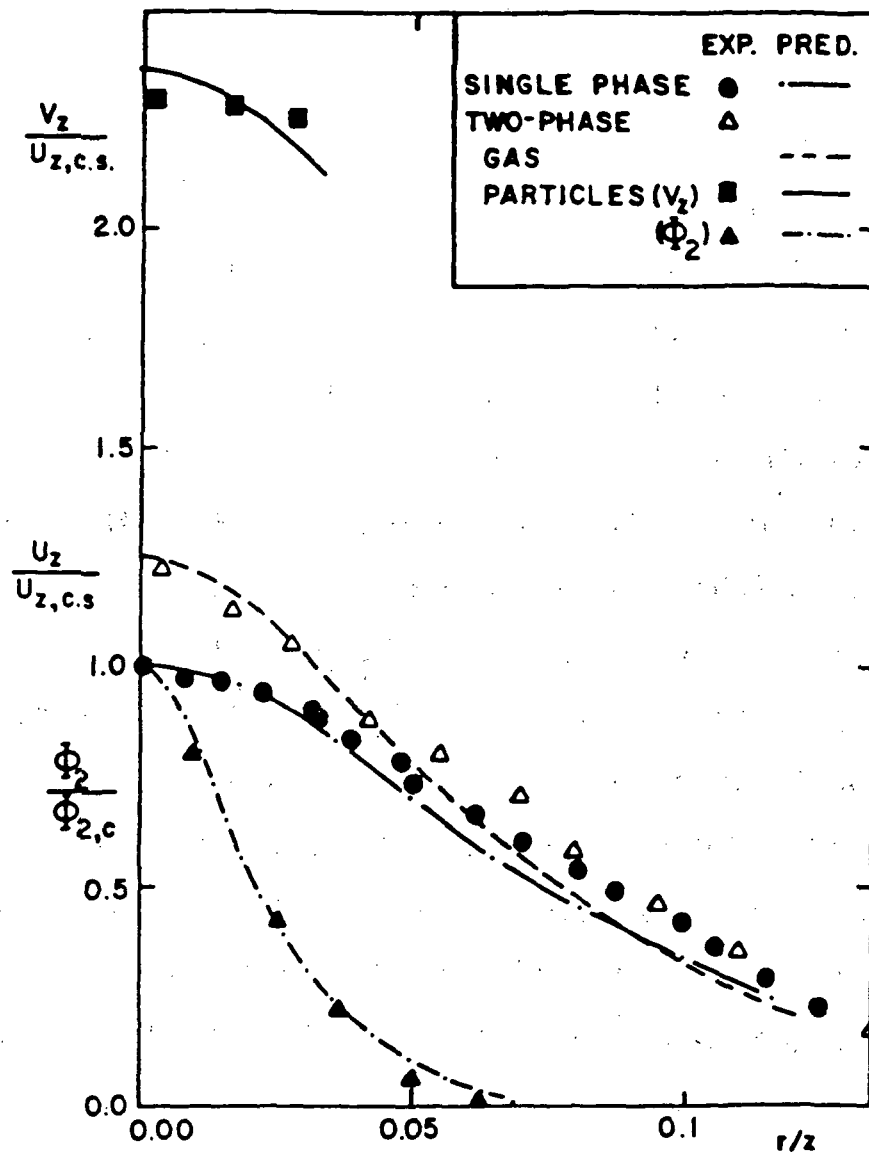FIGURE 7-2 RADIAL DISTRIBUTION OF THE MEAN
AXIAL VELOCITIES AT z/D = 20 (CASE 2)

FIGURE 7-3 RADIAL DISTRIBUTION OF THE MEAN
AXIAL VELOCITIES AT z/D = 20 (CASE 3)

119

Case 1, 75% for Case 2, and 25% for Case 3). This behavior can be explained by the fact that particles are confined to the inner region of the jet. Due to this confinement and the high inertial forces of the particles, their centerline velocity decays with the downstream distance at a slower rate than that of the fluid (see Figure 7-8), and thus they become a source of momentum to the fluid. Also due to the confinement, the number density of the particles which is a strong parameter in the momentum transfer between the particles and the carrier phase at any cross section is maximum at the jet centerline. The confinement of the particles is evident in Figures 7-2 and 7-3 where the concentration of the solid particles vanishes at a radial distance of r/z = 0.06, while the fluid spreads to at least three times this distance. This confinement can be explained by the fact that heavy particles do not respond well to fluid turbulence fluctuations ($v_p \ll v_t$), thus the main force that accelerates the particles in the radial direction is the viscous drag. This drag force is proportional to ($U_r - V_r$), and since U_r is negative in the outer region of the jet and $V_r < U_r$), the resulting force will be directed inwards thereby limiting the radial spread of the particles.

The influence of the loading ratio of the dispersed phase on the mean velocities at z/D = 20 for 50 μ particles is displayed in Figures 7-1 and 7-2. The inlet conditions for the two cases (1 and 2) are identical except for the loading ratio. By increasing the loading ratio from 0.32 (Case 1) to 0.85 (Case 2) the carrier phase velocity at the centerline increases from 30% to 75% relative to the corresponding velocity of the single-phase jet. It can be seen also from those two figures that the ratio between the centerline velocity of the dispersed phase to that of the single phase is 1.5 for Case 1 and 2 for Case 2. This can be explained by the fact that the initial momentum of the dispersed phase is proportional to the mass flow rate of that phase

since they have the same velocity distribution. Therefore, the initial momentum of the dispersed phase for Case 1 is about 2.7 times that for Case 2. This enhances the momentum transfer from the particles to the air, thereby enhancing the increase in the axial velocity of the latter compared with that of the single phase. Now, since the axial air velocity at any point on the jet axis at the higher loading case is greater than the corresponding value at the lower loading case, the momentum drain from the particles is expected to be inversely proportional to the particles' loading ratio. This explains the higher centerline velocity of the particles at the higher mass loading ratio.

The influence of the particles' diameter of the dispersed phase on the mean velocities at $z/D = 20$ is displayed in Figures 7-2 and 7-3 (Cases 2 and 3). The main difference between the two cases is the particle diameter, so any quantitative change in the mean velocity profiles is attributed to two factors: 1) the interphase surface area or the momentum exchange coefficient, and hence the source terms of the momentum equations, and the K and ϵ equations; 2) the particles' response to the turbulent fluctuations, thus the additional turbulence dissipation caused by the fluctuating particle slip velocity and its correlation with the fluid velocity fluctuation. The surface area in Case 2 is four times that in Case 3, since, for nearly the same loading ratio, the number of the 50 μ particles is 64 times that of the 200 μ particles. This increase in the number of particles or the interphase area results in augmenting the momentum source of the carrier fluid consequently reducing the rate of decay of its centerline velocity (see Figure 7-8).

Figure 7-4 shows the reduction in the shear stress due to the existence of the particles with the air in the same control volume for 50 μ and 200 μ particles. Due to the reduction in the turbulence kinetic energy
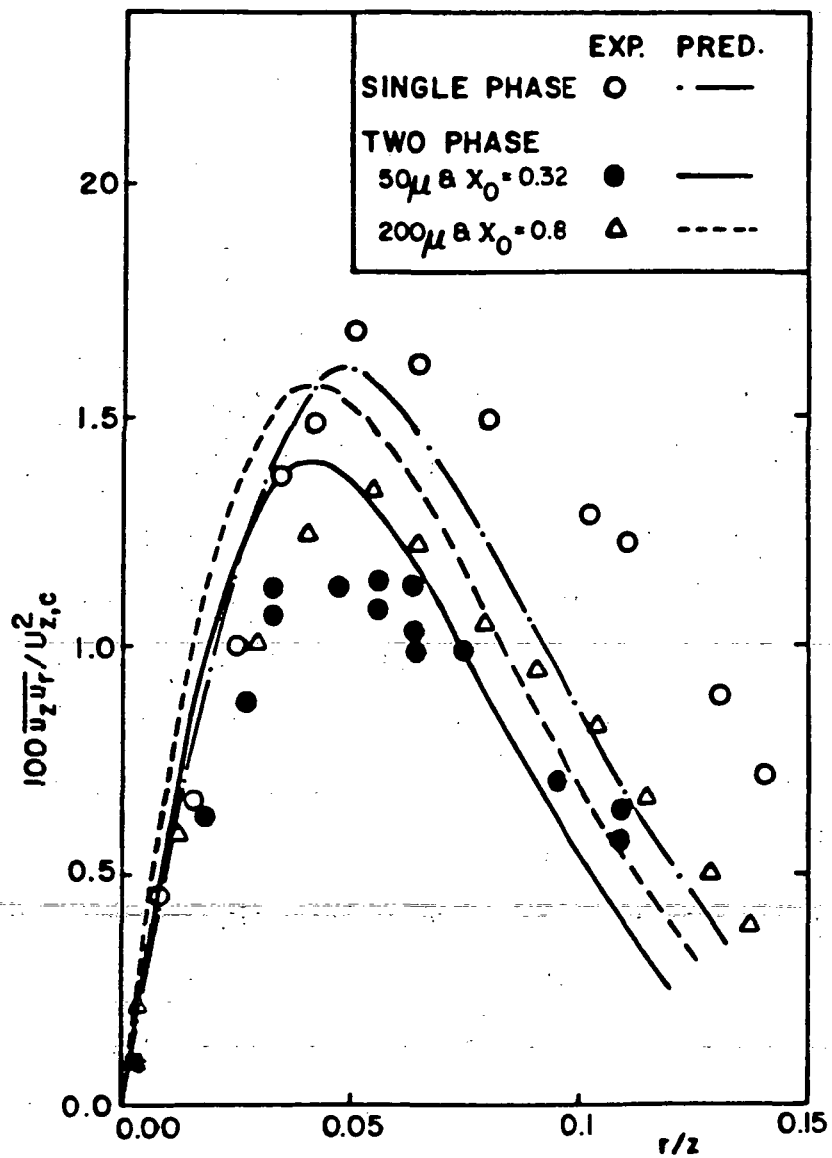
121

FIGURE 7-4 RADIAL DISTRIBUTION OF THE SHEAR STRESS AT z/D = 20 (SOLID PARTICLES)

compared with that of the single phase, which is associated with additional turbulence dissipation, the carrier phase momentum diffusivity is reduced. Figure 7-4 shows that the reduction in the shear stress for 50 μ particles is greater than that of 200 μ particles. This reduction in the turbulent diffusion coefficient reduces the rate of decay of the centerline air mean velocity (see Figure 7-8).

It is also clear from Figures 7-1, 7-2, and 7-3 that the single-phase jet is wider than the particle-laden jet; this will be discussed later in this section. Figures 7-1, 7-2, and 7-3 display in general good agreement between the measured and predicted velocity and concentration profiles.

In order to distinguish between the dispersed phase effects on the mean motion (inertia and drag) and on turbulence (diffusion), the mean velocity profiles obtained by solving the governing equations for the mean motions (Equations 3.26 to 3.33 together with the single-phase K and ε equations (i.e., Equations 3.34 and 3.35 without the additional production and dissipation terms due to the dispersed phase) are shown in Figure 7-1 and 7-2. The resulting increase in the fluid centerline velocity, as compared with that of the single-phase jet, is only half that measured and predicted by the new K-ε model. Stated differently, the modulation of the fluid mean velocity profile by the dispersed phase is not only due to the particles' inertia and drag but equally due to the additional turbulence dissipation. This in turn reduces the fluid momentum diffusivity resulting in a peaked velocity profile near the jet centerline. The additional turbulence dissipation is caused mainly by the fluctuating particle slip velocity and its correlation with the fluid velocity fluctuation that appeared in Equations 3.34 and 3.35. The consequent reduction in the fluid turbulence intensity and shear stress is displayed in Figures 7-4 and 7-5 where the agreement between the measurement
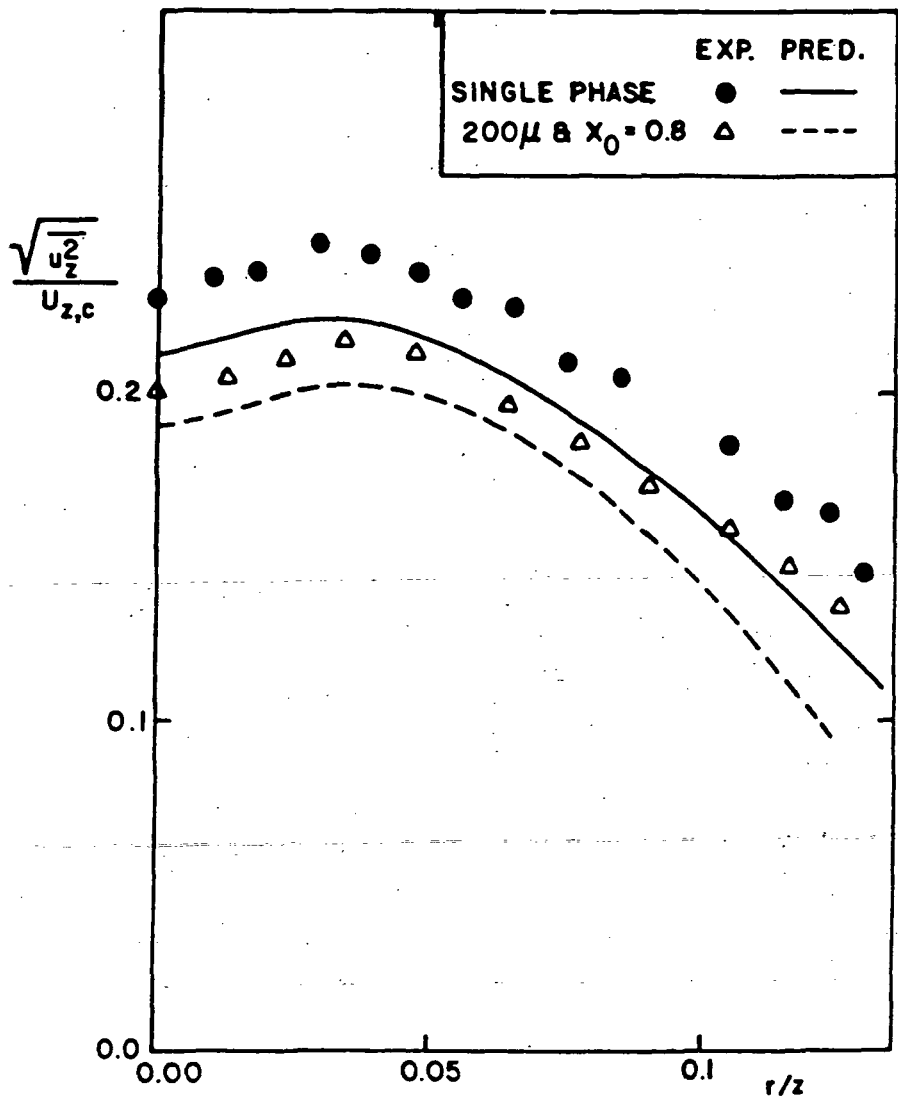
123

FIGURE 7-5 TURBULENCE INTENSITY DISTRIBUTION
(CASE 3)

and prediction is good.

Figure 7-6 compares the concentration distribution of 50 μ particles (Case 2) with that of 200 μ (Case 3) particles. Since the mass eddy diffusivity is inversely proportional to $(\vec{U}-\vec{V})^2/\bar{v}^2$ (Equation 5.30), it is consequently higher for the 200 μ than that of the 50 μ particles, so one would expect that the particles of 50 μ will diffuse in the radial direction more than the of 200 μ. This is evident in Figure 7-6 where the agreement between the measurement and prediction is good.

Figure 7-7 shows the effect of the dispersed phase on the spreading rate of the jet by comparing the different $Y_{1/2}$ - z distributions of the three cases, where $Y_{1/2}$ is the radius at which the fluid mean axial velocity is half that at the centerline. While for a turbulent single-phase jet the value of the slope $(dY_{1/2}/dz)$ is constant ($\simeq 0.08$), the value for a two-phase jet is a function of the dispersed phase properties such as particle diameter and density and loading ratio. This dependence is displayed in Figure 7-7. For Case 3 (d = 200 μ, X_o = 0.8) the predicted slope value is 0.053, for Case 2 (d = 50 μ, X_o = 0.85) it is 0.046, and for Case 1 (d = 50 μ, X_o = 0.32) it is 0.064. Cases 3 and 2 have nearly the same loading ratio but the particle diameter in the latter is one quarter that of the former, the result being a reduction of the spreading rate by more than 13%.

Figure 7-7 also shows the discrepancy that results in predicting the spreading rate if the single-phase K-ε model is used instead of the proposed model. The former predicts for Case 1 a slope of 0.072 while the latter agrees with the experimental value of 0.064. As explained earlier this is due to the fact that the additional dissipation of turbulence energy as a result of the dispersed phase is accounted for in the proposed model.

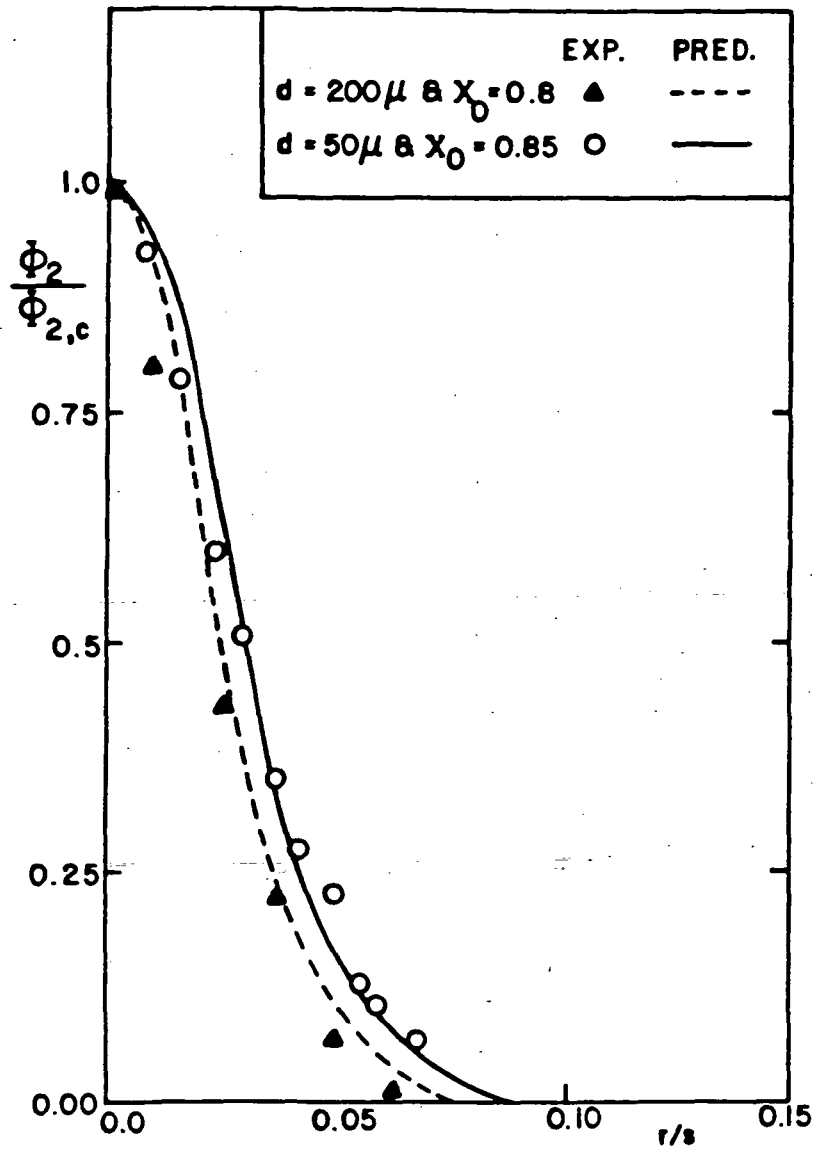Figure 7-8 shows the decay of the mean centerline velocities of the two

FIGURE 7-6 RADIAL DISTRIBUTION OF THE
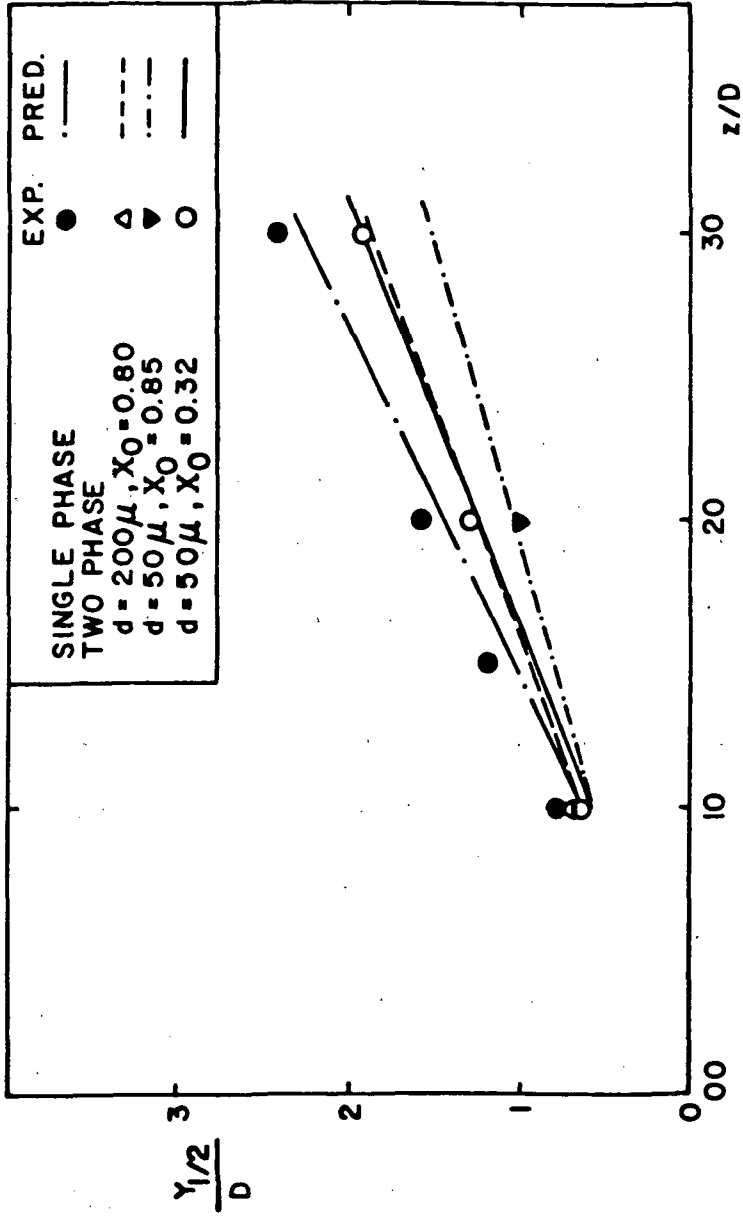PARTICLES VOLUME FRACTION AT z/D = 20
(SOLID PARTICLES)

126

FIGURE 7-7 THE DISTRIBUTION OF JET SPREAD RATES
(SOLID PARTICLES)

127

phases for Cases 1 and 3 compared with the single-phase values. Here $U_{z,o}$ is the carrier-phase centerline velocity at the pipe exit. It can be seen from Figure 7-8 that the two phases reach a local equilibrium situation, equal velocities, at about 10 pipe diameters and after that the relative velocity between the two phases along the jet centerline increases by increasing the downstream distance from the pipe exit. This behavior was previously analyzed in the discussion of Figures 7-1 through 7-3.

7.2 The Methanol Spray

The flow considered in the present study is identical to the flow of Modarress et al. (1984) except that the solid spheres are replaced by methanol droplets of a given size distribution at the exit of the pipe (Figure 1-2). The goal here is to mimic the flow of an idealized spray that has well-defined initial conditions. In the present study the good agreement between prediction and experimental data in the cases of a round gaseous jet laden with solid particles allows the use the of the latter while adding the complexity of mass transfer and the resulting size changes in the same jet.

A turbulent round jet laden with multisize evaporating liquid droplets is considered in this section. Atmospheric air carrying methanol liquid droplets of diameters 100, 80, 60, 40 and 20 μm issues vertically downwards from a cylindrical pipe of diameter D (= 0.02 m). The initial mean velocity and the turbulence intensity distributions are assumed to be those of the fully developed pipe flow as in the work of Modarress et al. (1984). The ratio between the velocity of the dispersed phase to that of the carrier phase at the centerline is equal to 0.7. The carrier fluid Reynolds number is equal to 30,000. The temperature of methanol droplets is assumed to be uniform at the steady state saturation conditions. The initial mass flow rates of the
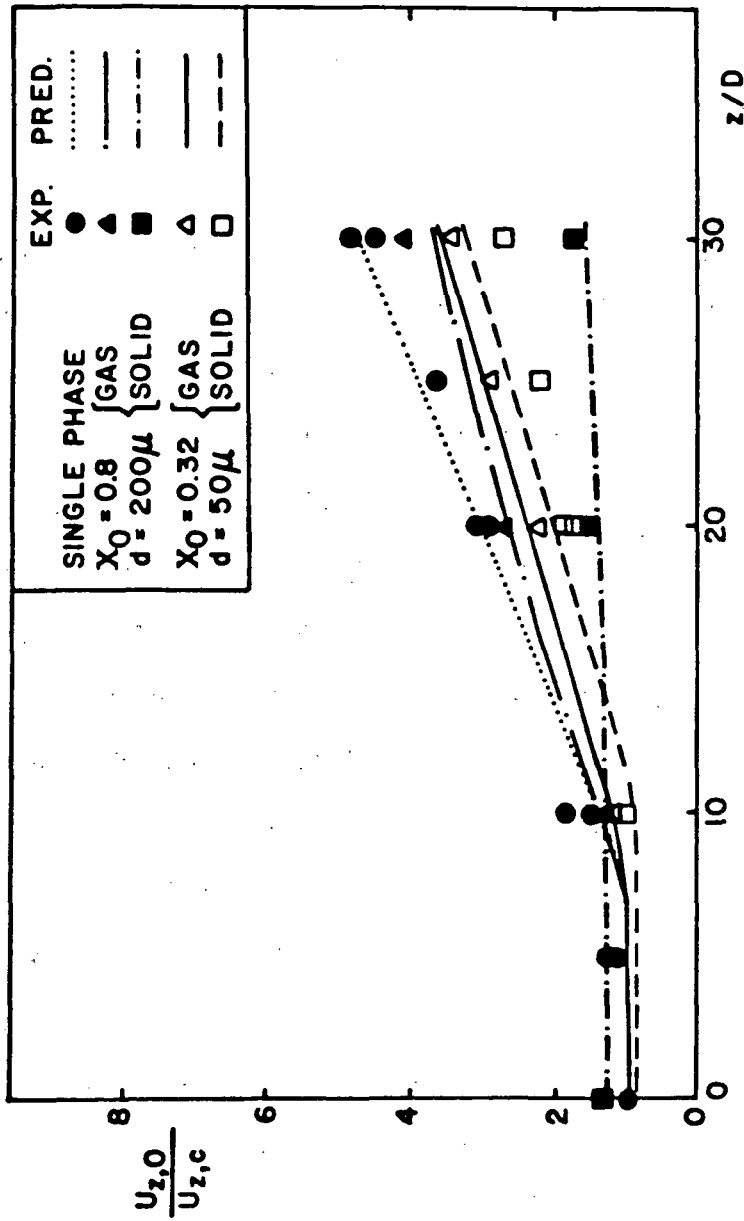
FIGURE 7-8 THE DISTRIBUTION OF THE CENTER LINE
VELOCITIES (SOLID PARTICLES)

different size groups are assumed to be equal and have a plug profile for volume fractions. Three different mass loading ratios of 0.1, 0.25, and 0.5 (Case 6) are considered.

In what follows, the predicted mean velocities, volume fractions of each phase, turbulence intensity, and shear stress of the carrier phase under the three mass loading ratios are presented.

The normalized radial profiles of the mean quantities of the different phases at 20 pipe diameters from the exit plane at $X_0 = 0.5$ are shown in Figure 7-9. The mean velocities of the carrier phase and those of the five groups ($k = 1,2,...,5$) of droplets are normalized by the centerline velocity of the single phase jet, $U_{z,c.s.}$. Here $k = 1$ refers to the group that has the largest diameters, and $k = 5$ the smallest ones. It can be seen from this figure, as one expected, that the difference between the velocity of the carrier phase and that of the largest diameter group is greater than that of any other group. This is attributed to the balance between the inertia of the droplet and the momentum exchange force. The inertia force is proportional to $(d^k)^3$ whereas the momentum exchange force is proportional to the droplet diameter with an exponent ranging from 1 to 1.7 (for a Reynolds number less than 100). If all the turbulent correlations in Equation 3.31 due to their small values compared with the mean momentum exchange term are now dropped, the equation becomes independent of ϕ^k. If the droplet size is then increased, the inertia becomes much greater than the momentum exchange force, and as a result the relative velocity between the droplets and the carrier phase ($U_z - V_z^k$) increases. The volume fraction profile of each group normalized by the centerline value of the first group is shown also in Figure 7-9. Since the reduction rate of the droplet diameter due to the evaporation process is inversely proportional to the square of the diameter, the smaller the droplet
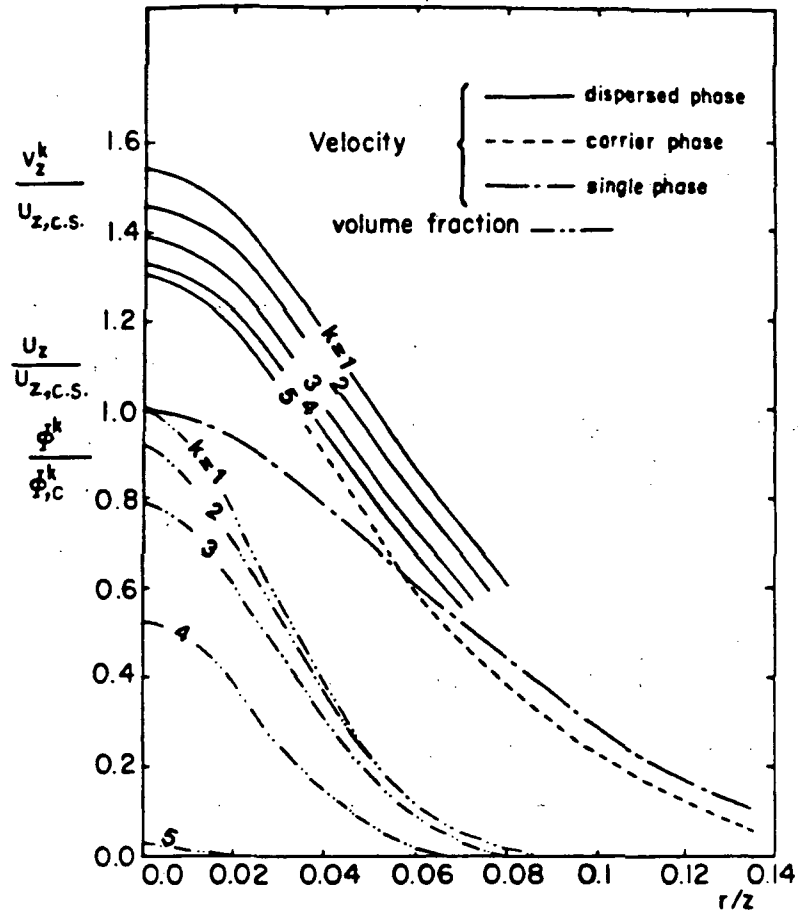
FIGURE 7-9 RADIAL DISTRIBUTION OF THE NORMALIZED
MEAN VELOCITIES AND VOLUME FRACTIONS AT $z/D = 20$
AND AT $X_o = 0.5$ (CASE 4)

diameter is, the more reduction in the volume fraction. Figure 7-9 also shows that the smaller the mean droplet diameter is, the less peaked the volume fraction profile of its group. This is attributed to the turbulent diffusion coefficient (v_p^k) of the droplet which decreases with the increase of the relative velocity or the droplet diameter (Equation 5.30). It can also be seen from Figure 7-9 that the mean velocity of the carrier phase is affected by the presence of the dispersed phase especially in the inner region. Elghobashi et al. (1983) discussed in detail how the entrainment and the negative radial velocity of the carrier phase in the jet outer region influence the volume fraction distribution of the dispersed phase. They showed that the entrainment flow creates an inward force exerted on the droplets towards the jet centerline. This force combined with the small turbulent diffusivity of the droplets, compared with that of the carrier phase, renders the volume fraction profile of the dispersed phase significantly narrower than the velocity profile of the carrier phase. Since the momentum exchange between the two phases is a linear function of the droplets volume fraction, it could be expected, that the momentum transfer to the carrier phase is maximum at the jet centerline. At the same time the reduction in the turbulence kinetic energy of the carrier phase and the increase of the dissipation rate of that energy due to the presence of the dispersed phase in the same control volume lead to a less turbulent diffusion coefficient for the carrier phase and hence a less radial diffusion of that phase compared with the single phase. These two factors make the velocity of the carrier phase at the jet centerline much greater than that of the single-phase jet (30% higher) and less than its corresponding value in the jet outer region.

The influence of the loading ratio of the dispersed phase on the carrier

132

fluid turbulence intensity and shear stress is displayed in Figures 7-10 and
7-11. The reduction in the turbulence energy or the increase in the
dissipation rate of that energy is caused by the fluctuating relative velocity
between the droplets and the carrier phase and the turbulent correlation
between this velocity and other fluctuating quantities, volume fractions and
carrier fluid velocity. It can be stated that the reduction in the turbulence
intensity and the shear stress is proportional to the mass loading ratio but
not linearly.

The concentration of the evaporated material in the carrier phase is
shown in Figure 7-12 at two different axial locations (z/D = 10 & 30) and at
X_0 = 0.5. Due to the continuous air entrainment by the jet and the turbulent
diffusion of the vapor, the concentration of the evaporating material in the
carrier fluid at z/D = 30 is less than the corresponding values at z/D = 10 at
the same distance from the jet axis, although the total evaporated mass
increases with downstream distance. This is also true even at the jet
centerline as will be seen in the discussion of Figure 7-15.

It can be seen from Figure 7-12 that C is minimum in the jet outer region
and maximum at the jet centerline. Since C_L, according to the assumption of
this study and the droplets' material, has a constant value of 0.12, the
transfer number (Equation 3.42) is maximum in the outer region of the jet.
Therefore, the diminution rate of the droplet diameter is greater in the outer
than in the inner region.

Figure 7-13 shows the centerline decay of the mean axial velocities of
the different groups and the carrier phase compared with the single phase
values for X_0 = 0.5. Here $U_{z,o}$ is the carrier-phase centerline velocity at
the pipe exit. It can be seen that the relative velocity between the droplets
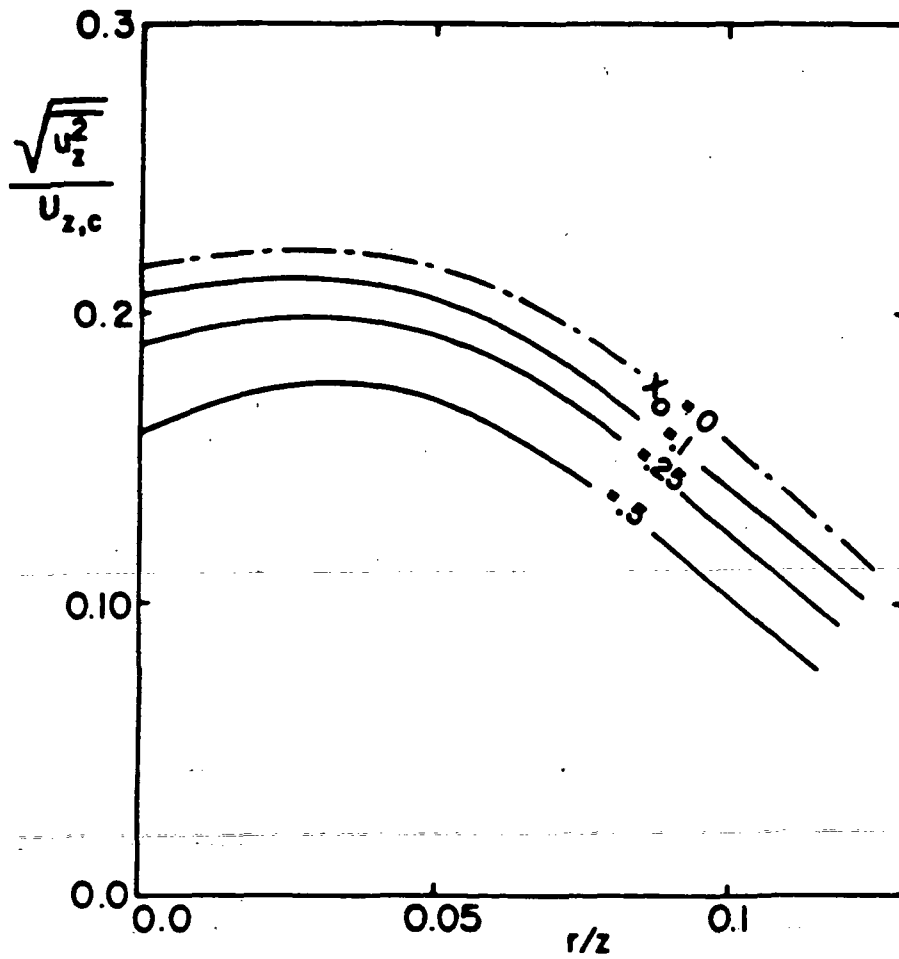and the carrier phase or the disequilibrium of the flow along the jet

FIGURE 7-10 RADIAL VARIATION OF THE TURBULENCE
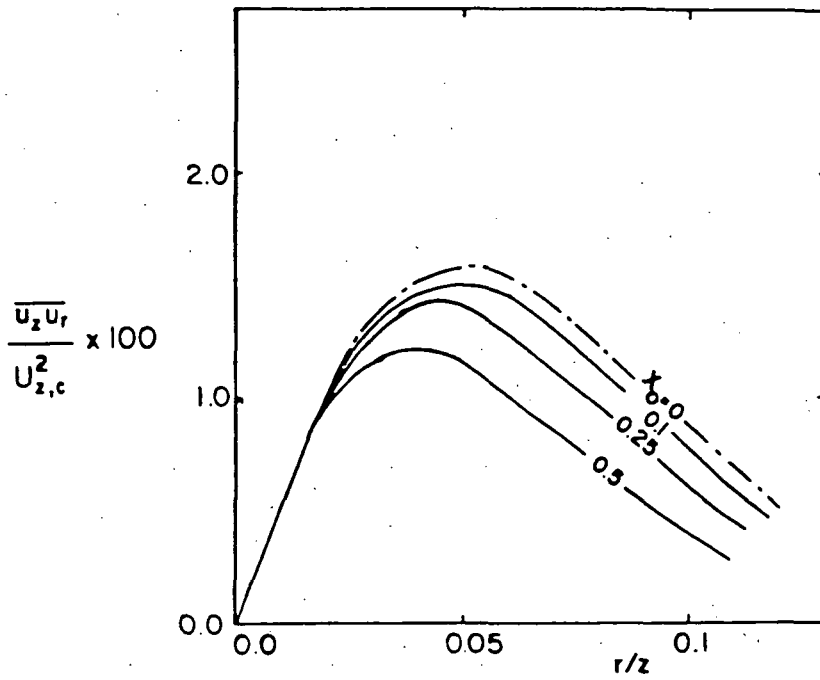INTENSITY WITH X_0 AT $z/D=20$ (CASE 4)

$$\frac{\overline{u_z u_r}}{U_{z,c}^2} \times 100$$

FIGURE 7-11 RADIAL VARIATION OF THE SHEAR
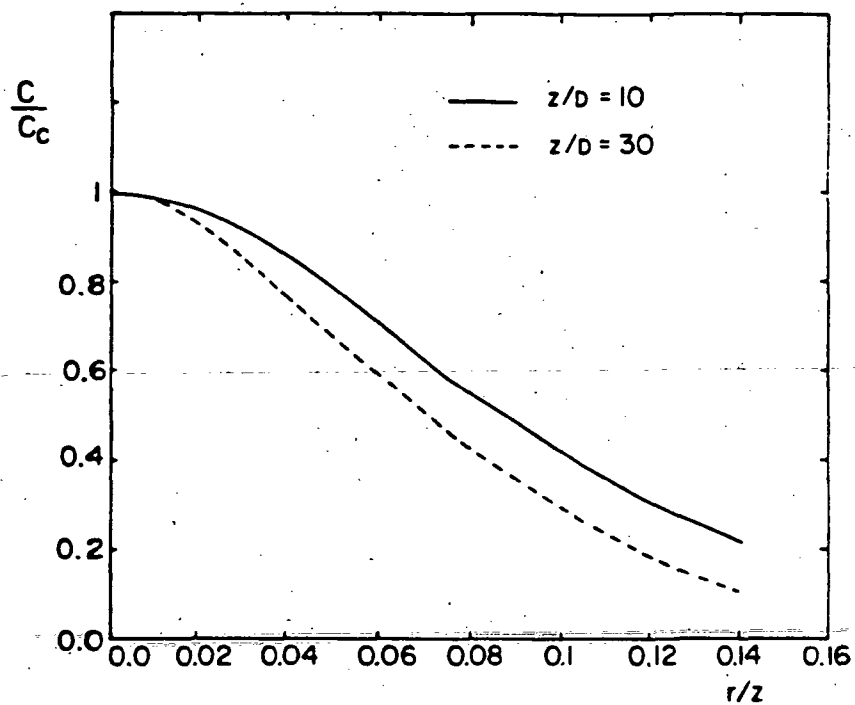STRESS WITH X_o AT $z/D = 20$ (CASE 4)

FIGURE 7-12 RADIAL DISTRIBUTION OF THE
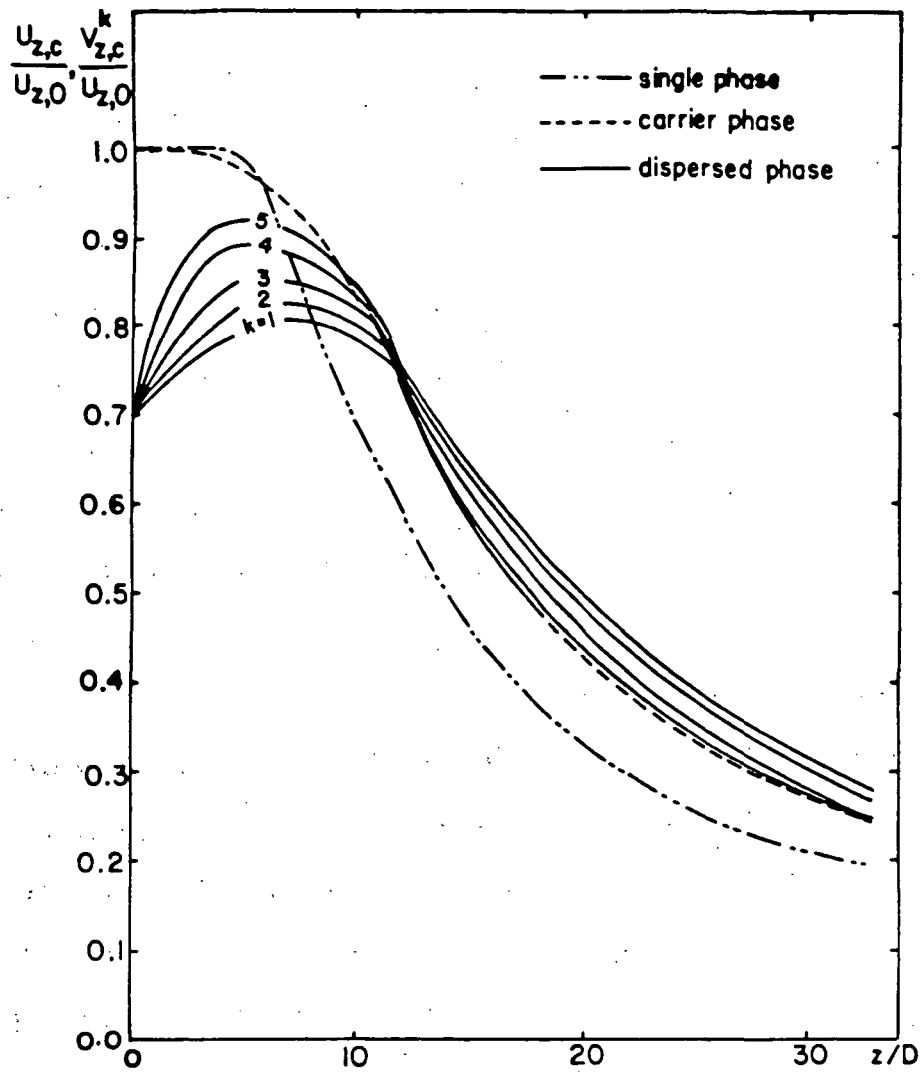VAPOR CONCENTRATION (CASE 4)

FIGURE 7-13 AXIAL DISTRIBUTION OF THE MEAN VELOCITIES
AT $X_0 = 0.5$ (CASE 4)

centerline, increases with increasing the droplet's diameter. It is worth noting that the carrier-phase centerline velocity is about 30% higher than the corresponding value of the single phase in the range $7 < z/D < 30$ as previously discussed.

Figure 7-14 exhibits the centerline decay of the volume fraction and mean droplet diameter based on the total surface area of the droplets for the five groups. The mean diameter is a quantity that is not used in any calculations but facilitates the display and discussion of the results. In the present work, it was possible to calculate the local diameter distribution within each group, thus from the maximum and minimum diameters at any station and the number of sizes to be solved, the diameter range for each group can be fixed (e.g., at $z/D = 10$, group $k = 1$ contains droplets ranging from 95 to 78 microns). It can be seen from Figures 7-9 and 7-14 that the smaller the droplet diameter is, the higher the evaporation rate, hence the rapid decay of the volume fraction and the mean diameter.

Figure 7-15 shows the axial distribution of the total volume fraction of the droplets and the centerline concentration of the methanol vapor in the carrier phase (C_c) for different mass loading ratios. Here $\phi_{2,c}/\phi_{2,o}$ is the total volume fraction of the dispersed phase at the centerline divided by that value at the pipe exit. The concentration of the evaporated material in the carrier phase first increases until $z/D = 10$ then monotonically decreases due to the continuous air entrainment by the jet and turbulent diffusion of the vapor.

The variation of the maximum turbulence intensity and maximum shear stress of the carrier phase with the axial distance is displayed in Figures 7-16 and 7-17 for the different mass loading ratios. It can be seen that the reduction in the turbulence quantities is proportional to the mass loading
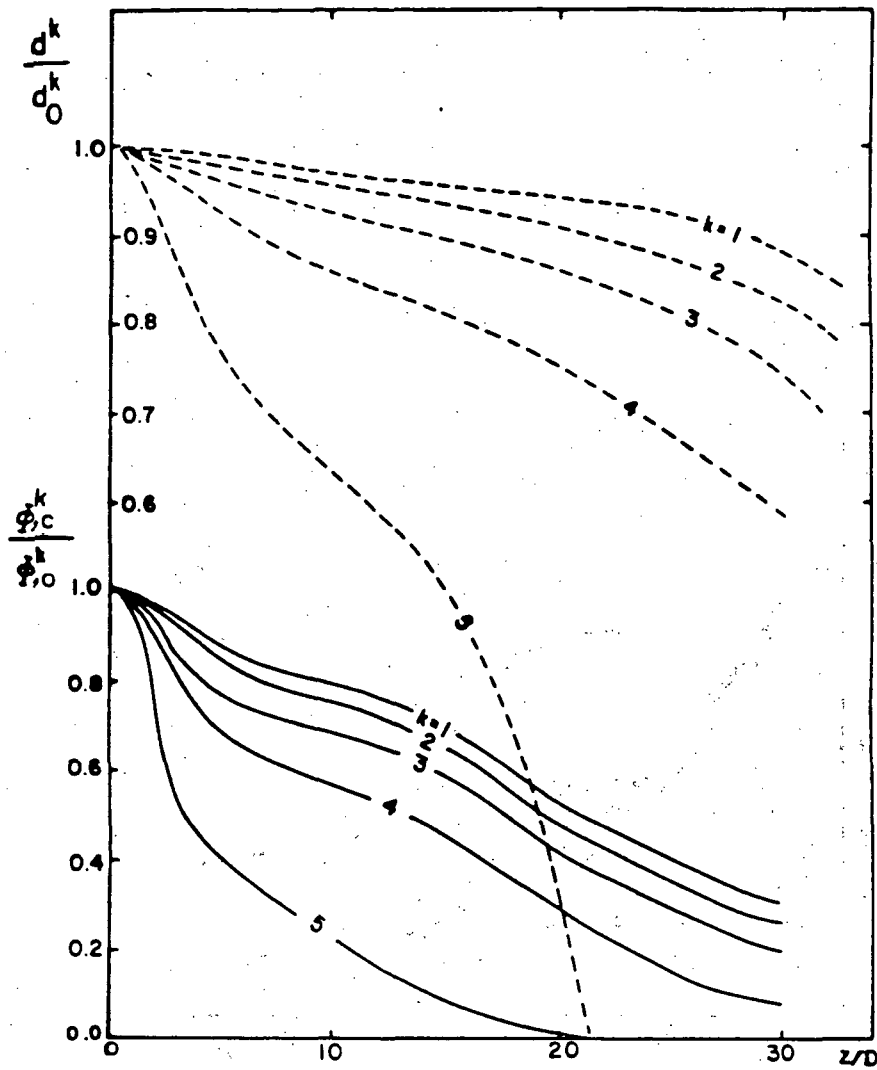
FIGURE 7-14 AXIAL VARIATION OF THE VOLUME FRACTIONS
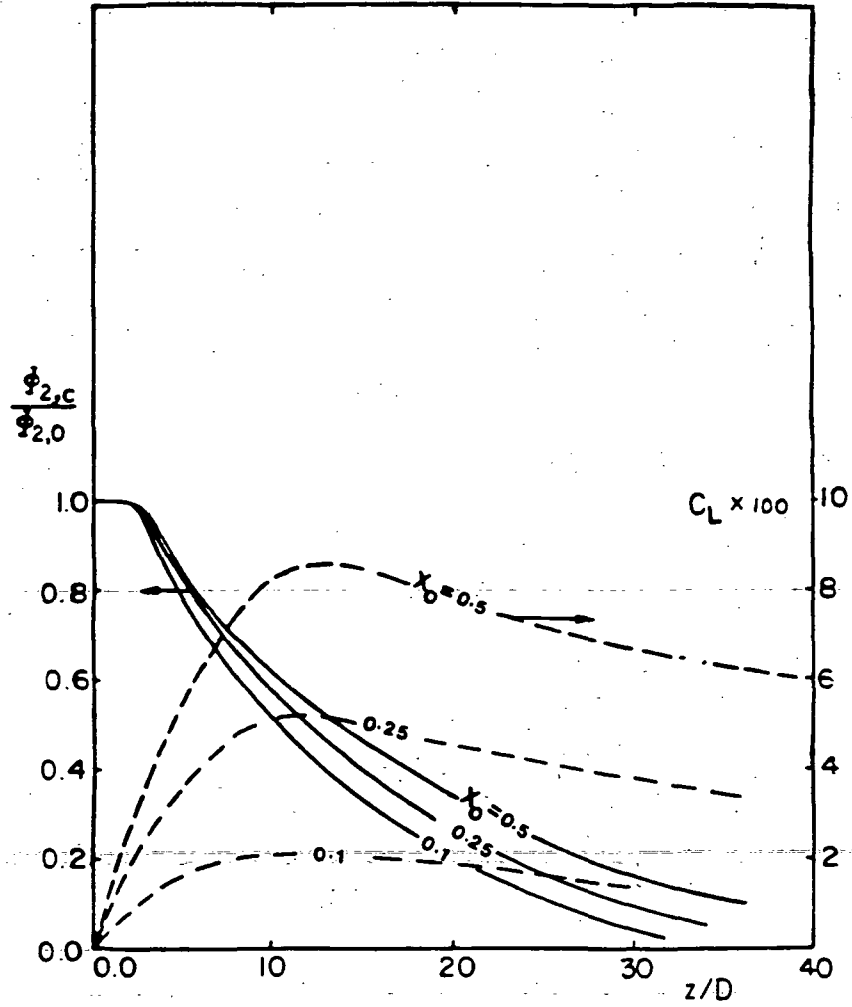AND THE AVERAGE DIAMETERS AT $X_0 = 0.5$ (CASE 4)

FIGURE 7-15 AXIAL VARIATION OF THE DROPLETS VOLUME

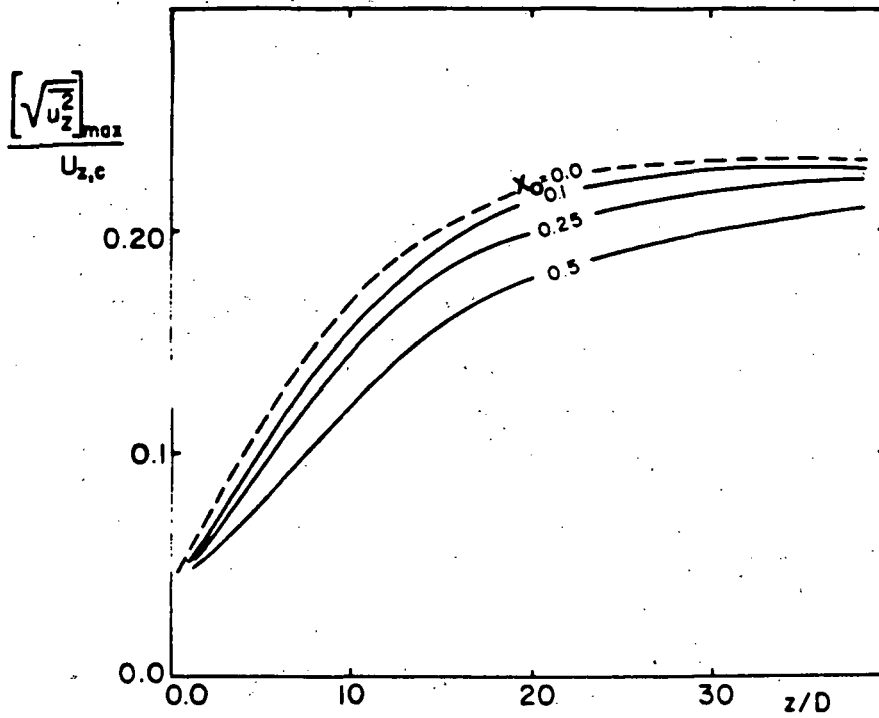FRACTION AND VAPOR CONCENTRATION WITH X_0 (CASE 4)

FIGURE 7-16 AXIAL VARIATION OF THE MAXIMUM
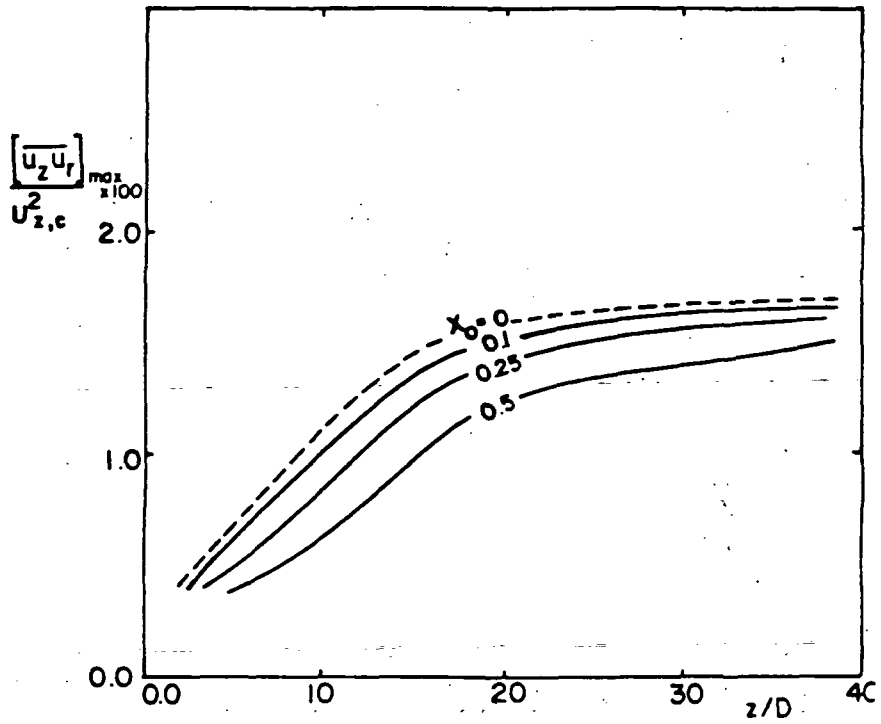TURBULENCE INTENSITY WITH X_o (CASE 4)

FIGURE 7-17 AXIAL VARIATION OF THE MAXIMUM
SHEAR STRESS WITH X_o (CASE 4)

ratio but again not linearly. These two figures also show that farther downstream from the pipe exit, the turbulence quantities are approaching their values for a single-phase jet due to the continuous diminution of the droplets' volume fraction.

The rate of evaporation is a function of both the transfer number and droplet Reynolds number, which are maximum in the outer region and minimum at the centerline. So the rate of evaporation is maximum in the outer region or the minimum droplet diameter. This explains the radial distribution of the droplet diameter at the various sections as shown in Figure 7-18. Also displayed is the monotonic reduction in droplet diameters with distance downstream for the five groups.

Figure 7-19 shows the effect of the evaporating spray on the spreading rate of the jet by comparing the different $Y_{1/2} \sim z$ distribution, where $Y_{1/2}$ is the radius at which the carrier-fluid mean axial velocity is half its value at the centerline. While for a turbulent-single phase jet the value of the slope $(dY_{1/2}/dz)$ is constant ($\simeq 0.08$), that for a two-phase jet is a function of the dispersed phase properties such as droplet diameter, density and mass loading ratio. This dependence was discussed in the work of Mostafa and Elghobashi (1983). In the developing region, the spreading rate of the spray case is much less than that of the single phase. As vaporization proceeds the effects of the droplets on the carrier fluid diminish allowing the fluid behavior to approach that of a single-phase jet.

7.3 The Flow of Shearer et al. (1979)

Shearer et al. (1979) measured the carrier phase properties in a turbulent two-phase round jet using a laser doppler anemometer, the droplet size distribution and the liquid mass flux using the inertial impaction
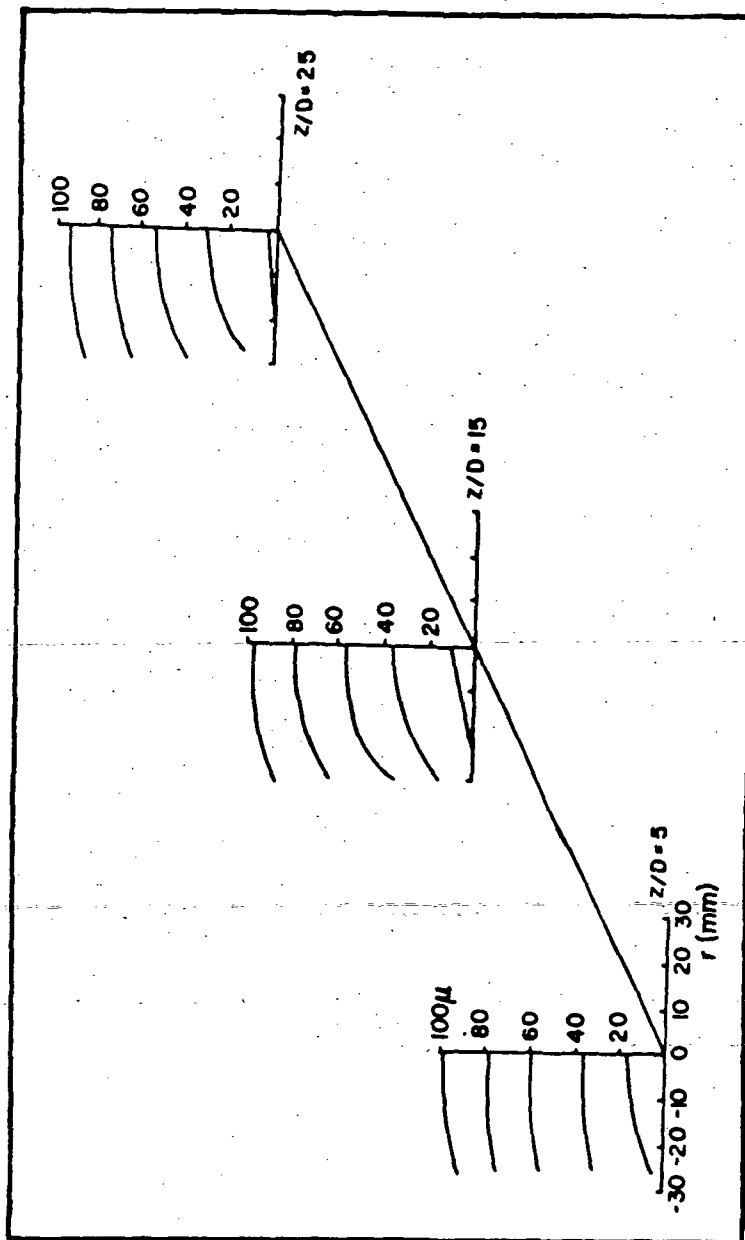
FIGURE 7-18 AXIAL DISTRIBUTION OF THE LOCAL DROPLET DIAMETERS
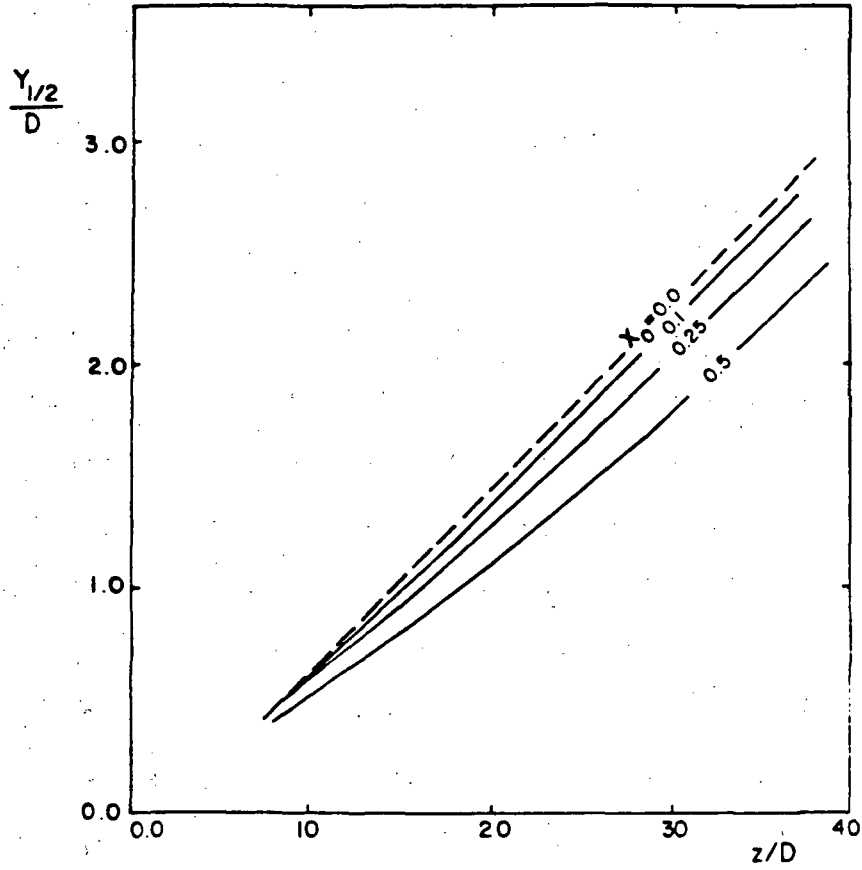
AT DIFFERENT AXIAL LOCATIONS (CASE 4)

144

FIGURE 7-19 SPREADING RATE UNDER DIFFERENT MASS LOADING RATIOS (CASE 4)

method. The Freon-11 spray was generated by an air-atomizing nozzle of 1.194 mm outer diameter (D). The ratio of the mass flow rate of Freon-11 spray at the nozzle exit to that of the air (X_o) is equal to 6.88 and the initial average velocity, $U_{z,o} = 74.45$ m/s. They also measured the mean mixture fraction by isokinetically sampling the flow at the gas velocity. Shearer et al. (1979) measured the radial profiles of the mean and rms velocity, and the Reynolds stress at three stations (z/D = 170, 340, and 510) for both isothermal single- phase and vaporizing spray jet flows. For computational purposes, the profiles of turbulence dissipation rate (ϵ) at z/D = 170 are obtained from the shear stress measurements and the axial velocity gradient at the same station (z/D = 170). Also, the velocity distribution of the droplets (one group with an average diameter = 27 μm) is assumed to be the same as that of the carrier phase. This assumption will be discussed at the end of the next section. From the measurements of the droplets' mass flux and velocity distribution, the volume fraction (Φ_2) is obtained. The profile of the freon vapor concentration in the carrier phase (C) is obtained from the mixture fraction measurements and the state relations given by Shearer (1979). Table C-3 (Appendix C) summarizes all the starting profiles needed for the computation for both the single-phase jet and the evaporating spray cases.

Temperature measurements of the carrier phase (with a bare wire chromelalumel thermocouple) showed only 5°C difference either in the radial or the axial directions (between z/D = 170 & 510). On the other hand, Shearer's analysis (1979) showed that the droplet's temperature at z/D = 170 is equal to the Freon's saturation temperature (240.3°K). In the present calculations it was assumed that the temperature of the carrier phase is equal to the surrounding air temperature (296°K) and the droplet's surface temperature is equal to the saturation one (240.3°K). At these conditions, the density of

146

the liquid Freon-11 is equal to 1518 Kg/m^3 and the vapor concentration at the droplet's surface (C_L in Equation 3.42) is equal to 0.292. In what follows we compare the predicted with the measured distributions of the mean velocity and shear stress of the carrier phase at z/D = 340 and 510.

Figure 7-20 shows the measured and predicted centerline decay of the mean axial velocity of the carrier phase compared with the single-phase values. Due to the fact that the inertia of the droplets is much greater than that of the carrier phase (ρ_2/ρ_1 = 1500) , the centerline velocities of the droplets in the region z/D < 170 are greater than those of the gas. As a result, the centerline velocity of the carrier phase would be expected to be greater than that of the single phase. This is due to 1) the continuous momentum transfer from the droplets to the gas since $V_{z,c}$ is greater than $U_{z,c}$ in the region close to the nozzle (z/D < 170) and 2) the reduction of the turbulence intensity (and hence turbulent diffusion) in the spray case compared with that of the single-phase jet (as will be seen later in Figures 7-23 and 7-24).

Figures 7-21 and 7-22 show the normalized radial profiles of the mean axial velocities at 340 and 510 nozzle diameters from the exit plane for both the single-phase jet and the evaporating spray cases. It can be seen from these figures that the jet width in the spray case is narrower than the single-phase one. This result can be attributed to the increase of the centerline velocity of the carrier phase compared with its corresponding value in the single-phase jet. The experimental data show that with increasing the distance downstream from the nozzle exit, the jet behavior approaches that of the single phase (Figure 7-22). The effect of the droplets on the radial shear stress distribution is displayed in Figures 7-23 and 7-24. It should be noted that the starting values of the turbulence quantities and mean velocity distribution of the vaporizing spray case differ (less shear stress) from
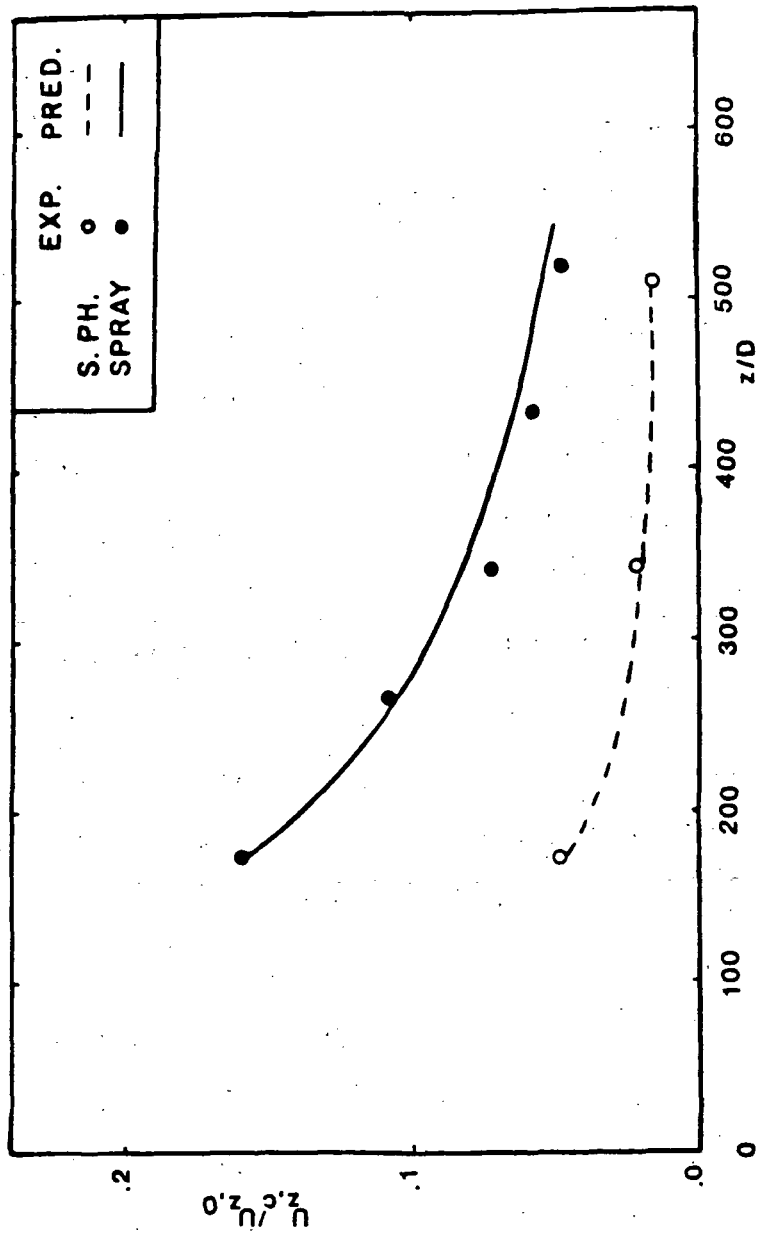
147

FIGURE7-20 AXIAL VARIATION OF THE MEAN CENTERLINE VELOCITY (CASE 5)

148

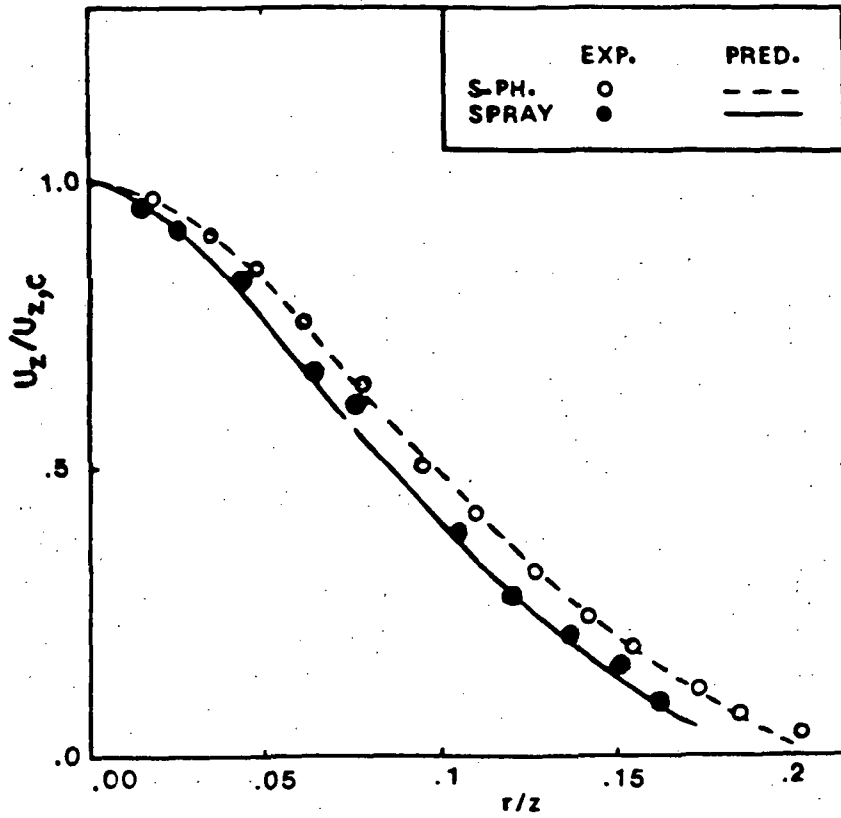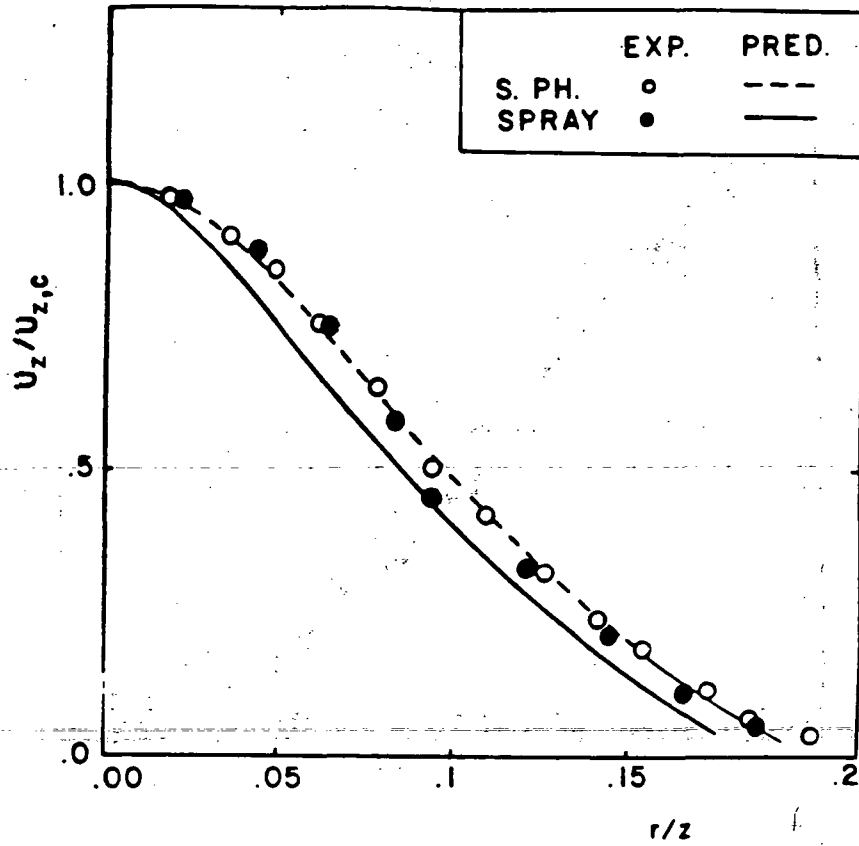FIGURE 7-21 RADIAL VARIATION OF THE MEAN AXIAL

VELOCITY AT z/D = 340 (CASE 5)

FIGURE 7-22 RADIAL VARIATION OF THE MEAN AXIAL
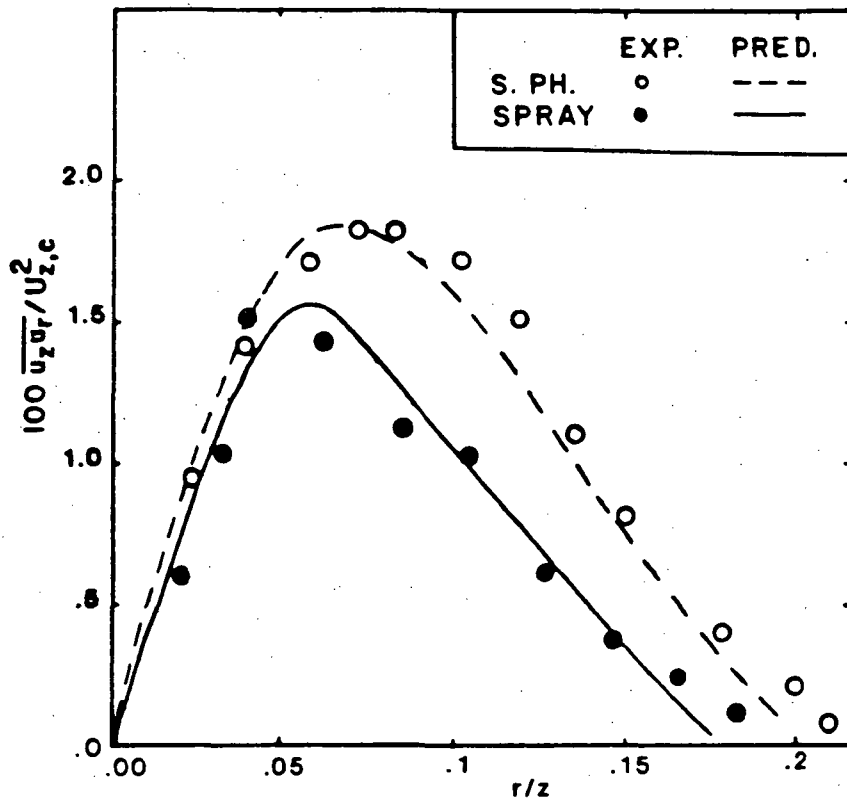VELOCITY AT z/D = 510 (CASE 5)

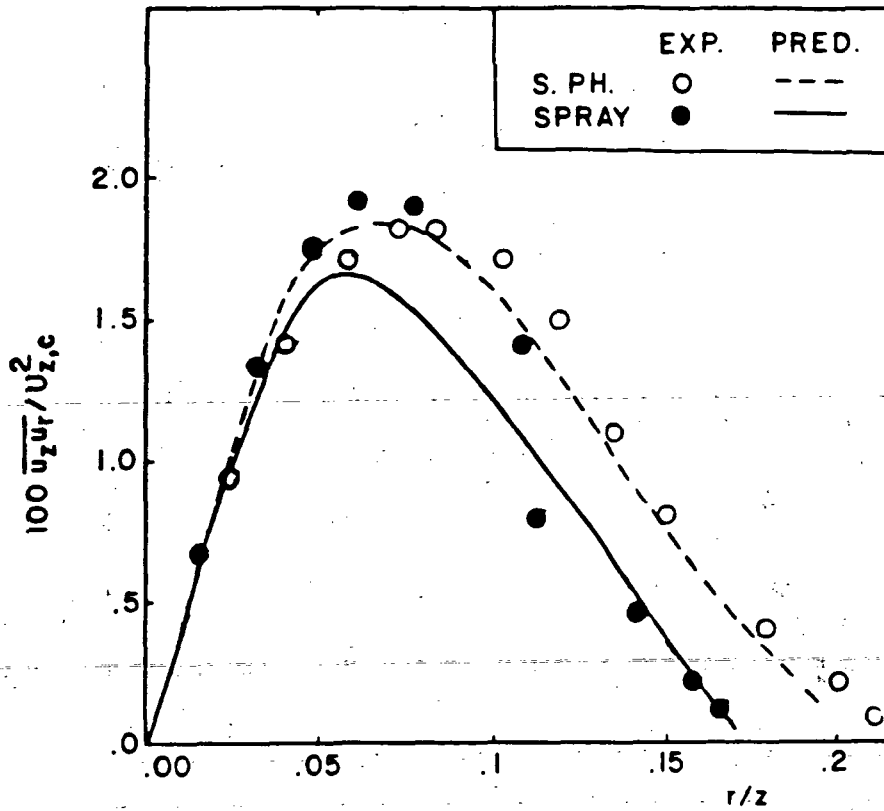FIGURE 7-23   RADIAL VARIATION OF THE SHEAR STRESS
AT z/D = 340 (CASE 5)

FIGURE 7-24 RADIAL VARIATION OF THE SHEAR STRESS
AT z/D = 510 (CASE 5)

those of the single phase. This may have some effects on the profiles downstream ($z/D = 340$). In general, there is a reduction in the shear stress or an increase in the dissipation rate of the turbulence kinetic energy due to the presence of the liquid droplets in the same control volume with the carrier phase. As vaporization proceeds the effects of the droplets on the turbulence quantities diminish allowing the fluid behavior to approach that of a single-phase jet (Figure 7-24).

In the present case it was assumed that the velocities of the droplets are equal to those of the gas. To study the effect of this assumption on the results, the droplets' velocity was increased by 20%; the effect on the carrier phase profiles was negligible. This result can be attributed to two factors: 1) the droplets' diameter, at the starting station, is equal to 27 μm or less, so the reduction rate of the mean slip velocity between the droplets and gas is considerable due to the vaporization; 2) since the droplets' mass fraction was measured, an increase in the velocity necessitates a reduction in the volume fraction. Thus, the effects of increased velocity are counterbalanced by those of decreased volume fraction.

It is important to note that the effects of density fluctuation in the calculation were neglected here. This assumption can be justified in the present study since the mean density gradient is very small compared with the velocity gradient. This is due to the negligible evaporated mass compared with the entrained air, so the properties of the carrier phase are almost those of the standard air.

7.4 The Flow of Solomon et al. (1984)

Solomon et al. (1984) presented some comprehensive measurements of the detailed structure of a two-phase turbulent round jet. Experiments considered

153

the same test rig of Shearer et al. (1979) to perform some detailed measurements of the droplets' properties. Two mass loading ratios (X_O = 7.71 and 15.78) were considered. Solomon et al. measured the carrier phase properties using a laser doppler anemometer, the droplet size and velocity using the shadow photograph technique, the liquid mass flux using inertial impaction method, and the mean mixture fraction by isokinetically sampling the flow. The radial distributions of these quantities were reported at four stations (x/D = 50, 100, 250, and 500) for the two mass loading cases. They classified the droplets into finite-size groups and measured the velocities and the number density distribution of each group. For computational purposes, the profiles of the turbulence dissipation rate (ϵ), the volume fraction of each droplets group (ϕ^k), and the freon vapor concentration in the carrier phase (C) are obtained from the different measured quantities at z/D = 50. ϵ is obtained from the distributions of the turbulent shear stress, the mean axial velocity gradient, and the turbulence kinetic energy at the same station. Seven groups (17.5, 22.5, 27.5, 32.5, 42.5, and 52.5 µm) are considered for X_O = 7.71 (Case 6) and ten groups (15, 25, 35, 45, 55, 65, 75, 85, 95, and 100 µm) are considered for X_O = 15.78 (Case 7). ϕ^k is obtained from the distributions of the liquid mass flux, and the mean velocity of the different droplets groups and their relative number density at z/D = 50. C is obtained from the mixture fraction measurements and the state relations given by Solomon et al. (1984). Table C-4 (Appendix C) summarized all the starting radial profiles of the main dependent variables at z/D = 50. This information is essential for accurately predicting the present flow to validate the turbulence model put forth in the present study.

Temperature measurements of the carrier phase (with a bare wire chromelalumel thermocouple) showed a maximum temperature difference of only

20°C either in the radial or in the axial directions. The analysis of Solomon et al. showed that the droplet's temperature reaches the Freon's saturation temperature at $z/D = 50$. It was assumed in the present calculations that the temperature of the carrier phase is equal to that of the surrounding air (300°K) while the droplet surface temperature is equal to that of the saturation conditions (240.3°K).

A comparison of the predicted with the measured distributions of the mean velocity, turbulence intensity and shear stress of the carrier phase, and the mean velocity of the droplets of the different-size groups follows.

Figures 7-25 and 7-26 show the measured and predicted centerline velocity distributions of the carrier phase and those of the different droplet groups for cases 6 and 7. Here $k = 1$ refers to the group that has the largest diameters, and $k = 7$ or 10 the smallest ones. The mean velocities are normalized by the average velocity at the nozzle exit ($U_o = 64.5$ m/s for case 6 and 29.64 m/s for case 7). It can be seen from the figures that the relative velocity between the carrier phase and the group of largest diameters is greater than that of any other group. This behavior is already explained in the analysis of Figure 7-9 (section 7.2). Figures 7-25 and 7-26 also show the continuous reduction in the relative velocity between the carrier phase and the group of smallest diameters as the distance measured from the nozzle exit plane increases. This can be attributed to the fact that the smaller the droplet diameter, the higher the reduction rate in the droplet diameter itself. Thus, by increasing the downstream distance, the smallest diameters group satisfies the local equilibrium conditions where the velocity of the droplet becomes equal to that of the carrier phase. It can be seen also from Figures 7-25 and 7-26 that the relative velocity between the carrier phase and the group of largest diameters increases with an increase in the downstream
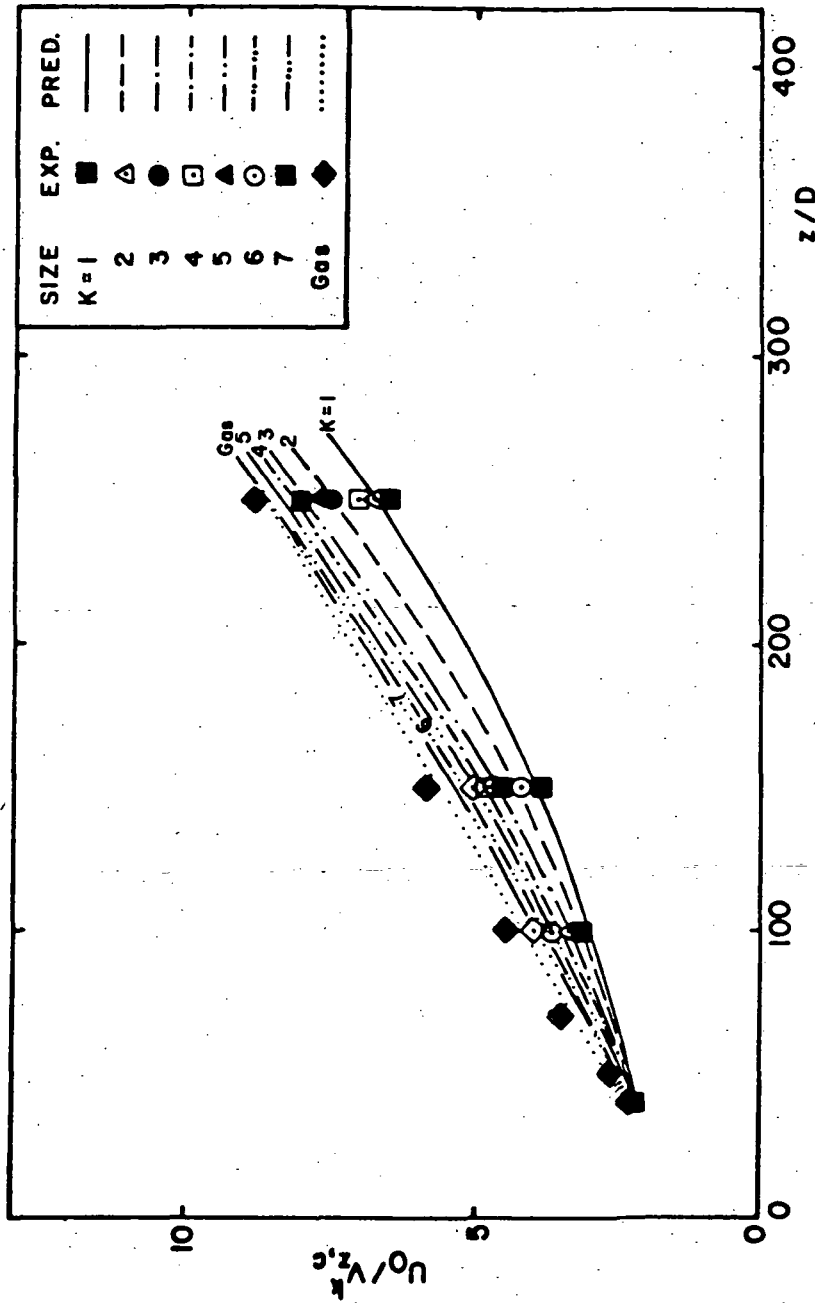
155

FIGURE 7-25 THE DISTRIBUTION OF THE JET CENTER LINE MEAN VELOCITIES
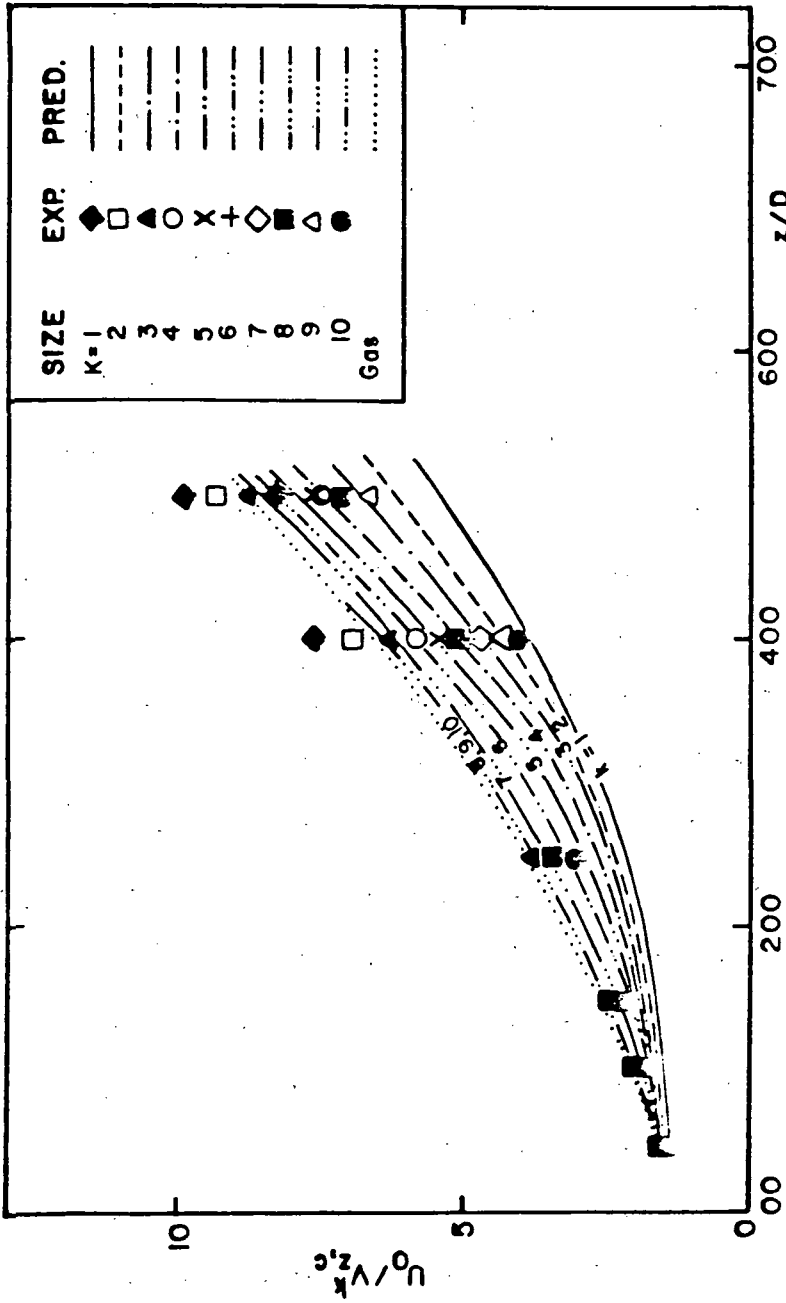(CASE 6)

156

FIGURE 7-26 THE DISTRIBUTION OF THE JET CENTER LINE MEAN VELOCITIES
(CASE 7)

157

distance. This behavior is already explained in the analysis of Figure 7-13 (section 7.2). Figures 7-25 and 7-26 display in general good agreement between the measured and predicted mean centerline velocities.

The influence of the loading ratio of the dispersed phase on the centerline mean velocity distributions of the carrier phase is illustrated in Figure 7-27. In this figure the increase in the mean centerline velocity of the carrier phase compared with the corresponding value of the single-phase jet is proportional to the mass loading ratio (but not linearly). This proportionality is analyzed in detail in the discussion of Figures 7-1 and 7-2 in section 7.1. Figures 7-28 to 7-30 show the normalized radial profiles of the mean axial velocities of the carrier phase at 100, 250, and 500 nozzle diameters from the nozzle exit plane for both the two loading ratios (Cases 6 and 7). It can be seen from these two figures that the jet width decreases with the increase of the mass loading ratio.

Figure 7-28 shows a maximum discrepancy of 30% between the predicted and measured velocities although the agreement is very good in Figures 7-29 and 7-30. Probably the measured quantities are overestimated at this station since Solomon et al. reported the same discrepancy between the measurements and their predictions at the same station, using the Lagrangian frame of work.

The influence of the dispersed phase on the carrier fluid turbulence kinetic energy and shear stress is displayed in Figures 7-31 to 7-36. It can be stated that the reduction in the turbulence energy and the shear stress is proportional to the mass loading ratio but not linearly. These figures also show that farther downstream from the nozzle exit ($z/D = 500$), the turbulence quantities are approaching their corresponding values for a single-phase jet (based on the experimental data of Shearer et al., 1979).

To understand the nature of the turbulent interaction between the carrier
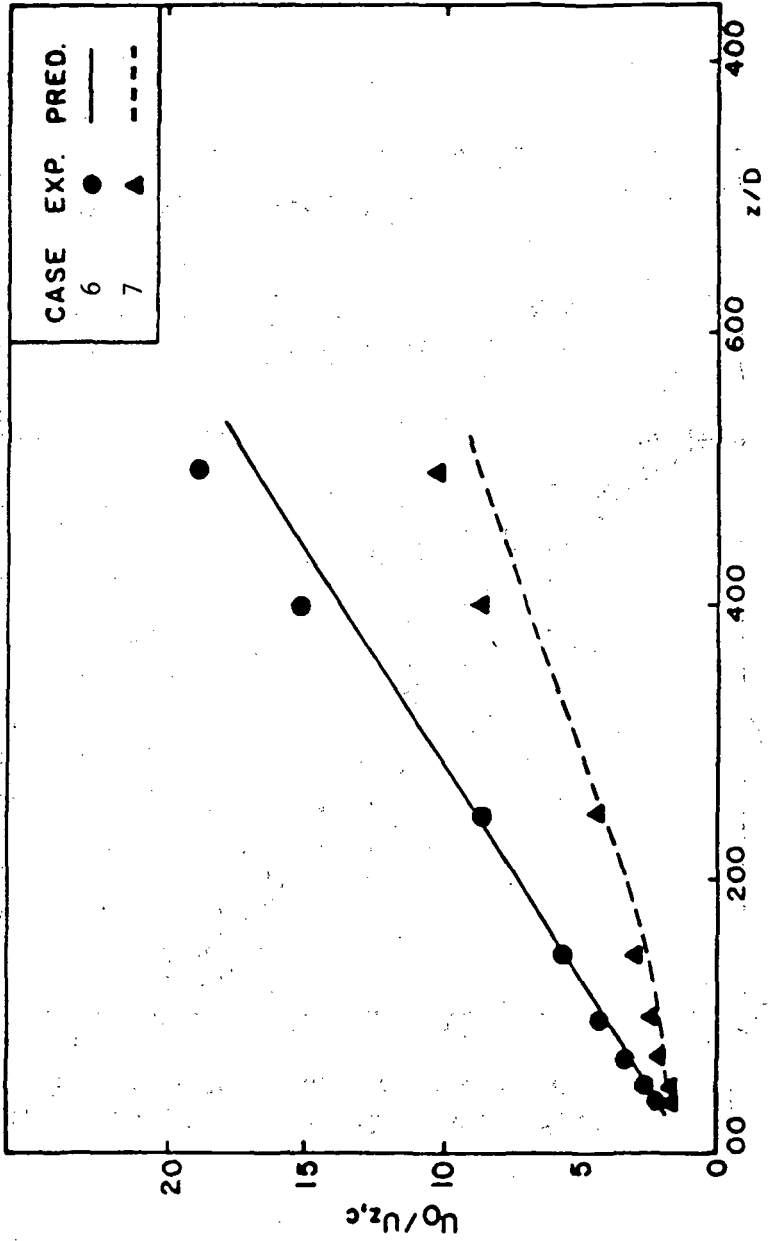
FIGURE 7-27 THE DISTRIBUTION OF THE CARRIER PHASE CENTER LINE
VELOCITY

159
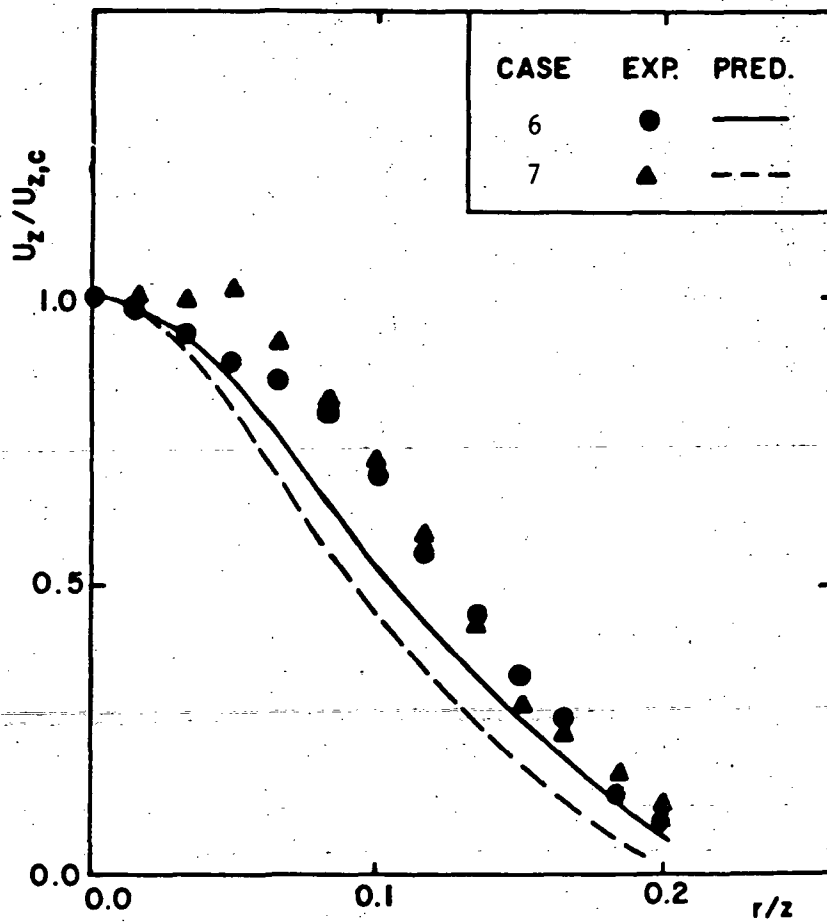
FIGURE 7-28 THE RADIAL DISTRIBUTION OF THE
MEAN GAS VELOCITIES AT z/D = 100
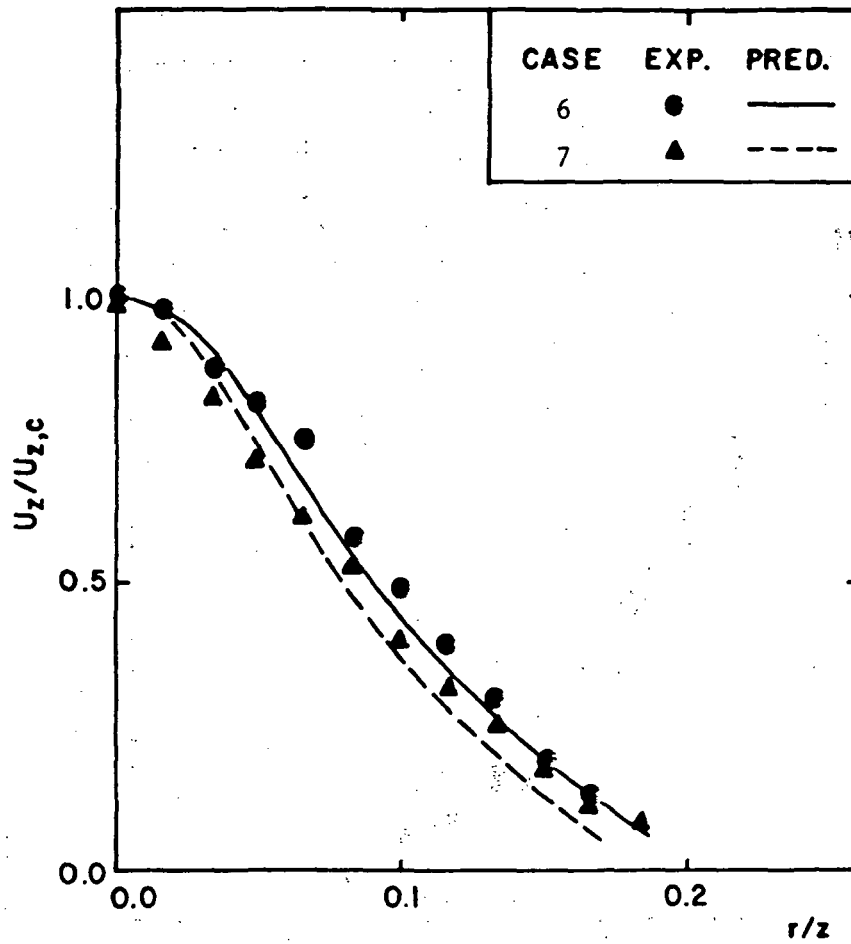
FIGURE 7-29 THE RADIAL DISTRIBUTION OF THE MEAN GAS VELOCITIES AT $z/D = 250$
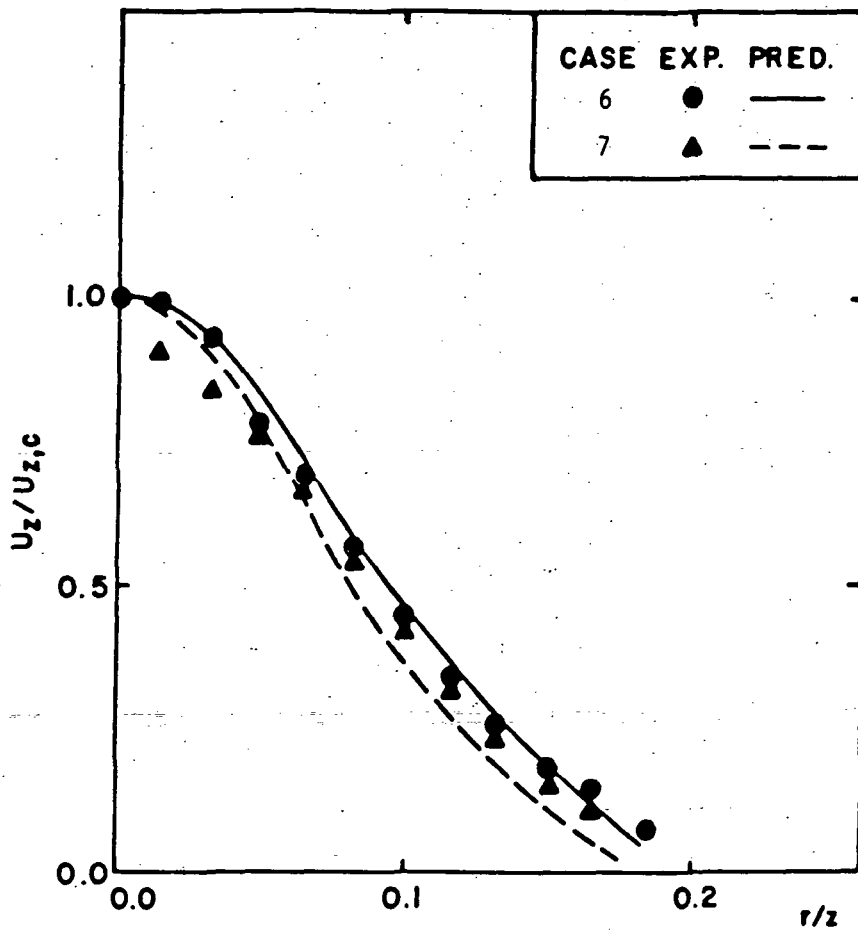
FIGURE 7-30 THE RADIAL DISTRIBUTION OF THE
MEAN GAS VELOCITIES AT z/D = 500
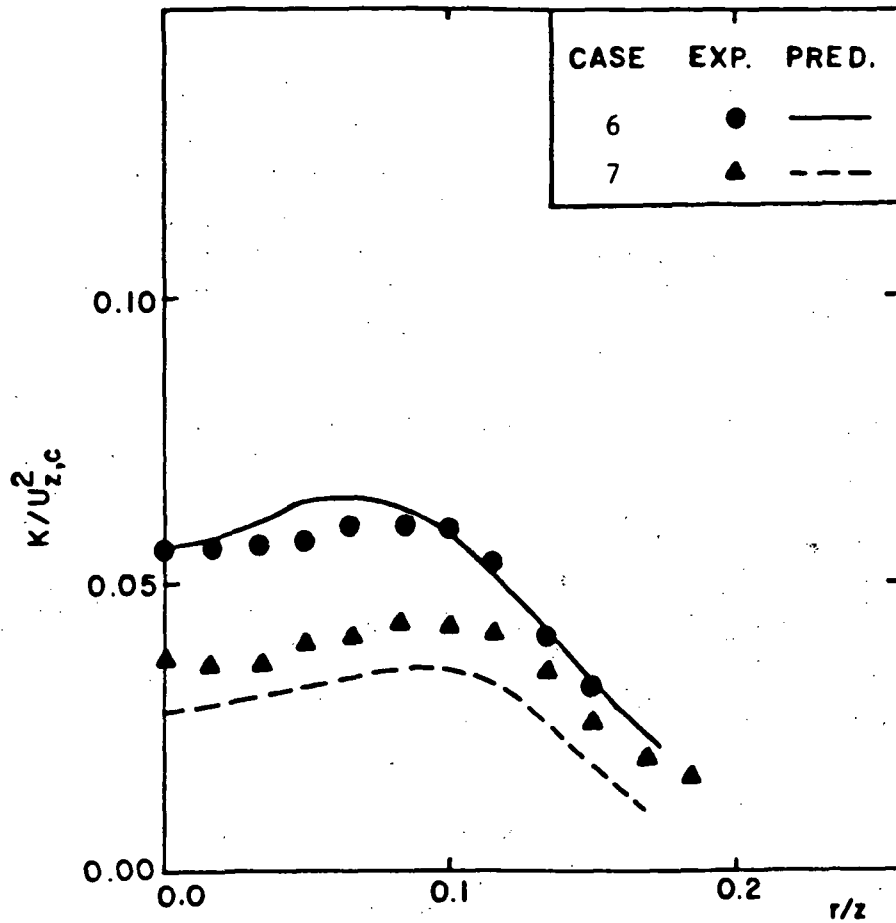
FIGURE 7-31 THE RADIAL DISTRIBUTION OF THE
KINETIC ENERGY OF TURBULENCE
AT z/D = 100

163
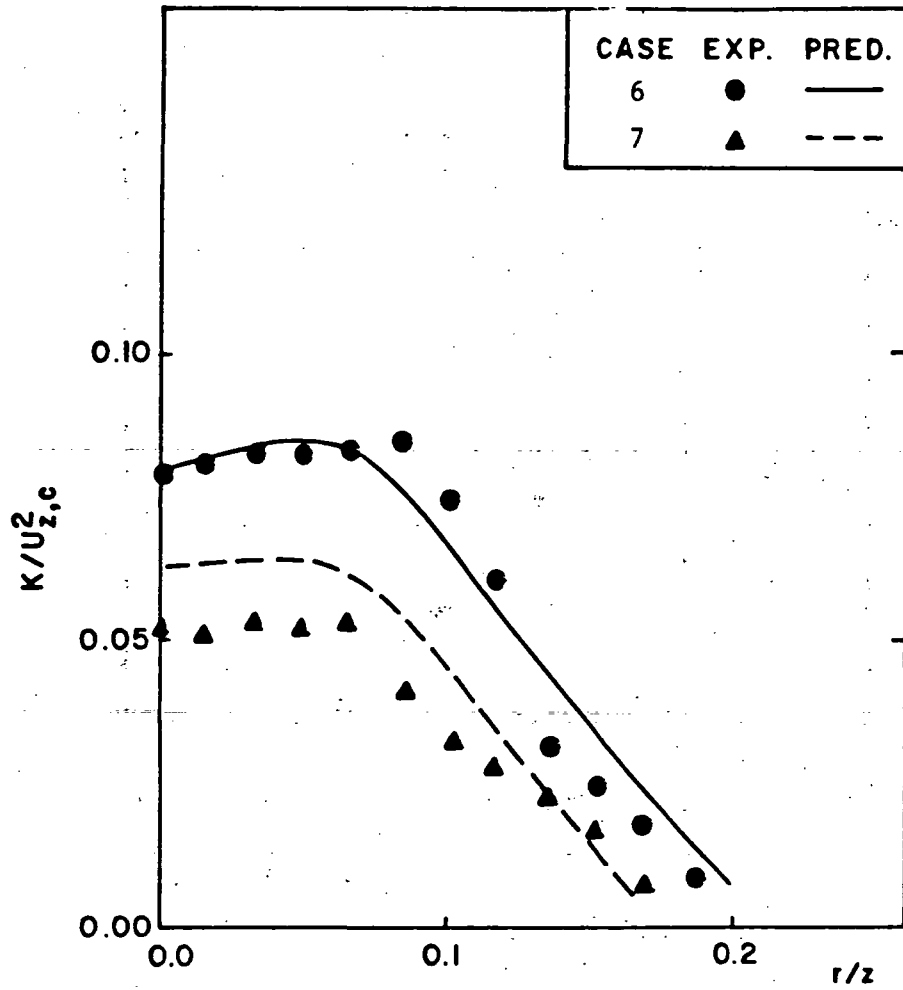
FIGURE 7-32 THE RADIAL DISTRIBUTION OF THE
KINETIC ENERGY OF TURBULENCE
AT $z/D = 250$

164
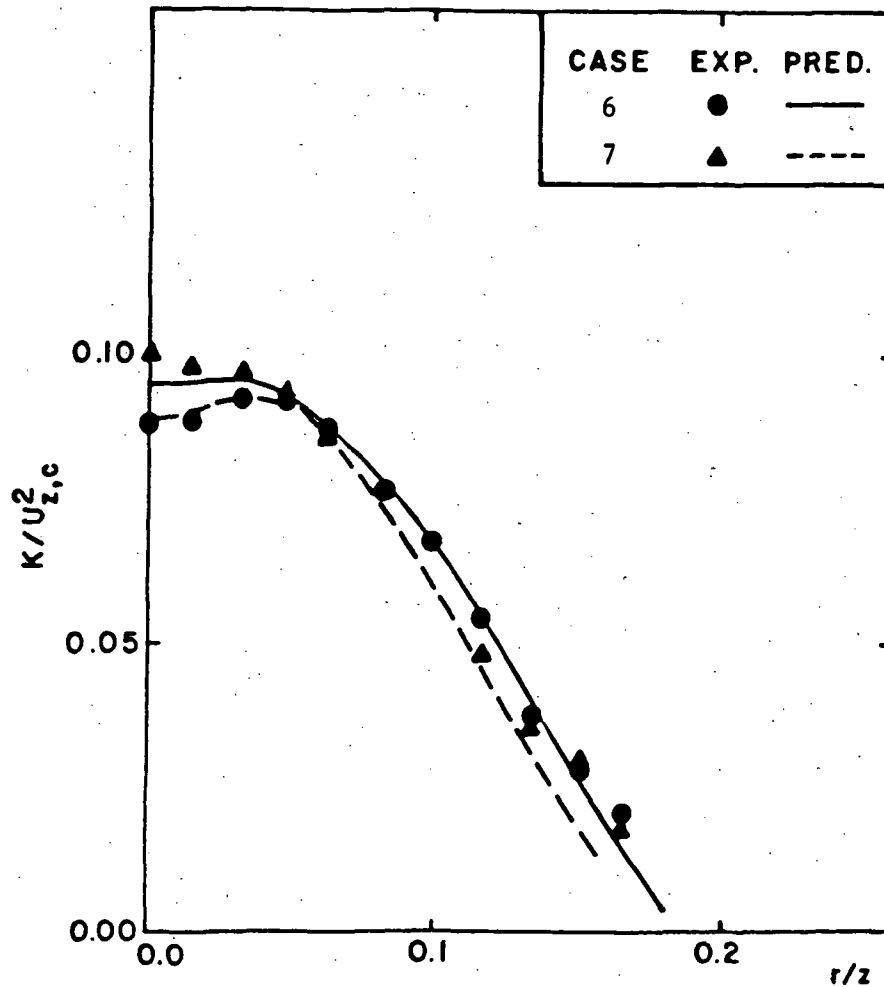
FIGURE 7-33 THE RADIAL DISTRIBUTION OF THE
KINETIC ENERGY OF TURBULENCE
AT z/D = 500
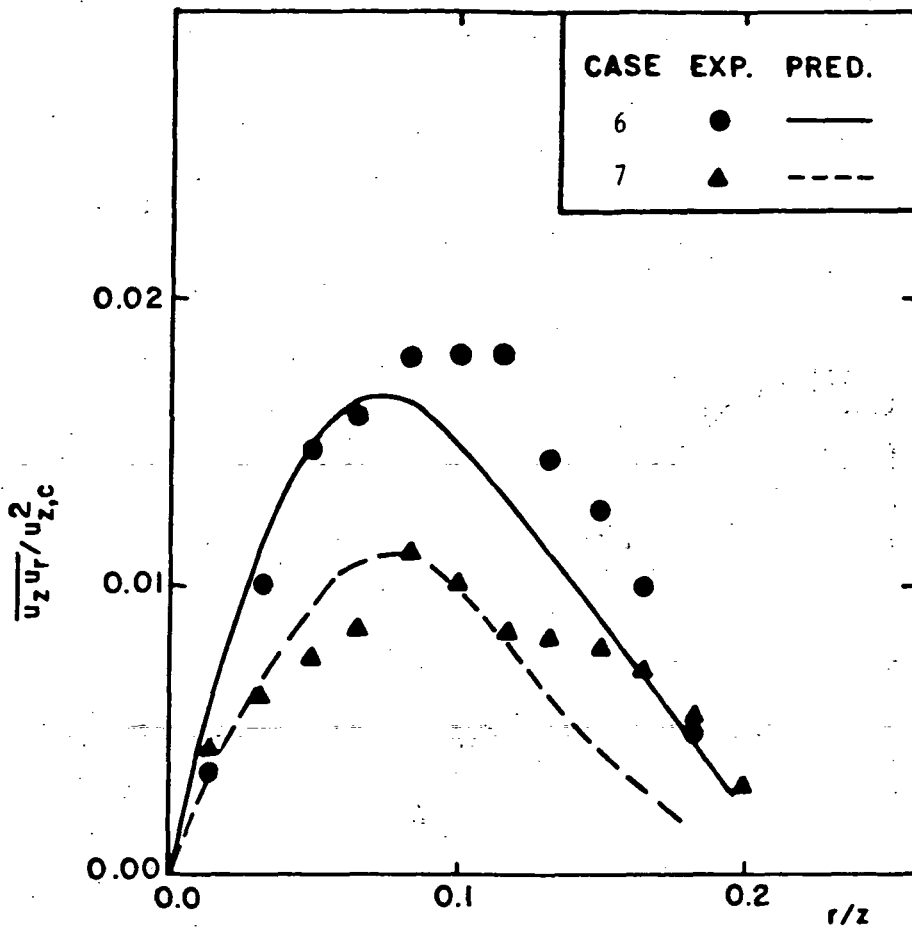
FIGURE 7-34 THE RADIAL DISTRIBUTION OF THE
SHEAR STRESS AT z/D = 100
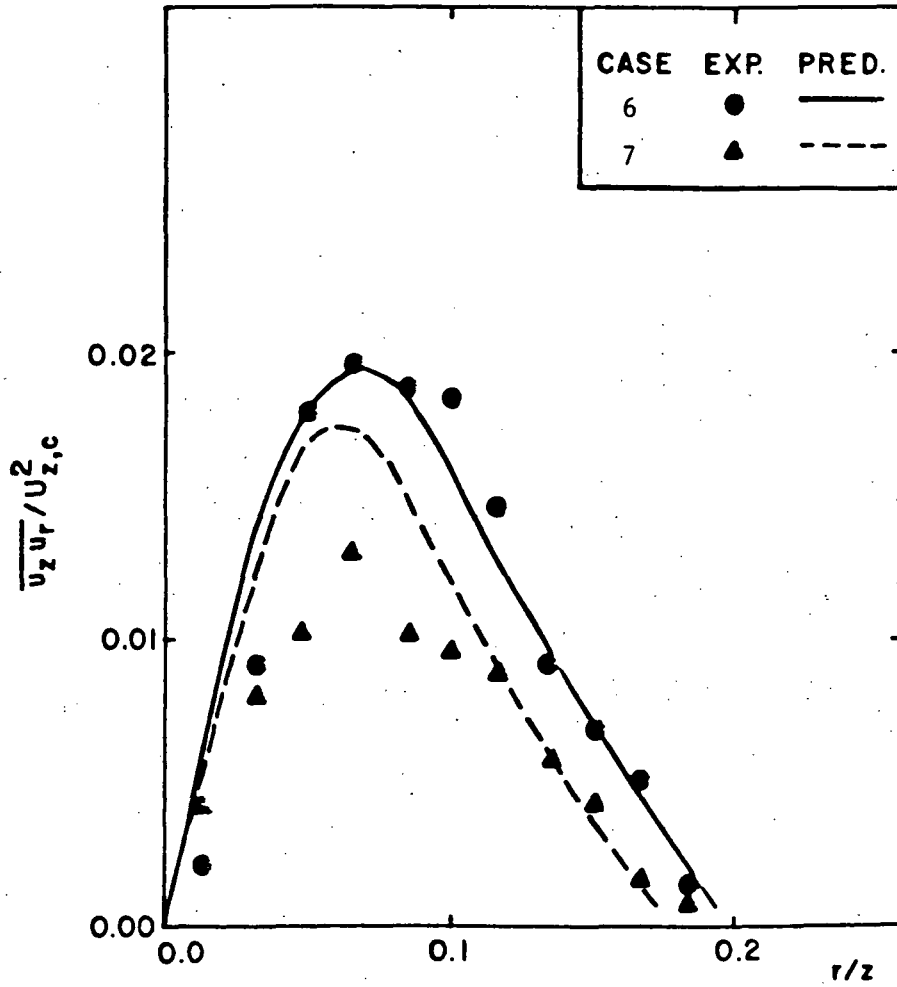
FIGURE 7-35 THE RADIAL DISTRIBUTION OF THE SHEAR STRESS AT z/D = 250
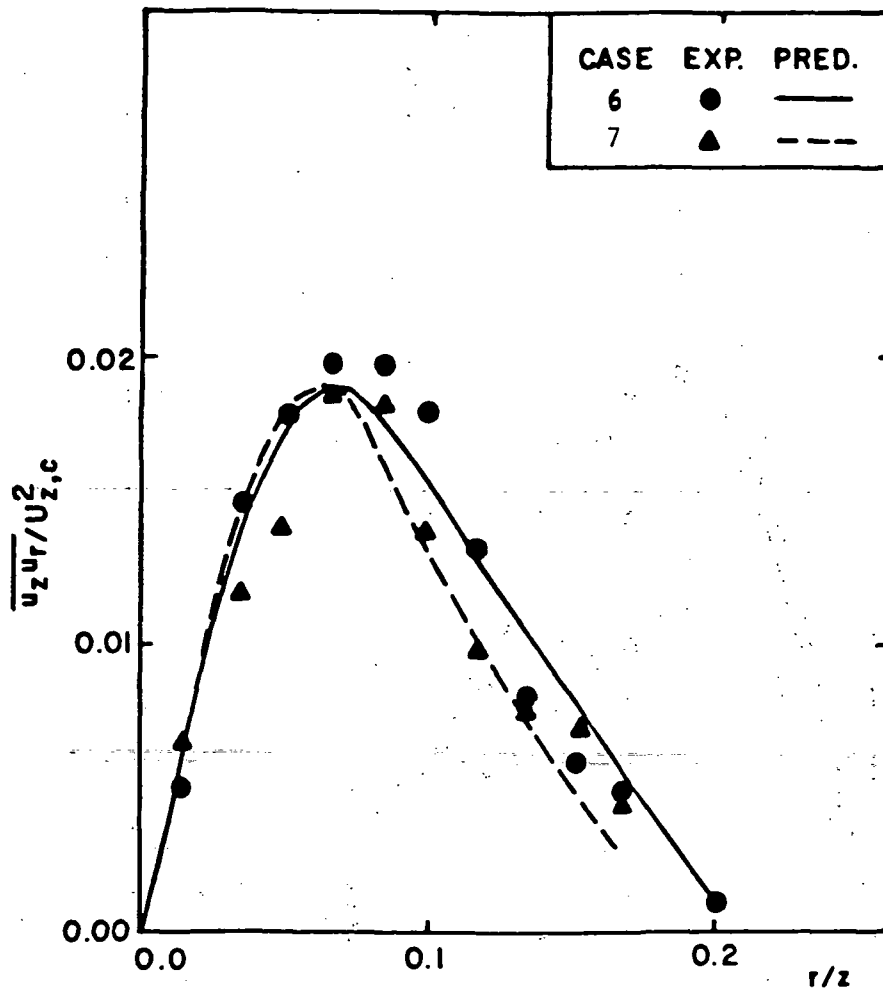
FIGURE 7-36 THE RADIAL DISTRIBUTION OF THE SHEAR STRESS AT z/D = 500

fluid and the vaporizing droplets, the main features of this type of flow are summarized as follows:

1. The toal mass of the dispersed phase continuously decreases and so does the volume fraction. Due to the reduction of the volume fraction, the momentum exchange terms (mean and/or fluctuating) are reduced.

2. The velocity of the evaporating material as it leaves the droplet surface is different from that of the carrier fluid. Thus, there is an additional momentum transfer that depends on the evaporation rate and the relative velocity.

3. The momentum exchange coefficient is inversely proportional to the droplet diameter with an exponent ranging from 2 to 1.3 (for a Reynolds number less than 100). Hence, as the diameter is reduced the momentum exchange coefficient increases.

4. The vaporization reduces the droplets' diameter and thus the total relative mean velocity ($\vec{U} - \vec{V}$) and the higher the turbulent diffusivity of the dispersed phase is.

Figures 7-31 to 7-36 display in general good agreement between the measured and predicted turbulence kinetic energy and shear stress of the carrier phase.

The predictions of the axial distribution of the Sauter mean diameter at the jet centerline compared with the experimental data is displayed in Figure 7-37. This diameter is given by

$$SMD = \frac{\sum_i (d_i)^3 n_i / V_i}{\sum_i (d_i)^2 n_i / V_i} \qquad 7.1$$

where n_i is the number of the droplets of diameter d_i. It is clear that there is also good agreement between the predictions and the data for the averaged

169
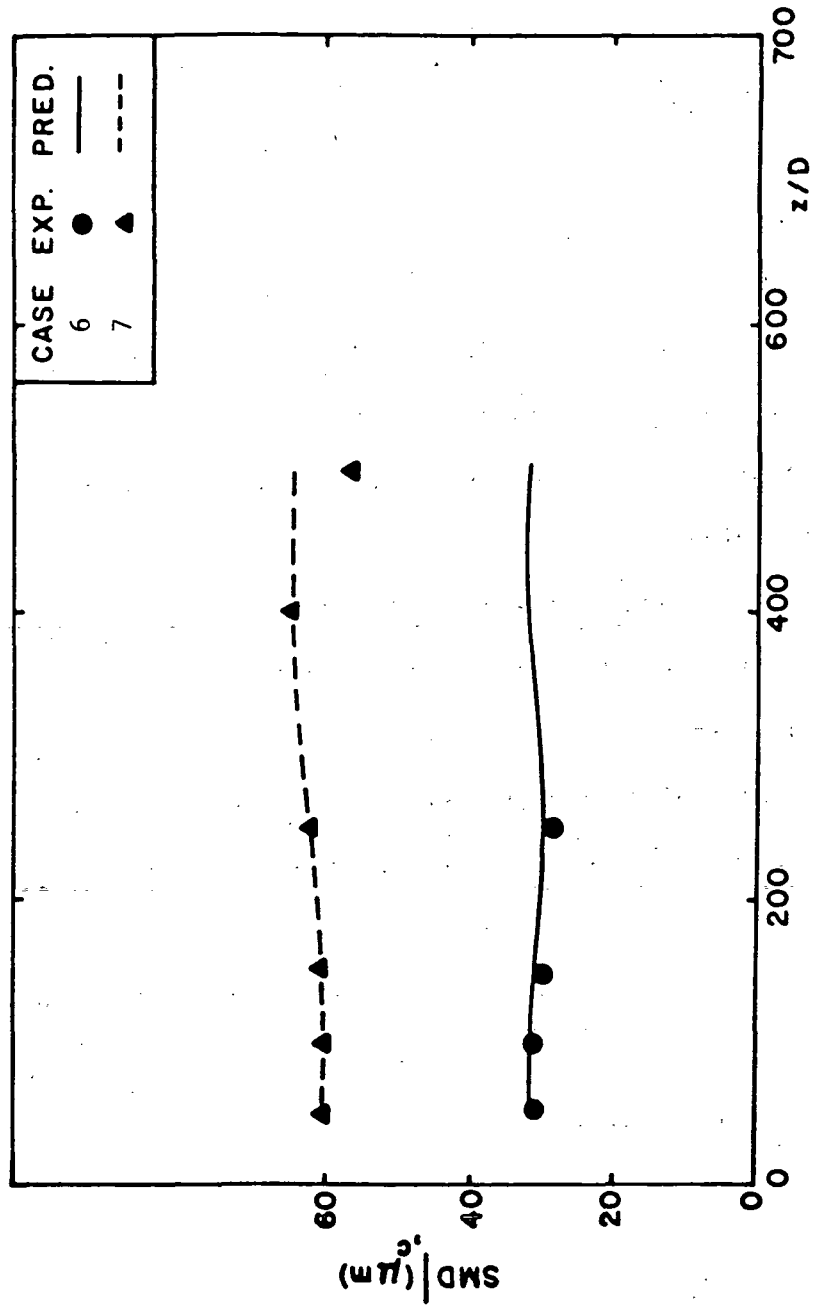
FIGURE 7-37 THE DISTRIBUTION OF THE SMD ALONG THE CENTER LINE

diameter.

It is important to note that the present study neglected the effects of density fluctuations in these two cases as in Case 5 (Shearer et al., 1979) and for the same reasons. It should be mentioned also that the prediction of Cases 6 and 7 are obtained with the coefficients of the turbulence model given by Table 3.1. The optimized value for $C_{\varepsilon 3}$ in these two cases is equal to 2.

8.0 CONCLUSIONS AND RECOMMENDATIONS

The main objectives of the present study were as follows:

1. to develop a mathematical model of turbulence for dilute two-phase flows starting from the exact transport equations of the turbulence kinetic energy and its dissipation rate;

2. to develop a reliable formula for the calculation of the lateral diffusivity of heavy particles suspended in a homogeneous turbulent field, and

3. to predict two-phase turbulent flows with phase changes based on modeled transport equations of mass, momentum of each phase, the concentration of vapor, and a two-equation turbulence model.

In the presented model, the third-order correlations containing particle volume fraction fluctuations are retained. The numerical results for all the predicted cases showed that those third-order correlations are negligible compared with the second-order ones (two orders of magnitude less). This means that the present study has only one new empirical coefficient in its turbulence model ($C_{\epsilon 3}$). This coefficient is determined from one set of data (Case 1) and used very successfully in all other cases of the same experiment. A sensitivity study was conducted to investigate the influence of the value of $C_{\epsilon 3}$ on the model predictions. By changing the value of $C_{\epsilon 3}$ by 10%, the maximum change in any radial profile is less than 3%.

The study of the effects of the dispersed phase on the carrier phase flow properties, mean and fluctuating components, shows the following results:

1. The momentum interchange between the two phases which reflects the degree of disequilibrium between the phases, is a function of the dispersed phase properties such as droplet diameter, density, and mass loading ratio. In the case of heavy particles suspended in a turbulent gaseous media, the momentum interchange terms and all the corresponding turbulent correlations should be considered in the governing equations of both the mean motion and the turbulence model.

2. The effect of partial or complete droplet evaporation is reflected on the velocity distribution of the different size groups. The smaller the diameter of the droplet is, the less the relative velocity between droplets and the fluid, and the higher the turbulent diffusivity of that group.

3. Due to the co-existence of the dispersed phase and the carrier phase in the same control volume, a significant reduction in the turbulent shear stress and the kinetic energy of turbulence of the carrier phase is observed. The reduction in the turbulence energy or the increase in the dissipation rate of that energy is caused by the fluctuating relative velocity between the particles and the carrier phase and the turbulent correlation between this velocity and other fluctuating quantities such as volume fractions and carrier fluid velocity. The reduction in the kinetic energy of turbulence is proportional to the loading ratio but not linearly.

A reliable expression for calculating the Schmidt number, defined as the ratio of particle diffusivity to fluid point diffusivity, of heavy particles

suspended in a turbulent flow is developed (Equations 5.30 to 5.33). The predictions using that formula are compared with recent well-defined experimental data for the dispersion of a single particle. The agreement between the predictions and data is very good.

Using the turbulence model presented in this work, predictions of the different cases for either solid particles or evaporating sprays, are generally in good agreement with the most recent well-defined experimental data.

Further extension of the present work includes:

1. obtaining optical measurements for the flow properties of the ideal spray experiment of Case 4 to validate the present model and to support the turbulent spray models in general.

2. predicting a ducted recirculating turbulent two-phase flow (elliptic flow). The predictions should be compared with a well defined data set.

3. predicting a ducted turbulent two-phase flow with heat transfer. The interaction between the evaporating droplet and the duct walls, and the heat and mass transfer to the wall, should be considered in the model. The density fluctuation effects should also be considered.

4. predicting the dense portion of the spray. Droplet-droplet interaction effects, collision, and shattering must be considered in the model.

REFERENCES

1. Abbas, A.S., Koussa, S.S. and Lockwood, F.C., 1981, "The Prediction of the Particle Laden Gas Flows," Eighteenth Symposium (International) on Combustion, The Combustion Institute, Pittsburgh, PA, 1427.

2. Abramovich, G.N., 1970, "The Effects of Admixture of Solid Particles, or Droplets, on the Structure of a Turbulent Gas Jet," Soviet Physics - Doklady, 15, 101.

3. Aggarwal, S.K., Lee, D.N., Fix, G.J. and Sirignano, W.A., 1983, "Numerical Optimization Studies of Axi-Symmetric Unsteady Sprays," J. Comp. Phys., 50, 101.

4. Ahmadzadeh, J. and Harker, J.H., 1974, "Evaporation from Liquid Droplets in Free Fall," Trans. Instn. Chem. Engrs., 52, 108.

5. Alonso, C.V., 1981, "Stochastic Models of Suspended Sediment Dispersion," A.S.C.E., 107, 733.

6. Al-Taweel, A.M. and Laundau, J., 1977, "Turbulence Modulation in Two-Phase Jets," Int. J. Multiphase Flow, 3, 341.

7. ASHRAE, 1969, "Thermodynamic Properties of Refrigerants," American Society of Heating, Refrigerating and Air-Conditioning Engineers, Inc., New York.

8. Batchelor, G.K., 1974, "Transport Properties of Two-Phase Materials with Random Structure," Annual Review of Fluid Mechanics, 6, 227.

9. Beard, K.V., 1976, "Terminal Velocity and Shape of Cloud and Precipitation Drops Aloft," J. Atmos. Sci., 33, 851.

10. Beard, K.V. and Pruppacher, H.R., 1969, "A Determination of the Terminal Velocity and Drag of Small Water Drops by Means of a Wind Tunnel," J. Atmos. Sci., 26, 1066.

11. Berlemont, A., Gouesbet, G. and Picart, A., 1982, "The Code DISCO-2 for the Prediction of the Dispersion of Discrete Particles in Turbulent Flow," Int. Rep. Mado/82/g/V. (France).

12. Bondarenko, O.N. and Shaposhnikova, 1980, "Investigation of Isothermal Flow of a Mixture of Gas and Particles in a Channel of Variable Section," Fluid Dynamics, 6, 850.

13. Boure, J.A., 1979, "On the Form of the Pressure Terms in the Momentum and Energy Equations of Two-Phase Flow Models," Int. J. Multiphase Flow, 5, 159.

14. Boyson, F. and Swithenbank, J., 1979, "Spray Evaporation in Recirculating Flow," Seventeenth Sympoiium (International) on Combustion, The Combustion Institute, Pittsburgh, PA, 443.

15. Buckingham, A.C. and Siekhaus, 1981, "Interaction of Moderately Dense Particle Concentrations in Turbulent Flow," AIAA Paper NO. 81-0346.

16. Buevich, Yu. A. and Markov, V. G., 1973, "Continual Mechanics of Monodisperse Suspensions Integral and Differential Laws of Conservation," Fluid Dynamics, 5, 846.

17. Calabrese, R.V. and Middleman, S., 1979, "The Dispersion of Discrete Particles in a Turbulent Fluid Field," AIChE J., 25, 1025.

18. Chao, B.T., 1964, "Turbulent Transport Behavior of Small Particles in Dilute Suspension," Osterr, Ing. Arch., 18, 7.

19. Chen, P.P. and Crowe, C.T., 1984, "On the Monte-Carlo Method for Modeling Particle Dispersion in Turbulence," ASME Energy Sources Technology Conference, New Orleans, LA.

20. Clift, R., Grace, J.R. and Weber, M.E., 1978, "Bubbles, Drops and Particles," Academic Press, New York.

21. Corrsin, S., 1974, "Limitations of Gradient Transport Models in Random Walks and in Turbulence," in Advances in Geophysics, Landsberg, H.E. and Van Mieghem, J. eds. (Academic, New York), 18A, 25.

22. Corrsin, S. and Lumley, J.L., 1956, "On the Equation of Motion for a Particle in a Turbulent Fluid," Appl. Sci. Res., 6A, 114.

23. Cox, R.G., and Mason, S.G., 1971, "Suspended Particles in Fluid Flow Through Tubes," Annual Rev. of Fluid Mech., 3, 291.

24. Crowe, C.T., 1978, "On Soo's Equations for the One-Dimensional Motion of Single-Component Two-Phase Flows," Int. J. Multiphase Flow, 4, 225.

25. Crowe, C.T., 1980, "On the Dispersed-Flow Equations," Two-Phase Momentum, Heat and Mass Transfer, (Edited by T. Durst and Afgan), 1, 25, London.

26. Crowe, C.T., 1981, "On the Relative Importance of Particle-Particle Collisions in Gas-Particle Flows," Paper 78-81, Conf. on Gas-Borne Particles, Inst. of Mech. Engr., Oxford, England, 135.

27. Crowe, C.T., 1982, "Review-Numerical Models for Dilute Gas-Particle Flows," ASME Journal of Fluids Engineering, 104, 297.

28. Crowe, C.T., Sharma, M.P. and Stock, D.E., 1977, "The Particle-Source-in-Cell Method for Gas Droplet Flow," ASME Journal of Fluids Engineering, 99, 325.

29. Csanady, G.T., 1963," Turbulent Diffusion of Heavy Particles in the Atmosphere," J. Atmos. Sci., 20, 201.

30. Daly, B.J. and Harlow, F.H., 1970, "Transport Theory of Turbulence," Univeristy of California, Report AL-DC-11207.

31. Danon, H., Wolfshtein, M. and Hetsroni, G., 1977, "Numerical Calculations of Two-Phase Turbulent Round Jet," Int. J. Multiphase Flow, 3,223.

32. Delhay, J.M., 1980, "Space-Averaged Equations and Two-Phase Flow Modeling," in Two Phase Momentum, Heat and Mass Transfer, eds. Durst, F., Tsikpauri, kV. and Afgan, N.H., Hemisphere Pub. Corp., 1,3.

33. DiGiacinto, M., Sabetta, F. and Piva, R., 1982, "Two-Way Coupling Effects in Dilute Gas-Particle Flows," ASME Paper No. 82-WA/FE-1.

34. Drew, D.A., 1971, "Averaged Field Equations for Two-Phase Media," Studies Applied Math; L, No. 2, 133.

35. Dukowicz, J.K., 1980, "A Particle-Fluid Numerical Model for Liquid Sprays," J. Comp. Phys., 35, 229.

36. Dukowicz, J.K., 1984, "Drag of Evaporating or Condensing Droplets in Low Reynolds Number Flow," Phys. Fluids, 27, 1351.

37. Durst, F., Milojevic, D. and Schonung, B., 1984, "Eulerian and Lagrangian Predictions of Particulate Two-Phase Flows: a Numerical Study," Appl. Math. Modelling, 8, 101.

38. Eisenklam, P., Arunachalam, S.A. and Weston, J.A., 1967, "Evaporation Rates and Drag Resistance of Burning Drops," Eleventh Symposium (International) on Combustion, The Combustion Institute, Pittsburgh, PA, 715.

39. El-Banhawy, Y. and Whitelaw, J.H., 1980, "Calculation of the Flow Properties of a Confined Kerosene-Spray Flame," AIAA J., 18, 1503.

40. El-Emam, S.H. and Mansour, H., 1983, "An Analytical Model for Two-Phase Flow Field of Liquid Sprays," Proceedings of the 3rd Multi-Phase Flow and Heat Transfer Symposium-Workshop, Miami Beach, Florida.

41. Elghobashi, S.E. and Abou-Arab, T.W., 1983, "A Two-Equation Turbulence Model for Two-Phase Flows," Phys. Fluids, 25, 931.

42. Elghobashi, S., Abou-Arab, T., Rizk, M. and Mostafa, A., 1984, "Prediction of the Particle-Laden Jet with a Two-Equation Turbulence Model," Int. J. Multiphase Flow (in press).

43 Elghobashi S.E. and Megahed, I.E.A. 1981, "Mass and Momentum Transport in a Laminar Isothermal Two-Phase Round Jet," Numerical Heat Transfer 4, 317.

44. El-Kotb, M.M., Elbahar, O.M.F. and Abou-Elail, M.M., 1983, "Spray Modeling in High Turbulent Swirling Flow," Fourth Symposium on Turbulent Shear Flows, F.R. Germany.

45. Faeth, G.M., 1977, "Current Status of Droplet and Liquid Combustion," Prog. Energy Combust. Sci., 3, 191.

46. Faeth, G.M., 1983, "Evaporation and Combustion of Sprays," Prog. Energy Combust. Sci., 9, 1.

47. Field, M.A., 1963, "Entrainment into an Air Jet Laden with Particles," BCURA Inf. Circular No. 273.

48. Friedlander, S.K., 1957, "Behavior of Suspended Particles in a Turbulent Fluid," AIChE. J., 3, 381.

49. Fuchs, N.A., 1959, "Evaporation and Droplet Growth in Gaseous Media," Pergamon Press, New York.

50. Fuchs, N.A., 1964, "The Mechanics of Aersols," The MacMillan Company, New York.

51. Galloway, T.R. and Sage, B.H. 1967, "Thermal and Material Transport from Spheres, Prediction of Macroscopic Thermal and Material Transport," Int. J. Heat Mass Transfer, 10, 1195.

52. Garner, F.H. and Lane, J.J., 1959, "Mass Transfer to Drops of Liquid Suspended in a Gas Stream, Part II: Experimental Work and Results," Trans. Inst. Chem. Eng., 37, 162.

53. Genchev, Zh.D. and Karpuzov, D.S., 1980, "Effects of the Motion of Dust Particles on Turbulence Transport Equations," J. Fluid Mech., 101, 833.

54. Girshovich, T.A., Kartushinskii, A.I., Laats, M.K., Leonov, V.A. and Mul'gi, A.S., 1981, "Experimental Investigation of a Turbulent Jet Carrying Heavy Particles of a Disperse Phase," Fluid Dynamics, 5, 658.

55. Goldschmidt, V. and Eskinazi, S., 1966, "Two-Phase Turbulent Flow in a Plane Jet," J. Applied Mech., Trans. ASME, 33E, 735.

56. Gosman, A.D. and Ioannides, E., 1981, "Aspects of Computer Simulation of Liquid Fueled Combustors," AIAA Paper No. 81-0323.

57. Gouesbet, G., Berlemont, A. and Picart, A., 1984, "Dispersion of Discrete Particles by Continuous Turbulent Motions Extensive Discussion of the Tchen's Theory, Using a Two-Parameter Family of Lagrangian Correlation Functions," Phys. Fluids, 27, 827.

58. Gray, W.G., 1975, "A Derivation of the Equations for Multi-Phase Transport," Chemical Engineering Science, 30, 229.

59. Hamielec, A.E., Hoffman, T.W. and Ross, L.L., 1967, "Numerical Solution of the Navier-Stokes Equation for Flow Past Spheres, Part I: Viscous Flow Around Spheres with and without Radial Mass Efflux," AIChE. J., 13, 212.

60. Hamielec, A.E. and Johnson, A.I., 1962, "Viscous Flow Around Fluid Spheres at Intermediate Reynolds Numbers," Can. J. Chem. Eng., 40, 41.

61. Hamielec, A.E., Storey, S.H. and Whitehead, J.M., 1963, "Viscous Flow Around Fluid Spheres at Intermediate Reynolds Numbers," Can. J. Chem. Eng., 41, 246.

62. Hanjalic, K. and Launder, B.E. 1972, "A Reynolds Stress Model of Turbulence and its Application to Thin Shear Flows," J. Fluid Mech., 52, 60.

63. Harlow, F.H. and Amsden, A.A., 1975, "Numerical Calculation of Multiphase Fluid Flow," J. Comput. Phys., 17, 19.

64. Hayashi, K. and Branch, M.C., 1980, " Concentration, Velocity and Particle Size Measurements in Gas-Solid Two-Phase Jets," J. Energy, 4, 193.

65. Hetsroni, G. and Sokolov, M., 1971, "Distribution of Mass Velocity, and Intensity of Turbulence in a Two-Phase Turbulent Jet," J. of Applied Mech., 38, 314.

66. Hinze, J.O., 1972a, "Turbulent Fluid and Particle Interaction," Progress in Heat and Mass Transfer, 6, 433.

67. Hinze, J.O., 1972b, "Momentum and Mechanical Energy Balance Equations for a Flowing Homogeneous Suspension with Slip Between the Two Phases," Appl. Sci. Res, 11, Section A., 33.

68. Hinze, J.O., 1975, "Turbulence," McGraw-Hill, N.Y.

69. Hjelmfelt, A.T. Jr. and Mockros, L.F., 1966, "Motion of Discrete Particles in a Turbulent Fluid," Appl. Sci. Res., 16, 149.

70. Ingebo, R.D., 1956, "Drag Coefficients for Droplets and Solid Spheres in Clouds Accelerating in Airstreams," NACA TN 3762.

71. Ishii, M., 1975, "Thermo-Fluid Dynamic Theory in Two-Phase Flow," Eyrolles, Paris.

72. Jackson, R. and Davidson, B.J., 1983, "An Equation Set for Non-Equilibrium Two Phase Flow, and an Analysis of Some Aspects of Choking, Acoustic Propagation, and Losses in Low Pressure Wet Steam," Int. J. Multiphase Flow, 9, 491.

73. Kalinin, A.v., 1970, "Derivation of Fluid-Mechanics Equations for a Two-Phase Medium with Phase Changes," Heat Transfer Soviet Research, 2, 83.

74. Kamimoto, T. and Matsuoka, S., 1977, "Predicting Spray Evaporation, in Reciprocating Engines," SAE Paper 770413.

75. Kassoy, D.R., Adamson, T.C. Jr. and Messiter, A.F., 1966, "Compressible Low Reynolds Number Flow Around a Sphere," Phys. Fluids, 9, 671.

76. Kinzer, G.D. and Gunn, R., 1951, "The Evaporation, Temperature and Thermal Relaxation-Time of Freely Falling Waterdrops," J. Meteorology, 8, 71.

77. Kramer, T.J. and Depew, C.A., 1972, "Analysis of Mean Flow Characteristics of Gas-Solid Suspensions," J. Basic Eng. Trans. ASME, 94D, 731.

78. Krestein, A.R., 1983, "Prediction of the Concentration PDF for Evaporating Sprays," Paper No. 83-34 presented at the Spring Meeting of the Western States Section of the Combustion Institute, Jet Propulsion Laboratory, Pasadena, CA.

79. Laats, M.K. and Frishman, F.A., 1970a, "Scattering of an Inert Admixture of Different Grain Size in a Two-Phase Axisymmetric Jet," Heat Transfer-Soviet Res., 2, 7.

80. Laats, M.K. and Frishman, F.A., 1970b, "Assumptions used in Calculating the Two Phase Jet," Fluid Dynamics, 5, 333.

81. Laats, M.K. and Frishman, F.A., 1973, "Development of Techniques and Investigation of Turbulence Energy at the Axis of a Two-Phase Turbulent Jet," Fluid Dynamics, 2, 304.

82. Labowski, M. and Rosner, D.E., 1976, "Conditions for 'Group' Combustion of Droplets in Fuel Clouds: 1. Quasi-Steady Predictions," Symposium on Evaporation - Combustion of Fluid Droplets Division of Petroleum Chemistry, Am. Ch. Soc.

83. Launder, B.E., Morse, A., Rodi, W. and Spalding, D.B., 1972, "The Prediction of Free Shear Flows - a Comparison of the Performance of Six Turbulence Models," Imperial College, TM/TN/19.

84. Launder, B.E., 1976, "Turbulence," edited by Bradshaw (Springer-Verlag).

85. Law, C.K., 1982, "Recent Status of Droplet Vaporization and Combustion," Prog. Energy Combust. Sci., 8, 171.

86. Levy, T. and Lockwood, F.C., 1981, "Velocity Measurements in a Particle Laden Turbulent Free Jet," Comb. and Flame, 40, 333.

87. Lumley, J.L., 1975," Modeling Turbulent Flux of Passive Scalar Quantities in Homogeneous Flows," Phys. Fluids, 18, 619.

88. Lumley, J.L., 1978a, "Two-Phase and Non-Newtonian Flows," Turbulence, ed. Bradshaw, P., Springer-Verlag, Berlin, 290.

89. Lumley, J.L., 1978b, "Turbulent Transport of Passive Contaminants and Particles: Fundamentals and Advanced Methods of Numerical Modeling," Lecture Series at the Von Karman Institute for Fluid Dynamics, Rhode-St-Genese, Belgium.

90. Marble, F.E., 1962, "Dynamics of a Gas Containing Small Solid Particles," Proceeding of the 5th AGARD Combustion and Propulsion Symposium, New York, Pergammon Press, New York, 175.

91. Marble, F.E., 1970, "Dynamics of Dusty Gases," Ann. Rev. Fluid Mech., 2, 397.

92. Martinelli, L., Reitz, R.D. and Bracco, F.V., 1984, "Comparisons of Computed and Measured Dense Spray Jets," Dynamics of Flames and Reactive Systems: Progress in Astronautics and Aeronautics (edited by J.R. Bowen, N. Manson, A.K. Oppenheim, and R.I. Soloukhin), AIAA, New York, 95, 484.

93. Maxey, M.R. and Riley, J.J., 1983, "Equation of Motion for a Small Rigid Sphere in a Nonuniform Flow," Phys. Fluids, 26, 883.

94. McDonald, J.E., 1954, "The Shape and Aerodynamics of Large Raindrops," J. Meteor., 11, 478.

95. Meek, C.C. and Jones, B.G., 1973, "Studies of the Behavior of Heavy Particles in a Turbulent Fluid Flow," J. Atmos. Sci., 30, 239.

96. Meek, C.C. and Jones, B.G., 1974, "Reply," J. Atmos. Sci., 31, 1168.

97. Melville, W.K. and Bray, K.N.C., 1979, "A Model of the Two-Phase Turbulent Jet," Int. J. Heat Mass Transfer, 22, 647.

98. Michaelides, E.E., 1984, "A Model for the Flow of Solid Particles in Gases," Int. J. Multiphase Flow, 10, 61.

99. Modarress, D., Tan, H., and Elghobashi, S., 1984, "Two-Component LDA Measurement in a Two-Phase Turbulent Jet," AIAA J., 22, 624.

100. Mongia, H.C. and Smith, K., 1978, "An Empirical/Analytical Design Methodology for Gas Turbine Combustors," AIAA Paper No. 78-998.

101. Mostafa, A.A. and Elghobashi, S.E., 1983, "Prediction of a Turbulent Round Gaseous Jet Laden with Vaporizing Droplets," Paper NO. 83-44, presented at the Fall Meeting of the Western States Section of the Combustion Institute.

102. Mostafa, A.A. and Elghobashi, S.E., 1984, "A Study of the Motion of Vaporizing Droplets in a Turbulent Flow," Dynamics of Flames and Reactive Systems: Progress in Astronautics and Aeronautics (edited by J.R. Bowen, N. Manson, A.K. Oppenhiem, and R.I. Soloukhin), AIAA, New York, 95,513.

103. Mostafa, A.A. and Elghobashi, S.E., 1985a, "A Two-Equation Turbulence Model for Jet Flows Laden with Vaporizing Droplets," Int. J. Multiphase Flow (in press).

104. Mostafa, A.A. and Elghobashi, S.E., 1985b, "On the Dispersion of Heavy Particles in a Homogeneous Turbulence," Submitted to Phys. Fluids.

105. Mostafa, A.A., 1985, "A Two-Equation Turbulence Model for Dilute Vaporizing Sprays," Ph.D. Thesis, University of California, Irvine.

106. Nagarajan, M. and Murgatroyd, W., 1971, "A Simple Model of Turbulent Glass Solids Flow in a Pipe," Aerosol Sci., 2, 15.

107. Nakano, Y. and Tien, C., 1967, "Approximate Solutions of Viscous Incompressible Flow Around Fluid Spheres at Intermediate Reynolds Numbers," Can. J. Chem. Eng., 45, 135.

108. Nigmatulin, R.I., 1967, "Equations of Hydromechanics and Compression Shock in Two-Velocity and Two-Temperature Continuum with Phase Transformations," Fluid Dynamics, 2, 20.

109. Nigmatulin, R.I., 1979, "Spatial Averaging of Heterogenous and Dispersed Phase Systems," Int. J. Multiphase Flow, 5, 353.

110. Nir, A. and Pismen, L.M., 1979, "The Effect of a Steady Drift on the Dispersion of a Particle in Turbulent Fluid," J. Fluid Mech., 94, 369.

111. No, H.C., 1982, "On Soo's Equations in Multidomain Multiphase Fluid Mechanics," Int. J. Multiphase Flow, 8, 297.

112. Oliver, D.L.R. and Chung, J.N., 1982, "Steady Flows Inside and Around a Fluid Sphere at Low Reynolds Numbers," AIAA-82-0981.

113. O'Rourke, P.J. and Bracco, F.V., 1980, "Modeling of Drop Interactions in Thick Sprays and a Comparison with Experiments," Stratified Charge Automotive Engines Conference, The Institution of Mechanical Engineers, London.

114. O'Rourke, P.J., 1981, "Collective Drop Effects on Vaporizing Liquid Sprays," Ph.D. Thesis, Dept. of Mechanical and Aerospace Engineering, Princeton University.

115. Owen, P.R., 1969, "Pneumatic Transport," J. Fluid Mech., 39, 407.

116. Panton, R., 1968, "Flow Properties from the Continuum Viewpoint of a Nonequilibrium Gas-Particle Mixture," J. Fluid Mech., 31, 273.

117. Peskin, R.L., 1971, "Stochastic Estimation-Applications to Turbulent Diffusion," Int. symposium on Stochastic Diffusion, C.L. Chiu, ed., Univ. of Pittsburgh, Pittsburgh, PA, 251.

118. Peskin, R.L., 1974, "Comments on "Studies of the Behavior of Heavy Particles in a Turbulent Fluid Flow," J. Atmos. Sci., 31, 1167.

119. Pismen, L.M. and Nir, A., 1978, "On the Motion of Suspended Particles in Stationary Homogeneous Turbulence," J. Fluid Mech., 84, 193.

120. Popper, J., Abuaf, N. and Hetsroni, G., 1974, "Velocity Measurements in a Two-Phase Turbulent Jet," Int. J. Multiphase Flow, 1, 715.

121. Pourahmadi, F. and Humphrey, J.A.C., 1983, "Modeling Solid-Fluid Turbulent Flows with Application to Predicting Erosive Wear," Int. J. PhysicoChemical Hydrodynamics, 4, 191.

122. Prakash, S. and Sirignano, W.A., 1980, "Theory of Convective Droplet Vaporization with Unsteady Heat Transfer in the Circulating Liquid Phase," Int. J. Heat Mass Transfer, 23, 253.

123. Pruppacher, H.R. and Beard, K.V., 1970, "A Wind Tunnel Investigation of the Internal Circulation and Shape of Water Drops Falling at Terminal Velocity in Air," J. Atmos. Sci., 96, 247.

124. Rajani, J.B., 1972, "Turbulent Mixing in a Free Air Jet Carrying Solid Particles," Ph.D. thesis, Queen Mary College, London University.

125. Rakhmatulin, Kh. A., 1956, "Fundamentals of the Gas Dynamics of Interpenetrating Motions of Compressible Media," Zhurnal Prikladnoi Matematiki i Mekhaniki, 20, 184 (in Russian).

126. Ranz, W.E., and Marshall, W.R., 1952, "Evaporation from Drops," Chem. Eng. Prog., 48, 141, 173.

127. Reeks, M.W., 1977, "On the Dispersion of Small Particles Suspended in an Isotropic Turbulent Fluid," J. Fluid Mech., 83, 529.

128. Rietema, K. and Van Den Akker, H.E.A., 1983, "On the Momentum Equations in Dispersed Two-Phase Systems," Int. J. Multiphase Flow, 9, 21.

129. Rivkind, V. Ia. and Ryskin, G.M., 1976, "Flow Structure in Motion of a Spherical Drop in a Fluid Medium," Fluid Dynamics, 11, 5.

130. Rivkind, V. Ia., Ryskin, G.M. and Fishbein, G.A., 1976, "Flow Around a Spherical Drop at Intermediate Reynolds Numbers," Fluid Dynamics, 10, 741.

131. Rizk, M.A. and Elghobashi, S.E., 1985, "A Two-Equation Turbulence Model for Two-Phase Dilute Confined Flows," to be submitted to Int. J. Multiphase Flow.

132. Roache, P.J., 1976, "Computational Fluid Dynamics," Albuquerque, New Mexico, Hermosa Publishers.

133. Rodi, W., 1971, "On the Equation Governing the Rate of Turbulent Energy Dissipation," Mech. Engng. Dept. Imperial College Rep. TM/TN/A/14.

134. Rudinger, Cr., 1965, "Some Effects of Finite Particle Volume on the Dynamics of Gas-Particle Mixtures," AIAA J., 3, 1217.

135. Sha, W.T. and Soo, S.L., 1978, "Multidomain Multiphase Fluid Mechanics," Int. J. Heat Mass Transfer, 21, 1581.

136. Shearer, A.J., 1979, "Evaluation of a Locally Homogeneous Flow Model of Spray Evaporation," Ph.D. Thesis, The Pennsylvania State University Park, PA.

137. Shearer, A.J., Tamura, H. and Faeth, G.M., 1979, "Evaluation of a Locally Homogeneous Flow Model of Spray Evaporation," J. Energy, 3, 271.

138. Shuen, J-S., Chen, L-D. and Faeth, G.M., 1983, "Evaluation of a Stochastic Model of Particle Dispersion in a Turbulent Round Jet," AIChE J., 29, 167.

183

139. Sirignano, W.A., 1983, "Fuel Droplet Vaporization and Spray Combustion Theory," Prog. Energy Combust. Sci., 9, 291.

140. Snyder, W.H. and Lumley, J.L., 1971, "Some Measurements of Particle Velocity Autocorrelation Functions in a Turbulent Flow," J. Fluid Mech. 48, 41.

141. Solbrig, C.W. and Hughes, E.D., 1975, "Governing Equations for a Seriated Continuum: An Unequal Velocity Model for Two-Phase Flow," ANCR-1193.

142. Solomon, A.S.P., Shuen, J-S., Zhang, Q-F., and Faeth, F.M., 1984, "A Theoretical and Experimental Study of Turbulent Evaporating Sprays," NASA Report No. 174760.

143. Soo, S.L., 1956, "Statistical Properties of Momentum Transfer in Two-Phase Flow," Chem. Engng. Sci., 5, 57.

144. Soo, S.L., 1967, "Fluid Dynamics of Multiphase Systems," Blaisdell, Waltham,

145. Spalding, D.B., 1971, "Concentration Fluctuations in a Round Turbulent Free Jet," Chem. Engng. Sci., 25, 95.

146. Spalding, D.B., 1978, "GENMIX: A General Computer Program for Two-Dimensional Parabolic Phenomena," Pergamon Press, Oxford.

147. Spalding, D.B., 1979, "Numerical Computation of Multiphase Flows," Lecture notes, Thermal Sciences and Propulsion Center, Purdue University, West Lafayette, Ind.

148. Subramanian, V. and Ganesh, R., 1982a, "Entrainment by a Concentric Jet with Particles in the Primary Stream," Letters in Heat and Mass Transfer, 9, 277.

149. Subramanian, V. and Ganesh, R., 1982b, "Entrainment by a Concentric Jet with Particles in the Secondary Stream," Can. J. Chem. Eng., 60, 589.

150. Synge, J.L., and Schild, A., 1978, "Tensor Calculus," Dover, New York.

151. Taylor, G.I., 1921, "Diffusion by Continuous Movements," Proc. London Math. Soc., Series 2, 20, 196.

152. Tchen, C.M., 1947, "Mean Value and Correlation Problems Connected with the Motion of Small Particles in a Turbulent Fluid," Ph.D. thesis, University of Delft.

153. Tennekes, H. and Lumley, J.L., 1972, "A First Course in Turbulence," MIT, Cambridge, Massachussettes.

154. Torbin, L.B. and Gauvin, W.H., 1959, "Fundamental Aspects of Solid-Gas Flow," Can. J. Chem. Eng., Vol. 37, 127, 167, 224.

155. Torbin, L.B. and Gauvin, W.H., 1960, "Fundamental Aspects of Solid-Gas Flow," Can. J. Chem. Eng., 38, 142, 189, 160.

156. Torbin, L.B. and Gauvin, W.H., 1961, "Fundamentals Aspects of Solid-Gas Flow," Can. J. Chem. Eng., 39, 113.

157. Tsuji, Y., Morikawa, Y. and Teraashima, K., 1982, "Fluid-Dynamic Interaction Between Tow Spheres," Int. J. Multiphase Flow, 8, 71.

158. Vargaftik, N.B., 1975, "Tables on the Thermophysical Properties of Liquids and Gases," Hemisphere Publishing Corporation, Washington.

159. Vasiliev, O.F., 1969, "Problems of Two-Phase Flow Theory," International Association of Hydraulic Research, Proceedings of the International Congress, 13, 39.

160. Vasil'kov, A.P., 1976, "Calculation of a Turbulent Two-Phase Isobaric Jet," Fluid Dynamics, 5, 669.

161. Wellek, R.M., Agrawal, A.K. and Skelland, H.P., 1966, "Shape of Liquid Drops Moving in Liquid Media," AIChE J., 12, 855.

162. Wells, M.R. and Stock, D.E., 1983, "The Effects of Crossing Trajectories on the Disprsion of Particles in a Turbulent Flow," J. Fluid Mech., 136, 31.

163. Westbrook, C.K., 1976, "Three Dimensional Numerical Modeling of Liquid Fuel Sprays," Sixteenth Symposium (International) on Combustion, The Combustion Institute, Pittsburgh, PA, 1517.

164. Whitaker, S., 1973, "The Transport Equations for Multi-Phase Systems," Chem. Engng. Sci., 28, 139.

165. Winnikow, S. and Chao, B.T., 1965, "Droplet Motion in Purified Systems," Phys. Fluids, 9, 50.

166. Wu, K-J., Coghe, A., Santavicca, D.A. and Bracco, F.V., 1984, "LDV Measurements of Drop Velocity in Diesel-Type Sprays," AIAA J., 22, 1263.

167. Yeung, W.-S., 1978, "Fundamentals of the Particulate Phase in a Gas-Solid Mixture," Lawrence Brekeley Laboratory, Berkeley, CA, Report No. LBL-8440.

168. Yeung, W.-S., 1982, "Similarity Analysis of Gas-Liquid Spray Systems," Journal of Applied Mechanics, 49, 687.

169. Yudine, M.I., 1959, "Physical Considerations on Heavy-Particle Diffusion," In Atmospheric Diffusion and Air Pollution: Adv. Geophys., 6, 185.

170. Yuen, M.C. and Chen, L.W., 1976, "On Drag of Evaporating Liquid Droplets," Combustion Science and Technology, 14, 147.

C-3

171. Yuen, M.C. and Chen, L.W., 1978, "Heat Transfer Measurements of Evaporating Liquid Droplets," Int. J. Heat Mass Transfer, 21, 537.

172. Yule, A.J., Seng, C. Ah, Felton, P.G., Ungut, A. and Chigier, N.A., 1982, "A Study of Vaporizing Fuel Sprays by Laser Techniques," Comb. and Flame, 44, 71.

173. Yuu, S., Yasukouchi, N., Hirosawa, Y. and Jotaki, T., 1978, "Particle Turbulent Diffusion in a Duct Laden Round Jet," AIChE J., 24, 509.

174. Zarin, N. and Nicholls, A., 1971, "Sphere Drag in Solid Rockets - Non-Continuum and Turbulence Effects," Comb. Sci. & Tech., 3, 273.

175. Zuev, Yu. V. and Lepeshinskii, I.A., 1981, "Mathematical Model of a Two-Phase Turbulent Jet," Fluid Dynamics, 6, 857.

APPENDIX A

Material Properties of the Spray

Table A-1
Physical Properties of Liquid Droplets*

Property	Methanol (CH_4O)	Freon 11 (CCL_3F)
Saturated vapor pressure (P_s), N/m^2	0.207	
Latent heat of vaporization (L), KJ/Kg	50.0	181.32
Density (ρ_2), Kg/m^3	810	1518
Saturation temperature (T_s), °K	292	240.3
Boiling temperature (T_B), °K	347.71	296.7
Molecular weight, W_v	32	137.37
Viscosity of liquid material, (μ_2), $10^4 Kg/ms$	5.09	4.05
Surface tension (γ), $10^3 N/m$	21.8	7.5
Diffusivity of the evaporating material (δ), $10^5 m^2/s$	1.35	2.85

* Obtained at 30°C and P = 1 atm. (Vargaftik 1975 and ASHRAE 1969)

Modeled Transport Equations in Cartesian Tensor Notations

Substituting in the time-averaged equations presented in the subsections 2.3 & 3.3 by the modeling approximations for various turbulent correlations discussed in the subsection 3.4, the modeled transport equations in Cartesian tensor notations are obtained and will be presented in this Appendix.

The continuity equations of the carrier phase

$$\rho_1(\Phi_1 U_i)_{,i} - \rho_1(\frac{\nu_t}{\sigma_c}\Phi_{1,i})_{,i} = \sum_k \dot{m}^k \phi^k \qquad \text{B-1}$$

The continuity equations of the kth phase

$$\rho_2(\Phi^k V_i^k)_{,i} - \rho_2(\frac{\sigma_p^k}{\sigma_c}\nu_t \Phi^k_{,i})_{,i} = -\dot{m}^k \phi^k \qquad \text{B-2}$$

The mean global continuity is

$$\Phi_1 + \sum_k \phi^k = 1 \qquad \text{B-3}$$

The momentum equation of the carrier phase

$$\rho_1\Phi_1 U_{i,j} U_j = -\Phi_1 P_{,i} - \sum_k \phi^k(F^k + \dot{m}^k)(U_i - V_i^k)$$

$$- \sum_k \dot{m}^k \frac{\sigma_p^k}{\sigma_c}\phi^k_{,i} - \rho_1 U_i(\frac{\nu_t}{\sigma_c}\Phi_{1,j})_{,j}$$

$$+ \sum_k F^k \frac{\nu_t}{\sigma_c}(1-\sigma_p^k)\phi^k_{,i} + \rho_1(\nu_t \Phi_1(U_{i,j}+U_{j,i}) + \frac{\nu_t}{\sigma_c}U_i\Phi_{1,j}$$

$$+ \frac{\nu_t}{\sigma_c}U_j\Phi_{1,i} + c_\phi \frac{\nu_t}{\sigma_c}(\frac{K}{\varepsilon})[(U_{i,\ell}+U_{\ell,i})(\nu_t\Phi_{1,j})_{,\ell}$$

Third Order Correlation

$$+ (U_{\ell,i} + U_{j,\ell})(\nu_t \Phi_{1,i}),_\ell]),_j \qquad \text{B-4}$$

<div align="center">Third Order Correlation</div>

The momentum equation of the kth phase

$$\rho_2 \phi^k V_{i,j}^k V_j^k = -\phi^k P,_i - F^k \phi^k (U_i - V_i^k)$$

$$+ \dot{m}^k \frac{\sigma_p^k}{\sigma_c} \phi^k,_i - \rho_2 V_i^k (\frac{\sigma_p^k}{\sigma_c} \nu_t \phi^k,_i),_i + g_i \phi^k (\rho_2 - \rho_1)$$

$$- F^k \frac{\nu_t}{\sigma_c}(1 - \sigma_p^k)\phi^k,_i + \rho_2 \sigma_p^k (\nu_t \phi^k (V_{i,j}^k + V_{j,i}^k) + \frac{\nu_t}{\sigma_c} V_i^k \phi^k,_j$$

$$+ \frac{\nu_t}{\sigma_c} V_j^k \phi^k,_i + c_\phi \frac{\nu_t}{\sigma_c}(\frac{K}{\epsilon})[(V_{i,\ell}^k + V_{\ell,i}^k)(\sigma_p^k \nu_t \phi^k,_j),_\ell$$

<div align="center">Third Order Correlation</div>

$$+ (V_{\ell,i}^k + V_{j,\ell}^k)(\sigma_p^k \nu_t \phi^k,_i),_\ell]),_j \qquad \text{B-5}$$

<div align="center">Third Order Correlation</div>

The conentration equation

$$\rho_1 \Phi_1 U_j C,_j = \sum_k \phi^k \dot{m}^k (1-C)$$

$$+ \frac{\rho_1}{\sigma_c}(\nu_t C \phi_{1,j} + \nu_t \phi_1 C,_j),_j - \rho_1 C(\frac{\nu_t}{\sigma_c}\phi_{1,j}),_j \qquad \text{B-6}$$

The turbulence kinetic energy equation (K)

$$\phi_1 U_\ell K,_\ell = \phi_1(\frac{\nu_t}{\sigma_k} K,_\ell),_\ell + \{\phi_1 U_{i,\ell} \nu_t (U_{i,\ell} + U_{\ell,i})$$

<div align="center">Production (P_k)</div>

$$+ c_\phi \frac{K}{\epsilon}\frac{\nu_t}{\sigma_c}(U_{i,j} + U_{j,i})(\nu_t \phi_{1,\ell}),_j + (U_{\ell,j} + U_{j,\ell})(\nu_t \phi_{1,i}),_j)\}$$

Third Order Correlation   Third Order Correlation

$$- \frac{1}{\rho_1} \sum_k (F^k + \dot{m}^k) \{(V_i^k - U_i) \frac{\nu_t}{\sigma_c} \sigma_p^k \phi^k_{,i}$$

extra dissipation (ε_p)

$$+ K(1 - \int_o^\infty (\frac{\Omega_1 - \Omega_R}{\Omega_2}) E(\omega) d\omega) \{\phi^k - c_\phi \frac{K}{\varepsilon} (\frac{\sigma_p^k}{\sigma_c} \nu_t \phi^k_{,\ell})_{,\ell}\}\}$$

Third Order Correlation

$$- \Phi_1 \varepsilon \qquad\qquad\qquad B-7$$

dissipation

The dissipation rate equation (ε)

$$\Phi_1 U_\ell \varepsilon_{,\ell} = \Phi_1 (\frac{\nu_t}{\sigma_c} \varepsilon_{,\ell})_{,\ell} - c_{\varepsilon 3} \frac{\varepsilon}{K} \cdot \varepsilon_p$$

$$+ (c_{\varepsilon 1} \frac{P_k}{\varepsilon} - c_{\varepsilon 2} \Phi_1) \frac{\varepsilon^2}{K} \qquad\qquad B-8$$

Initial Conditions of the Different Cases

Table C-2. Experimental Flow Conditions of Modarress et al. (1984)*

Gas-Phase (Air):	Case 1	Case 2	Case 3
Centerline velocity, $U_{x,c}$ (m/s)	12.6	12.6	13.4
Exponent, n, of power law velocity Profile $U_x/U_{x,c} = (1-(2r/D))^{1/n}$	<------------- 6.6 ------------->		
Turbulence Intensity $(u_x/U_{x,c})$	<--------(0.04 + 0.1 r/D)------>		
Density, ρ_1 (Kg/m^3)	<------------- 1.178 ----------->		
Mass flow rate $\dot{m}_1$ (Kg/s)	3.76×10^{-3}	3.76×10^{-3}	4×10^{-3}
Reynolds number $R_e = (4\dot{m}_1/\pi\mu_1 D)$	13300	13300	14100
Uniform mean velocity of surrounding stream, $U_{x,s}$ (m/s)	<------------- 0.05 ------------>		
Intensity of turbulence in surrounding $(u_{x,s}/U_{x,s})$	<------------- 0.1 ------------->		

* Measured at 0.1D Downstream of Pipe Exit

Solid-Phase (Glass Beads):	Case 1	Case 2	Case 3
Particle diameter (microns)	50	50	200
Particle density, ρ_2 (Kg/m^3)	<------------ 2990 ------------>		
Centerline velocity, $V_{x,c}$ (m/s)	12.4	12.4	10.2
Exponent, n, of power law velocity profile	<------------ 27.6 ------------>		
Mass flow rate $\dot{m}_2$ (Kg/s)	1.2×10^{-3}	3.2×10^{-3}	3.2×10^{-3}
Ratio of mass flow rates $\Phi_o = \dot{m}_2/\dot{m}_1$	0.32	0.85	0.8
Ratio of volumetric fractions = $\Phi_2/\Phi_1 = (\dot{m}_2/\dot{m}_1)(\rho_1 U_{x,av.}/\rho_2 V_{x,av.})$	1.1×10^{-4}	2.9×10^{-4}	3.52×10^{-4}

Table C-3: Experimental Flow Conditions of Shearer et al. (1979)* (Case 5)

$r \times 10^3$ m	U_z, m/s		K, m²/s²		ε, 10^{-2} m²/s³		$\Phi_2 \times 10^6$ m³ droplet/m³	C kg Vapor/kg
	S.ph.**	Spray	S.ph.	Spray	S.ph.	Spray		
0.0	9.6	11.7	7.1	9.6	7.06	17.4	2.25	0.24
5.0	9.0	11.0	7.1	9.6	7.06	17.4	1.8	0.22
10.0	7.9	9.41	6.8	9.3	5.42	15.2	1.2	0.19
15.0	6.2	7.30	6.0	8.7	3.35	5.98	0.51	0.14
20.0	3.6	5.20	4.5	7.2	2.04	6.29	0.2	0.09
25.0	3.2	3.27	3.0	5.2	1.17	3.92	0.14	0.05
30.0	2.1	1.93	1.8	3.1	0.487	1.56	0.08	0.02
35.0	1.1	0.94	0.09	1.4	0.25	0.53	0.04	0.01
40.0	0.4	0.0	0.03	0.0	0.1	0.0	0.0	0.0
42.5	0.0		0.0		0.0			

*   Measured at 170 D Downstream of the Injection Nozzle
** S.ph. = single phase flow

Table C-4. Experimental Flow Conditions of Solomon et.al. (1984)
Properties of the Carrier Phase at
50 D Downstream of the Nozzle (Cases 6 & 7)

$r \times 10^3$ m	U_z, m/s		K, m^2/s^2		$\varepsilon \times 10^{-3}$ m^2/s^3		C' kg vap/kg	
	Case 6	Case 7	Case 6	Case 7	Case 6	Case 7	Case 6	Case 7
0.0	24.0	16.0	16.1	4.6	0.59	0.28	0.292	.292
1.19	24.0	17.0	18.4	4.7	2.06	1.00	0.292	.292
2.39	23.3	18.7	20.6	6.5	5.59	2.67	0.269	.269
3.58	22.0	18.1	21.3	6.7	8.41	4.02	0.226	.226
4.78	19.9	16.0	21.3	9.2	9.12	4.36	0.183	.183
5.97	17.8	13.9	21.3	11.0	8.00	4.67	0.130	.130
7.17	15.4	11.7	21.0	11.5	7.82	4.45	0.083	.083
8.37	13.0	9.6	20.2	11.2	7.65	4.23	0.049	.049
9.56	10.6	9.56	19.0	9.5	7.65	4.23	0.024	.024
11.0	7.9	5.10	16.0	6.4	6.65	3.68	0.009	.009
12.0	4.0	2.30	9.92	3.0	4.26	2.00	0.005	.004
13.90	1.1	0.0	2.7	0.0	1.0	0.0	0.003	0.00
14.30	0.0		0.0		0.0		0.0	

194

Table C-4b. Properties of the kth Phases*
at 50 D Downstream of the Nozzle (Case 6)

r×10³ m	v¹	φ¹	v²	φ²	v³	φ³	v⁴	φ⁴	v⁵	φ⁵	v⁶	φ⁶	v⁷	φ⁷
0.0	27.8	1.7	28.3	1.41	27.5	2.15	28.4	2.07	28.5	2.87	28.5	1.81	27.2	0.44
1.19	28.2	1.79	28.1	1.48	27.4	2.11	28.2	2.05	27.7	2.84	27.8	1.80	26.2	0.45
2.39	28.6	1.89	27.9	1.55	27.3	2.0	27.9	2.0	26.8	2.81	27.1	1.80	25.2	0.47
3.58	28.6	1.94	27.9	1.58	27.3	1.87	27.9	1.93	26.8	2.76	27.1	1.78	25.2	0.48
4.78	25.5	1.95	24.8	1.58	24.8	1.72	24.7	1.84	24.0	2.64	24.0	1.72	22.4	0.48
5.97	22.3	1.95	21.6	1.53	22.2	1.51	21.4	1.72	21.1	2.50	20.8	1.65	19.5	0.46
7.17	20.2	1.92	19.2	1.49	18.6	1.29	18.3	1.57	17.9	2.32	17.5	1.54	16.6	0.44
8.37	18.2	1.85	16.7	1.42	14.9	1.08	15.2	1.41	14.7	2.10	14.2	1.40	13.6	0.41
9.56	18.2	1.75	16.7	1.31	14.9	0.86	15.2	1.20	14.7	1.81	14.2	1.34	13.6	0.37
11.10	15.1	1.53	14	1.13	13.2	0.623	12.2	0.97	11.8	1.46	11.3	1.00	10.7	0.31
12.00	11.9	0.82	11.3	0.58	11.4	0.31	9.1	0.53	8.9	0.81	8.3	0.55	7.8	0.16
13.90	6.0	0.2	5.7	0.14	5.7	0.08	4.6	0.13	4.5	0.20	4.2	0.14	3.9	0.04
14.30	0.0	0.0	0.0	0.0	0.0	0.0	0.0	0.0	0.0	0.0	0.0	0.0	0.0	0.0

* v^k in m/s and φ^k in 10⁵ m³/m³

Table C-1: The Considered Cases

Case Number	Dispensed Phase Material	Diameter of Particles d m	Mass Loading Ratio X_o	Region of Study z/D	Reference
1	Glass	50	0.32	0.1-20	Modarress et al. (1984)
2	Glass	50	0.85	0.1-20	Modarress et al. (1984)
3	Glass	200	0.8	0.1-20	Modarress et al. (1984)
4	Methanol	20-100	0.1-0.5	0.1-20	Idealized Flow
5	Freon-11	27	6.88	170-510	Shearer et al. (1979)
6	Freon-11	17.5-52.5	7.71	50-500	Solomon et al. (1984)
7	Freon-11	15-100	15.78	50-500	Solomon et al. (1984)

Table C-4c. Mean Velocities of for k^{th} Phases *
at 50 D Downstream of the Nozzle (Case 7)

$r \times 10^3 m$	v^1	v^2	v^3	v^4	v^5	v^6	v^7	v^8	v^9	v^{10}
0.0	19.5	18.8	19.3	20.5	20.3	21.1	20.7	21.2	20.6	19.8
1.19	19.6	19.0	19.7	20.9	20.8	21.7	21.3	21.1	20.1	19.9
2.39	19.9	19.6	20.5	21.3	21.7	22.0	22.0	21.1	20.4	20.2
3.58	19.7	20.0	19.6	20.9	21.2	21.8	21.3	20.4	19.8	19.6
4.78	19.1	19.1	18.7	19.5	19.5	19.6	19.1	18.2	17.4	17.2
5.97	18.3	18.3	17.9	18.8	17.7	17.4	16.9	16.0	15.0	14.9
7.17	17.4	17.5	17.0	16.9	16.4	15.9	14.8	13.1	11.6	11.4
8.37	16.5	16.6	16.1	15.7	15.1	14.3	12.8	10.2	8.2	7.8
9.56	15.0	15.0	14.1	13.4	12.6	11.8	10.2	7.9	5.9	5.5
11.00	13.0	12.9	11.5	10.4	9.5	8.7	7.1	5.7	4.1	3.7
12.00	8.5	8.2	6.7	5.5	4.8	3.6	3.0	2.7	1.7	1.5
13.90	0.0	0.0	0.0	0.0	0.0	0.0	0.0	0.0	0.0	0.0

* v^k in m/s

197

Table C-4d. Volume Fractions of the kth Phases *
at 50 D Downstream of the Nozzle (Case 7)

$rx10^3$ m	Φ^1	Φ^2	Φ^3	Φ^4	Φ^5	Φ^6	Φ^7	Φ^8	Φ^9	Φ^{10}
0.0	1.65	2.56	2.8	2.8	3.89	5.18	3.11	1.48	0.59	0.02
1.19	1.58	2.25	2.7	2.91	3.90	4.81	3.05	1.45	0.52	0.018
2.39	1.52	1.93	2.59	3.01	3.90	4.26	2.95	1.39	0.4	0.016
3.58	1.44	1.63	2.35	3.06	3.74	3.65	2.82	1.36	0.31	0.014
4.78	1.36	1.36	1.85	3.01	3.27	3.49	2.7	1.42	0.37	0.014
5.97	1.27	1.09	1.35	2.96	2.80	3.34	2.58	1.49	0.45	0.013
7.17	1.27	1.23	1.28	2.26	2.24	2.61	2.04	1.23	0.43	0.011
8.37	1.27	1.38	1.21	1.57	1.67	1.89	1.5	0.96	0.41	0.010
9.56	1.24	1.34	1.09	1.22	1.25	1.47	1.1	0.78	0.39	0.010
11.00	1.15	1.06	0.86	1.56	1.09	1.07	0.98	0.72	0.38	0.011
12.00	0.78	0.59	0.48	1.43	0.7	1.44	0.63	0.48	0.37	0.009
13.90	0.0	0.0	0.0	0.0	0.0	0.0	0.0	0.0	0.0	0.0

* Φ^k in 10^5 m^3/m^3

1. Report No. NASA CR-175063	2. Government Accession No.	3. Recipient's Catalog No.
4. Title and Subtitle Effect of Liquid Droplets on Turbulence in a Round Gaseous Jet		5. Report Date **February 1986**
		6. Performing Organization Code
7. Author(s) A.A. Mostafa and S.E. Elghobashi		8. Performing Organization Report No. None
		10. Work Unit No.
9. Performing Organization Name and Address University of California at Irvine Department of Mechanical Engineering Irvine, California 92717		11. Contract or Grant No. NAG 3-176
		13. Type of Report and Period Covered Contractor Report
12. Sponsoring Agency Name and Address National Aeronautics and Space Administration Washington, D.C. 20546		14. Sponsoring Agency Code 505-31-42

15. Supplementary Notes

Final report. Project Manager, Robert Tacina, Aerothermodynamics and Fuels Division, NASA Lewis Research Center, Cleveland, Ohio 44135.

16. Abstract

The main objective of this investigation is to develop a two-equation turbulence model for dilute vaporizing sprays or in general for dispersed two-phase flows including the effects of phase changes. The model that accounts for the interaction between the two phases is based on rigorously derived equations for the turbulence kinetic energy (K) and its dissipation rate (ϵ) of the carrier phase using the momentum equation of that phase. Closure is achieved by modeling the turbulent correlations, up to third order, in the equations of the mean motion, concentration of the vapor in the carrier phase, and the kinetic energy of turbulence and its dissipation rate for the carrier phase. The governing equations are presented in both the exact and the modeled forms. The governing equations are solved numerically using a finite-difference procedure to test the presented model for the flow of a turbulent axisymmetric gaseous jet laden with either evaporating liquid droplets or solid particles. The predictions include the distribution of the mean velocity, volume fractions of the different phases, concentration of the evaporated material in the carrier phase, turbulence intensity and shear stress of the carrier phase, droplet diameter distribution, and the jet spreading rate. Predictions obtained with the proposed model are compared with the data of Shearer et al. (1979) and with the recent experimental data of Solomon et al. (1984) for Freon-11 vaporizing sprays. Also, the predictions are compared with the data of Modarress et al. (1984) for an air jet laden with solid particles. The predictions are in good agreement with the experimental data.

17. Key Words (Suggested by Author(s)) Spray modeling Turbulence interactions Combustor	18. Distribution Statement Unclassified - unlimited STAR Category 07		
19. Security Classif. (of this report) Unclassified	20. Security Classif. (of this page) Unclassified	21. No. of pages 208	22. Price* A10

National Aeronautics and
Space Administration

Lewis Research Center
Cleveland. Ohio 44135

SECOND CLASS MAIL

ADDRESS CORRECTION REQUESTED

NASA